Future Energy
Service & Publishing

Trends in Renewable Energy

Volume 5, Issue 1, January 2019
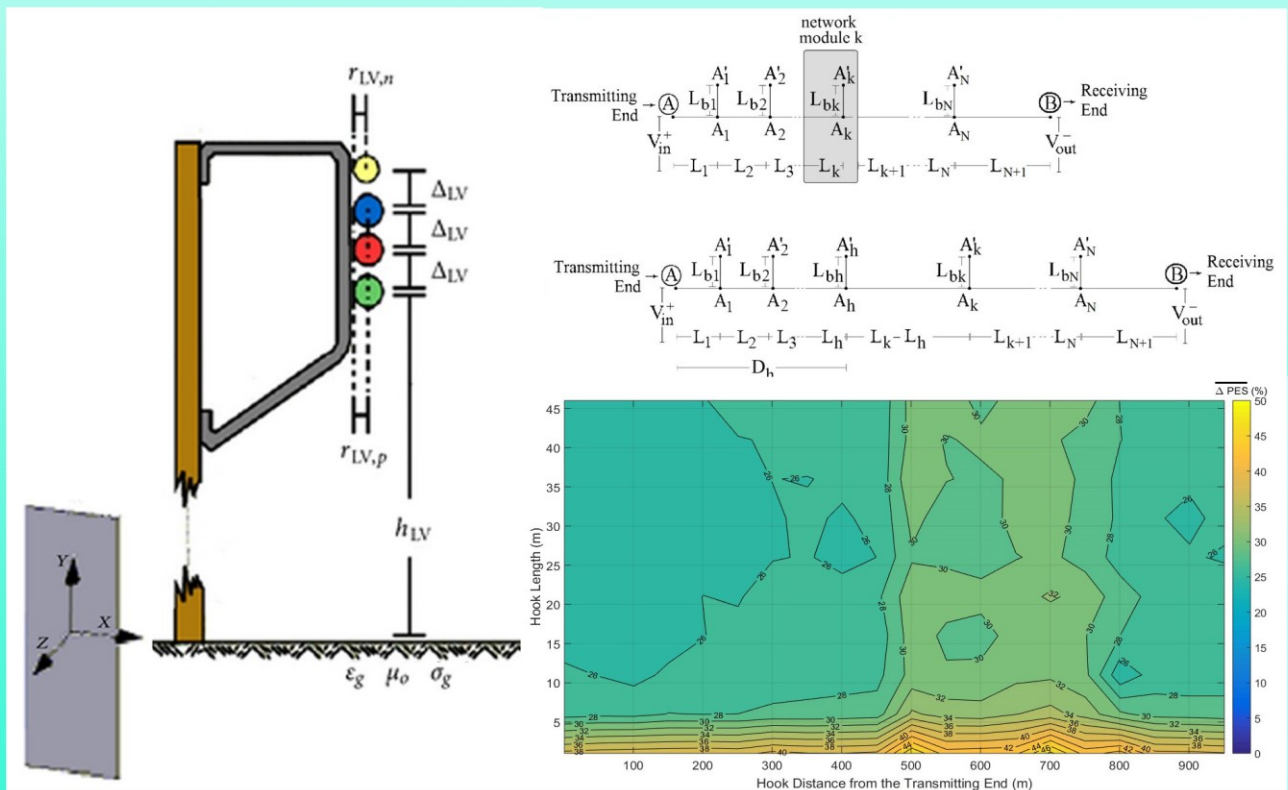
Cover image: Detection of the hook style energy theft, see articles by Lazaropoulos in this issue.

futureenergysp.com
thefutureenergy.org

Trends in Renewable Energy

_____

Trends in Renewable Energy is an open accessed, peer-reviewed semi-annual journal publishing reviews and research papers in the field of renewable energy technology and science.

The aim of this journal is to provide a communication platform that is run exclusively by scientists working in the renewable energy field. Scope of the journal covers: Bioenergy, Biofuel, Biomass, Bioprocessing, Biorefinery, Biological waste treatment, Catalysis for energy generation, Energy conservation, Energy delivery, Energy resources, Energy storage, Energy transformation, Environmental impact, Feedstock utilization, Future energy development, Green chemistry, Green energy, Microbial products, Physico-chemical process for Biomass, Policy, Pollution, Renewable energy, Smart grid, Thermo-chemical processes for biomass, etc.

The Trends in Renewable Energy publishes the following article types: peer-reviewed reviews, mini-reviews, technical notes, short-form research papers, and original research papers.

The article processing charge (APC), also known as a publication fee, is fully waived for the Trends in Renewable Energy.

III

Table of Contents

Volume 5, Issue No. 1, January 2019

Articles

Conversion of Food Processing Waste to Bioenergy: Bangladesh Perspective

Mohammad Shaiful Alam Amin[*], Musabbir Jahan Talukder, Rajarshi Roy Raju, Maksudur R. Khan

Department of Chemical Engineering and Polymer Science, Shahjalal University of Science and Technology, Sylhet 3114, Bangladesh.

Microbial fuel cell (MFC) is an attractive renewable and sustainable technology to meet up the drastic energy crisis of the world through waste water treatment. This Bioelectrochemical system (BES) converts biomass spontaneously into electricity by the metabolic activity of microorganisms. Food processing industry generally discharges large volume of wastewater, which creates adverse financial and ecological impacts to the industry and environment. In this present contribution, electricity production from food processing industry wastewater that serves as substrates in MFCs was investigated. Dual chambered mediator-less MFC was designed and fabricated using locally available materials. Performance of the MFC was evaluated by measuring potential parameters, such as current generation, current density, change in pH, and change in chemical oxygen demand at different operating conditions. Polarization experiments were conducted to find the maximum power density. Current generation increased with increasing sludge loading, and maximum results were recorded as 90 µA with 9 g of sludge and optimum pH value 8 in the anode chamber. This study documented a maximum power density of 7.42 mW/m^2 with the corresponding current density of 25 mA/m^2.

Introduction

The severely increased demand of limited fossil energy sources (*i.e.*, coal, petroleum, and natural gas); overwhelming climate changes due to air pollution; and the current escalation of energy cost considerably motivate the research toward searching new alternative energy production approaches. Like other countries due to the industrial revolution in Bangladesh, dependency and demand of electrical energy are increasing rapidly [1]. As a result, a variety of non-environmental friendly by-products such as greenhouse gases and hazardous solid wastes (e.g., radioactive wastes) are readily released to the environment. So, with this severe energy crisis, wastewater treatment is becoming another big issue for the present world [2-4]. Considering the socio-economic condition, we need both the industry and environment.

There are around 700 small and large food manufacturing industries operating in Bangladesh, including homemade processing units. Among all, nearly 30 enterprises are processing fruits and vegetables [5]. Overall 20% of the labor forces of the country are engaged this sector [6]. In total, all food processing enterprises are the source of 2% of the gross domestic product (GDP) [7]. Now-a-days, this sector is growing rapidly and creating new opportunities in investment and export along with the modern equipped technology. However, the distinctive characteristics of agricultural and food industries make its effluent treatment process differ from the conventional municipal wastewater treatment process. Although the discharged wastewater are biodegradable and nontoxic, but it is rich in high suspended solids (SS), chemical and biochemical oxygen (COD and BOD) [8, 9]. Therefore, these are industries are not only the source of opportunity; even so, there is a big concern on effluent treatment [10].

In this connection, microbial fuel cell (MFC) is a promising technology to meet the energy demand along with the food processing wastewater treatment [11-13]. MFC can utilize organic substances present in wastewater and be able to convert their chemical energy to electricity by using microorganisms as a catalyst [14-16]. For this benefit, interest on MFCs has massively grown in recent years. Number of researchers as well as the applications of this system are increasing, because of its simultaneous wastewater treatment and electricity generation [17, 18].

Design and construction of double chamber MFCs are widely studied for laboratory analysis. In this cell, organic matters of waste water are used as a fuel oxidized by bacteria and electrons are transferred to the anode. Electrons that pass along the circuit combine with electron acceptors. Thus, the biological electrochemical process and energy conversion are completed [19, 20]. In this present study, food processing industry wastewater has been used as substrate; anaerobic sludge was used for inoculation and potassium permanganate solution as oxidant. Different experiments have been carried out in a locally fabricated MFC to find the optimum condition for current generation and COD removal. Polarization experiments were conducted to find the maximum power density.

Materials and Methods

MFC Construction & Inoculation

Dual-chambered MFC was designed and fabricated in the laboratory using available local material. Two interconnected water bottle, 0.5 L of volume in each, was used as anode and cathode compartments. And each chamber was provided with sample port, wire point inputs (top), inlet and outlet ports (Figure 1). A Proton Exchange Membrane (PEM) membrane between two straight conduits was used to connect the two chambers. Two 1 cm long and 0.75 cm diameter plastic tubes were used for this purpose.

Food processing industry wastewater was collected from a renowned food processing industry in Sylhet, Bangladesh. Wastewater collected from the industry was used as the substrate in the anodic chamber of MFC. Sludge was collected from Drainage system of Surma Residential Area, Sylhet, Bangladesh.
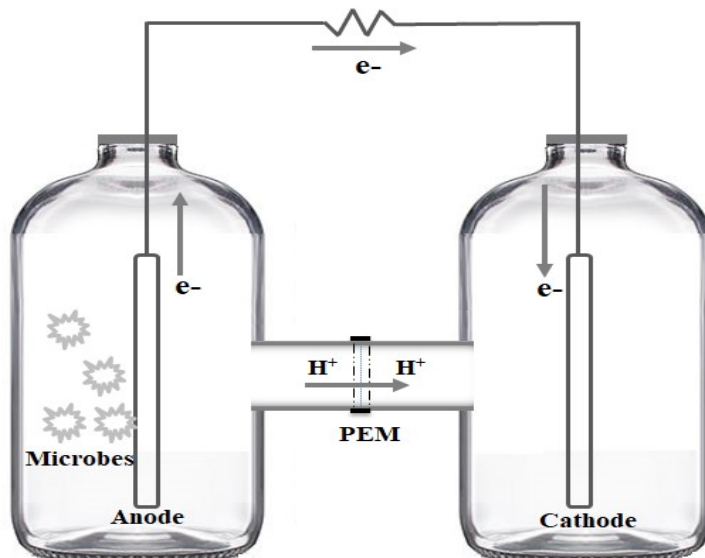
Figure 1. Schematic diagram of dual-chambered microbial fuel cell

Both the substrate and sludge were stored separately under anaerobic condition. This mixture was used as the original anodic inoculum. Before inoculation, the sludge was filtered through a sieve of 0.25 mm pore size to remove the impurities. The cells were operated in batch mode at room temperature ($28 \pm 2°C$) and at dark environment.

MFC Operations

The performance of MFC was investigated by conducting a series of experiments. Several experiments were conducted to find out the characteristics of the collected sample wastewater. The results can be summed up as pH: 3.1, phosphate content: 6785 mg/L, sulphate content: 1105 mg/L, nitrate: 15 mg/L, glucose: 7.2 g/L, TSS: 453 mg/L and TDS: 22mg/L. Then the experiment was conducted to explore the effect of sludge loading in MFC on electricity generation. To do so, MFCs were operated with 1 g, 3 g, 6 g and 9 g of sludge and one without sludge in the anode chamber. The changes of pH and voltage with time were noted. The subsequent experiments were conducted to scrutinize the effect of operating pH. In these experiments, we increased the anode pH by using NaOH. Three cells containing different influents pH of 7, 8 and 9 were operated simultaneously. For each cell, 9 g of sludge was used to inoculate the anode chamber containing 350 ml of waste water, while 200 ppm $KMnO_4$ was used in the cathode at room temperature. As like the earlier experiments, electricity generation and voltage generation both in closed and open circuits were monitored. Polarization and power density curves were used to obtain the maximum power density by varying the external resistance using a resistor box. Voltage vs. current density and power density vs. current density data, % COD removal, and effect of buffering were recorded at specified conditions which are demonstrated in the result and discussion section. Every experiment was conducted at least in duplicate at constant room temperature ($28 \pm 2°C$) and the average value was reported for all the data.

Analytics and Calculations

A digital multimeter (FL-9205A, SHEN-HENXL Electronic Co. Ltd, China) was continuously operated to record the cell voltage and current, with a fixed resistance. Relation between the power and voltage, $P=IV$ (where, I and V represents current (A) and voltage (V), respectively), was used to calculate the cell power. Obtained power and current were divided by the anodic surface area (m^2) to observe the power and current. During the experiments, pH and chemical oxygen demand (COD) of the anode chamber were continuously monitored by using the standard procedures [21].

Results and Discussion

Characterization of the Food Industry Wastewater

Several methods were conducted to find out the characteristics of the collected sample wastewater of the well-known food processing industry in Bangladesh. The results can be summed up as pH: 3.1, phosphate content: 6785 mg/L, Sulphate content: 1105 mg/L Nitrate: 15 mg/L, SS:356 mg/L, TS: 436 mg/L and DS: 70 mg/L. During the operation of MFCs, wastewater was undergoing some experiments to find out the characteristics of treated water. Following table listed some of the important determined results.

Table 1. Characterization of food processing wastewater

Parameter	Initial, mg/L	Final, mg/L
Suspended Solids (SS)	356	8
Dissolved Solids (DS)	70	61
Total Solids (TS)	436	69
% COD Removal	77.71%	

Effect of Sludge Loading in MFC

Effects of sludge loading in dual chamber MFC were analyzed by operating two cells having fixed amount of wastewater sample in each anode chamber. First cell was inoculated with 1g of sludge and the other was operated without the sludge. $KMnO_4$ was used as the oxidant in these cells and its concentration was kept constant at 200 mg/L. This experiment was conducted in the closed circuit and the cells were connected with an external resistance of 1 kΩ. From figures 2 and 3, it was clear that, MFC with sludge in the anode chamber has a great effect on current generation. Without sludge, the generation of current shows a decreasing trend.
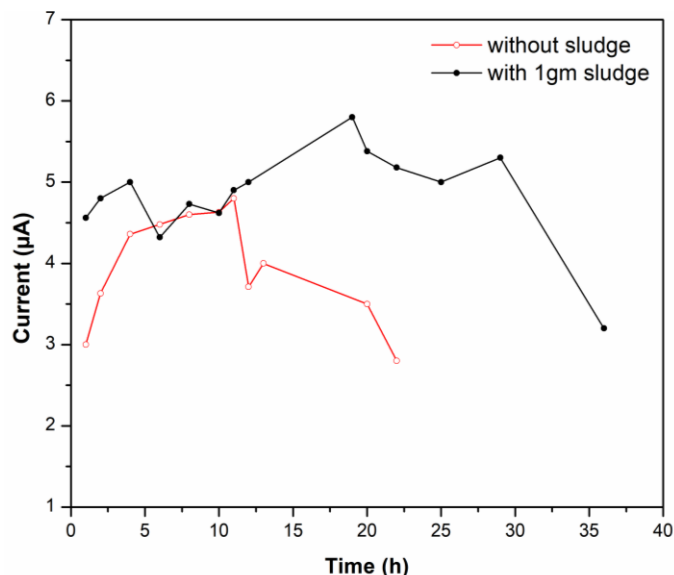
Figure 1. Comparison between MFCs running with sludge and without sludge

The graph (Figure 1) illustrates that, the cell using sludge at the anode chamber showed better current production and reached a peak value of 5.8 µA at 19th hour of operation. The current production in both cells increased initially and reached the decline phase after a bit unsteady performance. Sludge loading favors complex reactions, like hydrolysis, acidogenesis, electro-genesis and causes higher electricity generation undergone by micro-organisms [22]. Initial feed pH could be a cause of poor performance as unfavorable condition retards bacterial growth. As incorporation of sludge gives better performance, three more MFCs were operated with 3 g, 6 g and 9 g of sludge in the anode chambers, respectively (Figure 2). The experimental result reveals that increasing sludge loading at the anode chamber increases electricity generation. The cell operated by 9 g sludge provides better electricity production than the others and the cell operated without the sludge gives the least production of electricity.
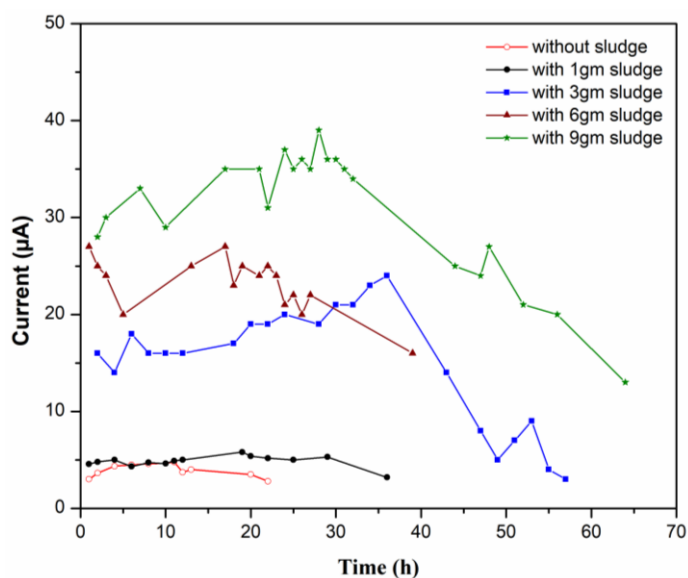
Figure 2. Effect of variable sludge loading in electricity generation

Initial electricity generations were 28, 27, 20, 4, 3 µA in 9, 6, 3, 1, 0 g sludge containing cells, respectively. Increment of sludge loading causes increment of bacterial population, which favors electricity generation. This supports the result found by Behera *et al.* [22].

Effect of Operating pH

Food processing industry wastewater is acidic in nature and neutralization of the wastewater is necessary for biological treatment. Higher acidity or alkalinity of wastewater affects both wastewater treatment efficiency and the environment inside the reactor [23]. The pH of wastewater needs to be maintained near neutral to protect microorganisms to favor biological treatment processes. For acidic or alkaline industrial wastewaters, the pH is corrected to near neutral by addition of suitable alkali or acid before biological treatment. The capacity of the anaerobic reactors to handle the loading rates depends on the feed pH and the alkalinity generating capability of the wastewater to counteract the changes in pH. Therefore, in this study, the performance of MFC was evaluated under different anodic pH values.
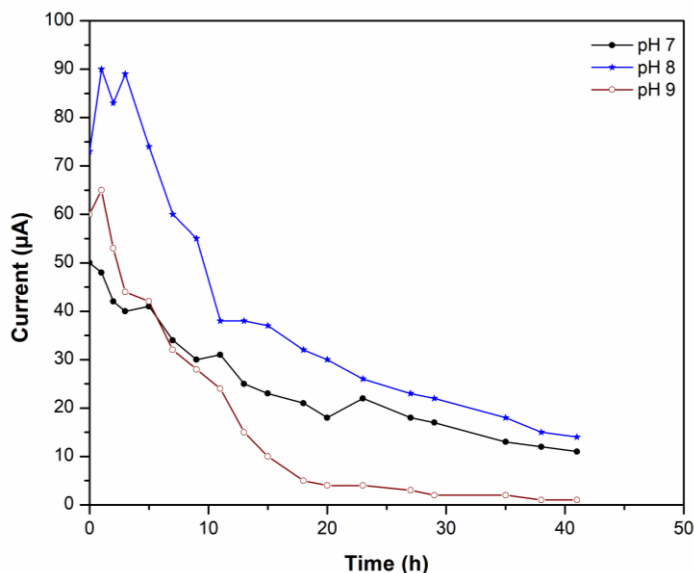
Figure 3. Effect of feed pH in electricity generation

From Figure 3, the experimental results clearly demonstrate that the MFC performance is dependent on the anodic pH. The possible reason for higher current generation at pH 8.0 might be attributed to the effective extracellular electron transfer at this pH microenvironment, where electrogenic bacterial growth was favored [24, 25]. As the feed pH was not constant in none of anode chamber, electricity also decreased sharply over time.

Polarization and Power Curve

The polarization curve characterizes the cell voltage as a function of current. In the microbial fuel cell, the current generation was depended on the size of the electrical load. In this regard, the polarization curve was used to explain the electrochemical efficiency with respect to the operating current.

Polarization and Power Curve for Variable Sludge Loading

From Figure 4, it is observed that, when the current density of the cells increased, the cell potential decreased. It can be also seen that, potential energy increased when a higher amount of sludge was loaded. It can be explained as, because of the enhanced microbial population prevails in the presence of larger amount of sludge in the anode chamber. The maximum potential was recorded as 308 mV from the cell containing 9 g of sludge. Power densities were also measured at variable external resistances. Current generation in different resistors was observed once the maximum voltage was attained, the maximum power density was recorded as 0.97 mW/m^2 at the current density of 5.6 mA/m^2 for the cell containing 9 g sludge in the anode chamber.
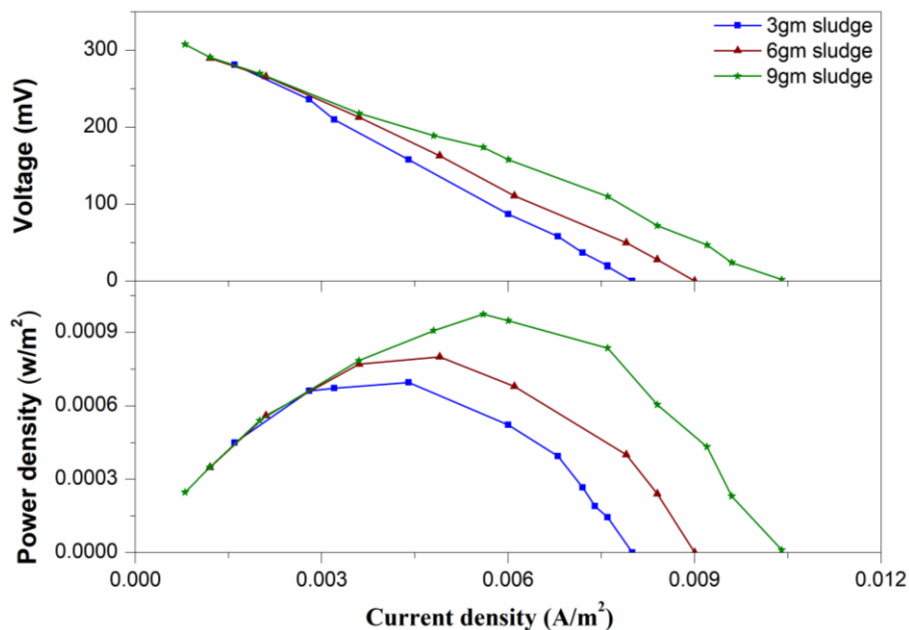
Figure 4. Power density curve and voltage behavior versus current density for three MFCs using variable sludge loading

At first, the power densities showed an incremental trend with increasing external resistance. After that, the power density started to decrease slowly with increasing resistance and current density. This typical fuel cell behavior was also reported by the researchers [26]. When a higher resistance was used, relatively less power density was observed. Relatively less voltage drop was observed at lower resistance indicating less potential drop. Voltage stabilization was comparatively rapid at higher resistances studied. Effective electron discharge observed at lower resistances might be the probable reason for further potential drop and slow stabilization of the voltage at lower resistances. Oxidation of substrates by microbes was more at lower resistance than at higher resistance, where microbes donated electrons to the anode as the electrons were discharged in a closed circuit compared the current generation potentiality of different substrate and source inoculums [2]. The power produced reported in our study is relatively moderate comparing to other researchers working with same substrate. Relatively lower power observed in this study might be due to the use of graphite electrode without any coating.

Polarization & Power Curve for different feed pH
        Current density and voltage generation with respect to the power density were observed at feed pH 8 compared to others. The potential favor on biofilm generation at optimum pH is likely to be the reason [22]. The cell potential decreased with the increment of current density.
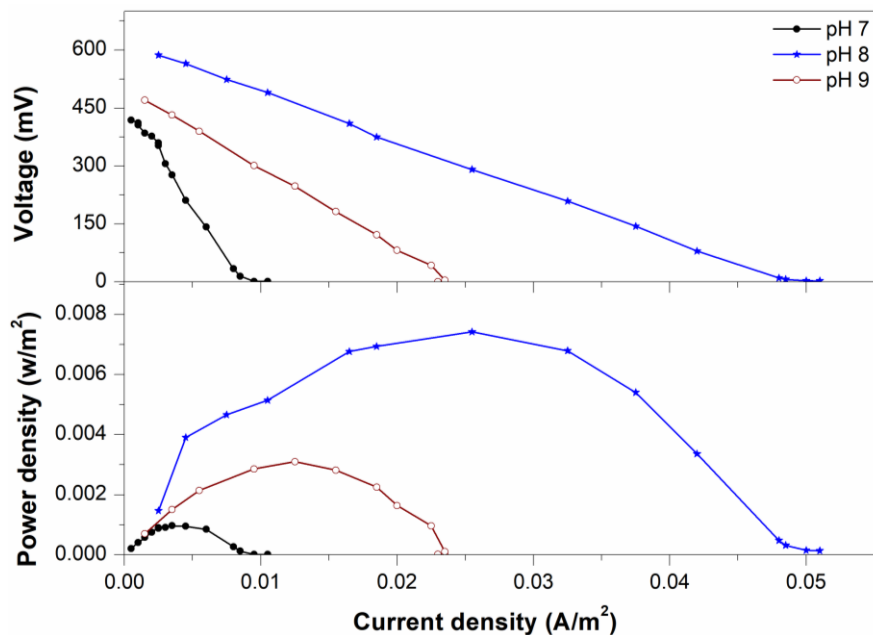
Figure 5. Power density curve and voltage behavior versus current density for three MFCs using different feed pH.

        It can be seen (Figure 6) that the maximum value of 587 mV was achieved at current density 25 mA/m^2 for feed pH 8. The utmost power density of 7.4 mW/m^2 was achieved with current density of 25 mA/m^2 at feed pH 8.

Removal of COD in Anode Chamber
        It has been reported that microorganisms can convert organic matters into electricity using MFCs while simultaneously accomplishing wastewater treatment [27]. Figure 6 shows the COD removal ratio of three MFCs containing 3, 6 and 9 g of sludge. In 64 hours of operation, the cells showed a COD removal efficiency of 30.73%, 44.56% and 55.13% for the cells containing 3, 6 and 9 g of sludge in the anode chambers, respectively.
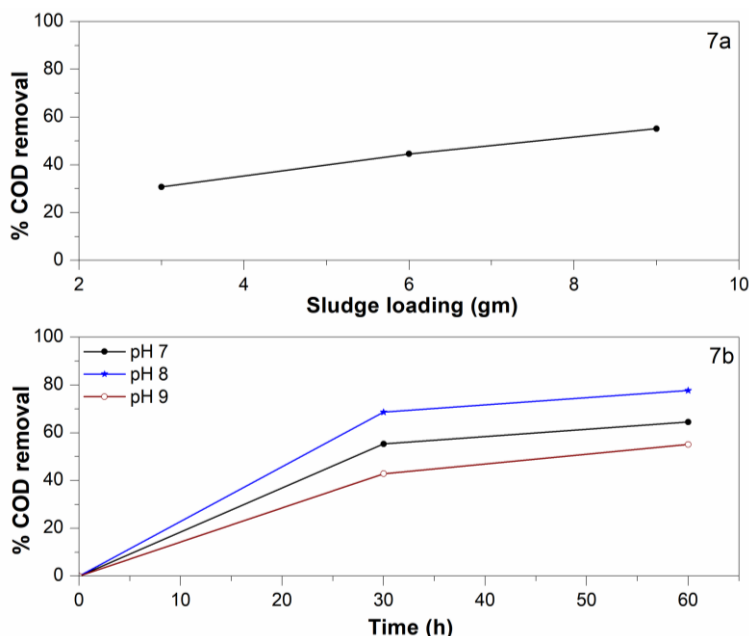
Figure 6. Percentage of COD removal of three MFCs having a) different sludge loading and b) feed pH

The cells showed a COD removal efficiency of 64.51%, 77.71% and 55.54% for the cells containing having feed pH 7, 8 and 9 in the anode chambers over 52 hours of operation, respectively. So, the removal of COD is found to be higher for the cell which showed higher current production especially at the optimum pH. This result is expected, because higher current production means higher utilization of the organic substrate in the anode chamber.

Conclusion

Dual chamber microbial fuel cell was fabricated and constructed with local available materials. Food processing industry wastewater was used as the substrate. Effect of sludge loading was investigated and found that, current generation of an MFC increased for a given concentration substrate with the increment of sludge. The effect of anode feed pH was explored. At the optimum pH, a higher current was produced. Polarization and power curves were plotted for particular sets of MFCs. Due to the ohmic and external resistances, sharp drop in the voltage was observed with the increase of the current density. The removal of COD was found to be higher for the cell showing higher current density at optimum pH. Though the power output was relatively low, 7.42 mW/m^2, it will be sufficient to run low-energy lighting or to recharge batteries for a host of devices such as cell phones. Therefore, it is necessary to expand this research work database by giving special attention to the digital data acquisition system, new types of electrode and membrane materials and scaling up of MFCs. So, the application of MFCs in Bangladesh can be effective to produce green electricity generation as well as the reuse of organic wastes to maintain the healthy and pollution free environment.

CONFLICTS OF INTEREST

The authors declare that there is no conflict of interests regarding the publication of this paper.

REFERENCES

[1]   K Hossain, A., and Badr, O. (2007). Prospects of renewable energy utilisation for electricity generation in Bangladesh. *Renewable and Sustainable Energy Reviews*, 11(8), 1617-1649.

[2]   Pant, D., Bogaert, G. V., Diels, L., and Vanbroekhoven, K. (2010). A review for the substrate used in microbial fuel cell (MFCs) for sustainable energy production. *Bioresource Technology*, 101(6), 1533-1543.

[3]   Logan, B. E., and Regan, J. M. (2006). Microbial fuel cells: Challenges and applications. *Environ. Sci. Technol.*, 41, 5172-5180.

[4]   Papaharalabos, G., Greenman, J., Melhuish, C., and Ieropoulos, I. (2015). A novel small scale Microbial Fuel Cell design for increased electricity generation and waste water treatment. *International Journal of Hydrogen Energy*, 40(11), 4263-4268.

[5]   Latif, M. A., Rahman, M. H., and Ehasan, M. A. (2015). Agro-industrial development and sustainability in Bangladesh-A study. *Int. J. Agril. Res. Innov. & Tech.*, 5(2), 37-43.

[6]   (2018).*https://en.wikipedia.org/wiki/Food_industry_in_Bangladesh*. [19/06/2018]

[7]   Hussain, S. S., and Leishman, D. (2013). Gain Report on Food Processing Industries in Bangladesh. pp: 2-3.

[8]   Khan, M. R., Amin, M. S. A., Rahman, M. T., Akbar, F., and Ferdaus, K. (2013). Factors affecting the performance of double chamber microbial fuel cell for simultaneous wastewater treatment and power generation. *Polish Journal of Chemical Technology*, 15(1), 7-11.

[9]   Agency, E. E. (2001). Indicator: Biochemical oxygen demand in rivers European Environment Agency, Copenhagen, Denmark.

[10]   Brião, V. B., and Tavares, C. R. G. (2007). Effluent generation by the dairy industry: preventive attitudes and opportunities. *Brazilian Journal of Chemical Engineering*, 24, 487-497.

[11]   Ravinder, K., Lakhveer, S., W., Z. A., and I., H. F. (2018). Microbial fuel cell is emerging as a versatile technology: a review on its possible applications, challenges and strategies to improve the performances. *International Journal of Energy Research*, 42(2), 369-394.

[12]   Cecconet, D., Molognoni, D., Callegari, A., and Capodaglio, A. G. (2018). Agro-food industry wastewater treatment with microbial fuel cells: Energetic recovery issues. *International Journal of Hydrogen Energy*, 43(1), 500-511.

[13]   Luo, H., Xu, G., Lu, Y., Liu, G., Zhang, R., Li, X., Zheng, X., and Yu, M. (2017). Electricity generation in a microbial fuel cell using yogurt wastewater under alkaline conditions. *RSC Advances*, 7(52), 32826-32832.

[14]   Logan, B. E., and Rittmaan, B. E. (2008). Opportunities for Renewable Bioenergy Using Microorganisms. *Biotechnology and Bioengineering*, 100(2), 203-212.

[15]   Oh, S. E., and Logan, B. E. (2005). Hydrogen and electricity production from a food processing wastewater using fermentation and microbial fuel cell technologies. *Water Res.*, 39, 4673-4682.

[16]   Du, Z., Li, H., and Gu, T. (2007). A state of the art review on microbial fuel cells: A promising technology for wastewater treatment and bioenergy. *Biotechnology Advances*, 25(5), 464-482.

[17]   Amin, M. S. A., Haque, T., Tarannum, R., and Khan, M. R. (2014). Wastewater treatment and electricity generation by membrane less microbial fuel *Int. J. Environmental Engineering*, 6(3), 314-323.

[18]   Mohan, S. V., Saravanan, R., Veer, S. R., Mohanakrishna, G., and Sarma, P. N. (2006). Bioelectricity production from wastewater treatment in dual chambered microbial fuel cell (MFC) using selectively enriched mixed microflora: Effect of catholyte. *Bioresour. Technol.*, 99(3), 596-600.

[19]   You, S., Zhao, Q., Zhang, J., Jiang, J., and Zhao, S. (2006). A microbial fuel cell using permanganate as the cathodic electron acceptor. *J. Power Sour.*, 162, 1409-1415.

[20]   Trinh, N. T., Park, J. H., and Kim, S. S. (2010). Generation behavior of electricity in a microbial fuel cell. *Korean J. Chem. Eng.*, 27(2), 546-550.

[21]   APHA (1998). Standard methods for the examination of water and wastewater. American Public Health Association, Washington DC, USA.

[22]   Behera, M., and Ghangrekar, M. M. (2009). Performance of microbial fuel cell in response to change in sludge loading rate at different anodic feed pH. *Bioresource Technology*, 100(21), 5114-5121.

[23]   He, Z., Huang, Y., Manohar, A. K., and Mansfeld, F. (2008). Effect of electrolyte pH on the rate of the anodic and cathodic reactions in an air-cathode microbial fuel cell. *Bioelectrochemistry,* 74, 78-82.

[24]   Jiang, J., Zhao, Q., Zhang, J., Zhang, G., and Lee, D.-J. (2009). Electricity generation from bio-treatment of sewage sludge with microbial fuel cell. *Bioresource Technology*, 100(23), 5808-5812.

[25]   Gil, G.-C., Chang, I.-S., Kim, B. H., Kim, M., Jang, J.-K., Park, H. S., and Kim, H. J. (2003). Operational parameters affecting the performannce of a mediator-less microbial fuel cell. *Biosensors and Bioelectronics*, 18(4), 327-334.

[26]   Venkata Mohan, S., Saravanan, R., Raghavulu, S. V., Mohanakrishna, G., and Sarma, P. N. (2008). Bioelectricity production from wastewater treatment in dual chambered microbial fuel cell (MFC) using selectively enriched mixed microflora: Effect of catholyte. *Bioresource Technology*, 99(3), 596-603.

[27]   Liu, H., Cheng, S., and Logan, B. E. (2005). Production of Electricity from Acetate or Butyrate Using a Single-Chamber Microbial Fuel Cell. *Environmental Science & Technology*, 39(2), 658-662.

Detection of Energy Theft in Overhead Low-Voltage Power Grids – The Hook Style Energy Theft in the Smart Grid Era

Athanasios G. Lazaropoulos[*]

School of Electrical and Computer Engineering / National Technical University of Athens / 9 Iroon Polytechniou Street / Zografou, GR 15780

This paper investigates the possibility of detecting the hook style energy theft in the overhead low-voltage (OV LV) power grids when the smart grid conveniences are available. On the basis of the broadband over power lines (BPL) technology and the proposed method of the detection of the hook style energy theft (HS-DET method), a plethora of different scenarios concerning the hook style energy theft is considered so that the performance of HS-DET method can be assessed. The impact of OV LV BPL topologies, hook characteristics and measurement differences on the performance of HS-DET method is mainly assessed through appropriate metrics, such as derivative metrics of percent error sum (PES). Finally, appropriate contour plots against the hook style energy theft are proposed revealing the efficiency of HS-DET method against any relevant threat in any conditions.

1. Introduction

Energy theft defines a well-known problem either in traditional power systems or in the emerging smart grid [1]-[7]. In fact, a World Bank report indicates that up to 50% of electricity in developing countries is acquired via energy theft [8] while, in financial terms, utility companies have announced losses that reach up to $6 billion, $5 billion and $4.5 billion in United States, Brazil and India, respectively [9]-[11]. To cope with the energy theft, a plethora of detection schemes have been proposed in the literature, on behalf of the states and power utility companies, that exploit smart meters, wireless sensors and radio-frequency identification tags in order to provide a high detection accuracy. However, the main disadvantage of these detection schemes is the required extra investment cost that includes the device cost, the system implementation cost, the software cost and the operating/training cost [3], [12]-[15]. Also, compared to the traditional power grid, which can only be physically tampered, the smart grid is vulnerable to more types of attacks (*e.g.,* network attacks) [4].

On the basis of suitable broadband applications, such as this one that is presented in this paper, the interoperability of the smart grid with the broadband over power lines

(BPL) systems can offer significant help towards the combat against the energy theft and finally restore the financial losses of the power utility companies due to this issue. Here, it should be highlighted that among the available communications technologies that can interoperate under the aegis of the smart grid, the BPL technology can play the crucial role during the detection of the energy theft since the BPL technology exploits the already installed power grid infrastructure [16]-[18].

In this paper, the detection of the hook style energy theft of the overhead low-voltage (OV LV) power grids, which is a common type of energy theft in developing countries, is here analyzed on the basis of the installed BPL networks and the hybrid model [19]-[36]. Until now, hybrid model has extensively been employed to examine the behavior of various multiconductor transmission line (MTL) configurations in transmission and distribution BPL networks and, of course, in OV LV BPL networks such those that are examined in this paper. Actually, the hybrid model consists of two interconnected modules, namely: (i) the bottom-up approach module that is based on an appropriate combination of MTL theory and similarity transformations; and (ii) the top-down approach module that is based on the concatenation of multidimensional transmission matrices of the cascaded network BPL connections. On the basis of broadband performance metrics supported by the hybrid method such as channel attenuation, spectral efficiency and capacity, a number of BPL broadband applications, such as Topology Identification Methodology (TIM) [37], Fault and Instability Identification Methodology (FIIM) [38], methodology to preserve power system stability [39], [40] and main line fault localization methodology (MLFLM) [41]-[43], have already been demonstrated. In this paper, the hook style energy theft detection method (HS-DET method) is proposed and aims at coping with the detection of hook style energy theft in OV LV BPL networks.

The proposed HS-DET method is investigated either in theoretical or in real operation conditions of OV LV BPL networks. Already been mentioned in [37]-[39], [41]-[44], measurement differences between the real results collected by in-situ measurements and the theoretical results derived from the hybrid model occur during the channel attenuation determination that further affect the computation of the broadband performance metrics. In accordance with [37]-[39], [42], [45], [46], to deal with the measurement differences, the measurement differences can comfortably be handled as error distributions such as continuous uniform distributions (CUDs). Anyway, HS-DET method adopts the metric of percent error sum (PES), which has extensively applied in the aforementioned BPL broadband applications, as its main performance metric in order to assess the power grid integrity and allow the detection of energy theft.

The rest of this paper is organized as follows: In Section 2, a brief synopsis of MTL configurations of OV LV power grids, indicative OV LV BPL topologies, signal transmission and signal coupling is given. Section 3 deals with the measurement differences as well as PES and HS-DET method. In Section 4, numerical results and discussion are provided, aiming at practically evaluating the possibility of detecting a hook style energy theft and assess the detection performance of HS-DET method when measurement differences occur and hook style energy theft exists. Section 5 concludes this paper.

2. OV LV BPL Network Synopsis

2.1 OV LV MTL Configuration

A typical case of an OV LV distribution line is depicted in Fig. 1. Overhead distribution lines hang above the ground. OV LV distribution lines consist of three parallel non-insulated phase conductors of radius r_p^{OVLV} while the lowest phase conductor is hung at height h^{OVLV} above the ground. Above the three phase conductors, there is a neutral conductor of radius r_n^{OVLV}. The vertical spacing of the four conductors is equal to Δ^{OVLV}. More details regarding the material properties and dimensions of OV LV MTL configurations are given in [19].

As the ground properties are concerned, the ground is considered as the reference conductor while its conductivity and relative permittivity are assumed to be equal to σ_g=5mS/m and ε_{rg}=13, respectively [19], [21], [22], [25], [27]-[29]. The consideration of an imperfect ground defines a realistic scenario whose impact on high frequency signal propagation and transmission through OV LV power lines is detailed in [19]-[25], [27]-[29], [47]-[52].
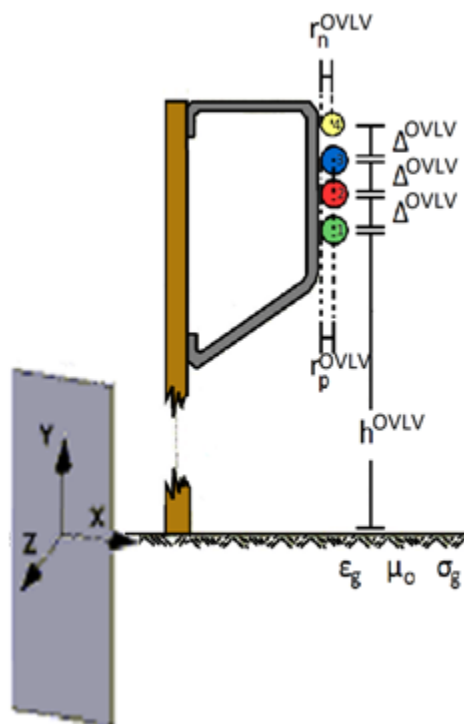
Fig. 1. Typical OV LV MTL configurations [19].

2.2 Indicative OV LV BPL Topologies and Hook Insertion Impact

In accordance with [1], [37]-[43], [53], BPL networks constitute a feedback loop control system that relies on measurement data that are collected by BPL units, meters and sensors, which are deployed across the power lines as well as their surrounding environment. In fact, BPL networks are divided into cascaded BPL connections, which can be treated separately. Each BPL connection is bounded by the transmitting end and

receiving end repeaters that allow the amplification and regeneration of the attenuated BPL signals. Between the transmitting and receiving end of a BPL connection, the number of branches as well as the topological characteristics may vary depending on the type of the supported power grid. On the basis of its topological characteristics, each BPL connection can be treated as a different OV LV BPL topology. In Fig. 2(a), a typical BPL topology with N branches is shown. With respect to Fig. 2(a), one of the main inputs of the hybrid model is the topological profile of the examined OV LV BPL topology. In Table 1, the topological characteristics of indicative OV LV BPL topologies are reported.
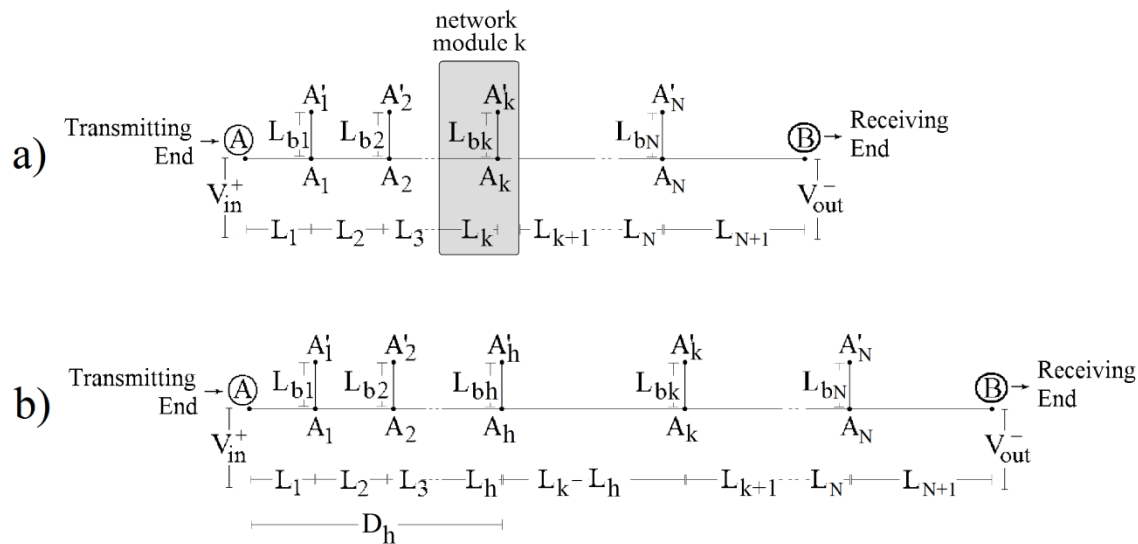
Fig. 2. (a) Original end-to-end OV LV BPL topology with N branches [19], [54], [55]. (b) Modified end-to-end OV LV BPL topology due to the hook insertion.

Table 1. Indicative OV LV BPL Topologies [46]

Topology Name	Topology Description	Number of Branches	Length of Distribution Lines	Length of Branching Lines
Urban case A	Typical OV urban topology	3	L_1=500m, L_2=200m, L_3=100m, L_4=200m	L_{b1}=8m, L_{b2}=13m, L_{b3}=10m
Urban case B	Aggravated OV urban topology	5	L_1=200m, L_2=50m, L_3=100m, L_4=200m, L_5=300m, L_6=150m	L_{b1}=12m, L_{b2}=5m, L_{b3}=28m, L_{b4}=41m, L_{b5}=17m
Suburban case	OV suburban topology	2	L_1=500m, L_2=400m, L_3=100m	L_{b1}=50m, L_{b2}=10m
Rural case	OV rural topology	1	L_1=600m, L_2=400m	L_{b1}=300m
"LOS" case	OV Line-of-Sight transmission	0	L_1=1000m	-

Since the HS-DET method in OV LV power grids is examined in this paper, a hook insertion modifies the examined indicative OV LV BPL topologies of Table 1 as indicated in Fig. 2(b). Let assume that a hook is hung at the position A_h that is located at distance $D_h = L_h + \sum_{i=1}^{k-1}(L_i)$ from the transmitting end. Hence, the distance between the hook and the kth branch is equal to $L_k - L_h$. The length of the hook, which is treated as a branch from the hybrid model, is assumed to be equal to L_{bh}. From Fig. 2(b), it is evident that each examined indicative OV LV BPL topology is modified depending on the hook location and the hook length.

Apart from the topological characteristics of Table 1, a set of assumptions concerning the transmission and propagation of the BPL signal as well as the circuital characteristics of the OV LV MTL configurations have been detailed in [19]-[27], [29], [31], [56]-[60]. Except for the aforementioned assumptions, the hook termination is assumed to be open circuit while the hook interconnection with the distribution lines is assumed to be complete (*i.e.,* hook derivation points at the same distance from the transmitting end on all the three phases) and horizontal. Therefore, the hook can be treated by the hybrid model as a branch. The previous assumptions are made in order to simplify the following analysis.

2.3 BPL Signal Transmission and Coupling

Hybrid method that deals with the BPL signal propagation and transmission across MTL configurations of OV LV BPL networks gives as output the $n^G \times n^G$ channel transfer function matrix $\mathbf{H}\{\cdot\}$ that relates line voltages $\mathbf{V}(z) = [V_1(z) \quad \cdots \quad V_{n^G}(z)]^T$ at the transmitting (z=0) and the receiving (z=L) ends where n^G is the number of the conductors of the examined MTL configuration and $[\cdot]^T$ denotes the transpose of a matrix. Then, according to how signals are injected onto and extracted from the lines of OV LV BPL networks, different coupling schemes may occur [19], [22], [25], [27]-[29], [54], [55]. In [54], [55], CS2 module has been introduced and is adopted in this paper. In accordance with [54], [55] where a number of restrictions is detailed, the coupling scheme channel transfer function of a coupling scheme module that relates output BPL signal V^{out-} and input BPL signal V^{in+} is given by

$$H^c\{\cdot\} = \frac{[V^{out-}]^C}{[V^{in+}]^C} = [\mathbf{C}^{out}]^C \cdot \mathbf{H}\{\cdot\} \cdot [\mathbf{C}^{in}]^C \qquad (1)$$

where $\mathbf{C}^{in}$ is the input coupling vector, $\mathbf{C}^{out}$ is the output coupling vector and $[\cdot]^c$ denotes the applied coupling scheme. With reference to [54], [55] and eq. (1), three types of coupling schemes can be supported: (i) *Coupling Scheme Type 1: Wire-to-Ground (WtG) or Shield-to-Phase (StP) coupling schemes*; (ii) *Coupling Scheme Type 2: Wire-to-Wire (WtW) or Phase-to-Phase (PtP) coupling schemes*, and (iii) *Coupling Scheme Type 3*: MultiWire-to-MultiWire (MtM) or MultiPhase-to-MultiPhase (MtM) coupling schemes. Depending on the applied coupling scheme, $\mathbf{C}^{in}$ and $\mathbf{C}^{out}$ are properly defined and, then, the coupling scheme channel transfer function $H^c\{\cdot\}$ is straightforward computed. Apart from the applied coupling scheme, the coupling scheme channel transfer function depends on the frequency, the OV LV BPL topology, the physical properties of the cables and the geometry of the MTL configuration [19], [21], [46], [58], [61].

3. Measurement Differences, PES and HS-DET

3.1 Measurement Differences

Although the theoretical computation of the coupling scheme channel transfer function, as described in eq. (1), is a well-defined straightforward process and, at the same time, experimentally verified, a set of practical reasons and "real-life" conditions can create significant differences between experimental measurements and theoretical results. These differences are denoted as measurement differences while the causes of the measurement differences can be grouped into six categories [37], [41], [44]. In mathematical terms, the measured coupling scheme transfer function $\overline{H^C}\{\cdot\}$ for given coupling scheme can be determined by

$$\overline{H^C}(f_i) = H^C(f_i) + e(f_i), \ i=1,\ldots,u \qquad (2)$$

where f_i, $i=1,\ldots,u$ denotes the measurement frequency, $e(f_i)$ synopsizes the total measurement difference in dB due to the six categories and u is the number of subchannels in the examined frequency range. As it is usually done [41]-[44], the total measurement difference can be assumed to follow continuous uniform distribution (CUD) with minimum value $-a_{CUD}$ and maximum value a_{CUD}.

It is evident that the determination of the measured coupling scheme transfer function of original and modified end-to-end OV LV BPL topologies suffers from the same total measurement differences, and thus same CUD of measurement difference, for given MTL configuration, OV LV BPL topology and measurement equipment. With reference to eq. (2), $H_{or}^C\{\cdot\}$ and $H_{mod}^C\{\cdot\}$ are the original and modified theoretical coupling scheme channel transfer functions, respectively, while $\overline{H_{or}^C}\{\cdot\}$ and $\overline{H_{mod}^C}\{\cdot\}$ are the original and modified measured coupling scheme channel transfer functions, respectively.

3.2 PES

As already been mentioned, a number of BPL broadband applications, such as TIM [37], FIIM [38], power system stability methodology [39], [40] and MLFLM [41]-[43], have already been demonstrated while their theoretical core is the cooperation of the hybrid model with the performance metric of percent error sum (PES). In accordance with [40], [44], PES assessed the approximation accuracy when piecewise monotonic data approximation methods have been applied in BPL networks. In this paper, PES is going to be employed so as to assess the approximation accuracy of the original and modified coupling scheme transfer functions. Therefore, PES expresses as a percentage of the total sum of the relative differences between the examined coupling scheme transfer function and the theoretical coupling scheme transfer function for all the used frequencies. With reference to eq. (5) of [46] and Sec. 3.1 of this paper, four PES metrics can be computed, namely:

$$PES_{or} = 100\% \cdot \frac{\sum_{i=1}^{u}\left|H_{or}^C(f_i)-H_{or}^C(f_i)\right|}{\sum_{i=1}^{u}\left|H_{or}^C(f_i)\right|} = 0\% \qquad (3)$$

$$PES_{mod} = 100\% \cdot \frac{\sum_{i=1}^{u}\left|H_{mod}^C(f_i)-H_{or}^C(f_i)\right|}{\sum_{i=1}^{u}\left|H_{or}^C(f_i)\right|} \qquad (4)$$

$$\overline{PES_{or}} = 100\% \cdot \frac{\sum_{i=1}^{u}\left|\overline{H_{or}^C}(f_i)-H_{or}^C(f_i)\right|}{\sum_{i=1}^{u}\left|H_{or}^C(f_i)\right|} \qquad (5)$$

$$\overline{PES_{mod}} = 100\% \cdot \frac{\sum_{i=1}^{u}\left|\overline{H_{mod}^C}(f_i)-H_{or}^C(f_i)\right|}{\sum_{i=1}^{u}\left|H_{or}^C(f_i)\right|} \qquad (6)$$

where PES_{or}, PES_{mod}, $\overline{PES_{or}}$ and $\overline{PES_{mod}}$ assess the accuracy of the original theoretical coupling scheme channel transfer function, modified theoretical coupling scheme channel transfer function, original measured coupling scheme channel transfer function and modified measured coupling scheme channel transfer functions, respectively, in relation with the original theoretical coupling scheme channel transfer function.

3.3 HS-DET Method and ΔPES

With reference to eqs. (3)-(6), HS-DET method of the OV LV power grids can detect energy theft whether measurement differences occur or not through the respective PES submetrics:

$$\overline{\Delta PES} = \overline{PES_{mod}} - \overline{PES_{or}} \qquad (7)$$
$$\Delta PES = PES_{mod} - PES_{or} = PES_{mod} \qquad (8)$$

It is evident that when $\overline{\Delta PES}$ and ΔPES are greater than zero and all the other problematic cases of OV LV power grids are excluded (*e.g.,* faults and instabilities of [37], [38], [62], [41], [42], [43]), a possible energy theft may occur across the OV LV power grid. This assertion is the theoretical basis of HS-DET method while the performance assessment of HS-DET method with respect to the existence of measurement differences or not is examined in the following Section of the numerical results.

4. Numerical Results and Discussion

The numerical results of this Section focus on the ability of HS-DET method to successfully detect the potential energy theft. Then, the performance of HS-DET method is assessed when various OV LV BPL topologies and types of hooks (*i.e.,* different hook distances from the transmitting end and hook lengths) are assumed. Two main scenarios are examined, which are: (i) the absence of measurement differences; and (ii) the existence of different intensities of measurement differences.

4.1 HS-DET Method without Measurement Differences

The broadband performance, in terms of coupling scheme channel transfer function in the 3-88 MHz frequency band, is assessed by applying hybrid model and CS2 module when the indicative OV LV BPL topologies of Sec. 2.2 are considered. Also, one representative coupling scheme is considered in OV LV BPL topologies for the sake of simplicity; say, WtG[1] coupling scheme.

With reference to Fig. 2(b), let assume that a hook of length L_{bh} is inserted at distance D_h from the transmitting end. In Table 2, PES_{or}, PES_{mod} and ΔPES are reported when $L_{bh} = 5m$ and $D_h = 300m$ are assumed for the five indicative OV LV BPL topologies.

Table 2. PES Metrics of Indicative OV LV BPL Topologies when $L_{bh} = 5m$ and $D_h = 300m$

OV LV BPL Topology	PES_{or} (%)	PES_{mod} (%)	ΔPES (%)
Urban case A	0	34.19	34.19
Urban case B	0	28.17	28.17
Suburban case	0	49.43	49.43
Rural case	0	73.57	73.57
"LOS" case	0	247.19	247.19

From Table 2, as it was expected, PES_{or} is equal to zero while PES_{mod} assesses the asymmetry between the original and the modified OV LV BPL topology. In terms of ΔPES, the topology asymmetry after the hook insertion remains high when "LOS" LV BPL topology is examined since the almost stable behavior of coupling scheme transfer function of "LOS" case starts to obtain multipath characteristics, such as spectral notches, after the hook insertion. Conversely, low asymmetry through ΔPES is reported in OV LV BPL topology of urban case B. In this case, the already intense multipath environment with its high number and deep spectral notches is rearranged through the hook insertion. The shift and the depth change of spectral notches of the modified OV LV BPL topology in comparison with ones of the original urban case B does not create the significant increase of ΔPES already observed in the other OV LV BPL topologies, which is presented in Table 2. As for the other indicative OV LV BPL topologies, their ΔPES behavior remains almost the same when a hook insertion occurs. However, ΔPES remains above 10% in all the cases examined.

HS-DET method should detect any hook presence regardless of its characteristics, say; its distance from the transmitting end and its length. However, due to the multipath environment of OV LV BPL networks, the performance of HS-DET method depends on the aforementioned hook characteristics. To investigate the performance of HS-DET method, in Fig. 3(a), ΔPES is plotted versus the hook distance from the transmitting end and the hook length when the OV LV BPL topology of urban case A is assumed. In Figs. 3(b), 3(c), 3(d) and 3(e), same plots with Fig. 3(a) are given but for the case of the urban case B, suburban case, rural case and "LOS" case, respectively. Here, it should be noted that the hook distance from the transmitting end span and the hook length span are assumed to be equal to 50 m and 5 m, respectively, while the range of the hook distance from the transmitting end and the range of the hook length are from 1 m to 951 m and from 1 m to 46 m, respectively, for all the examined contour plots of this paper. The selection of the previous plot specifications has been done for the sake of plot clarity and the computational speed.

(a)

(b)

(c)

(d)

(e)
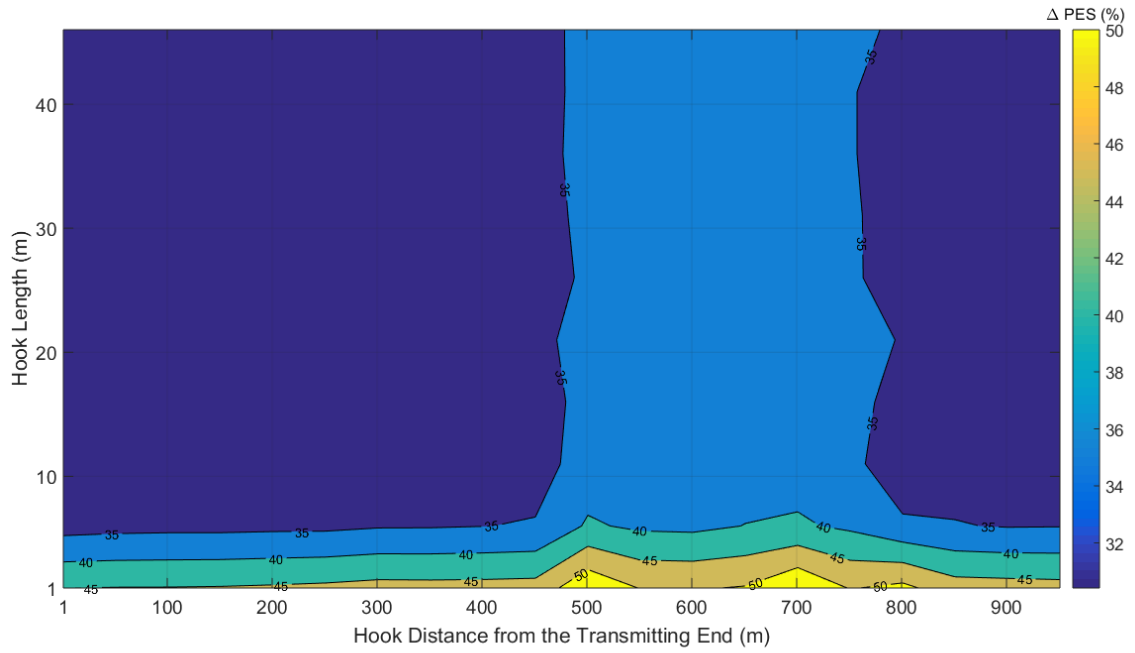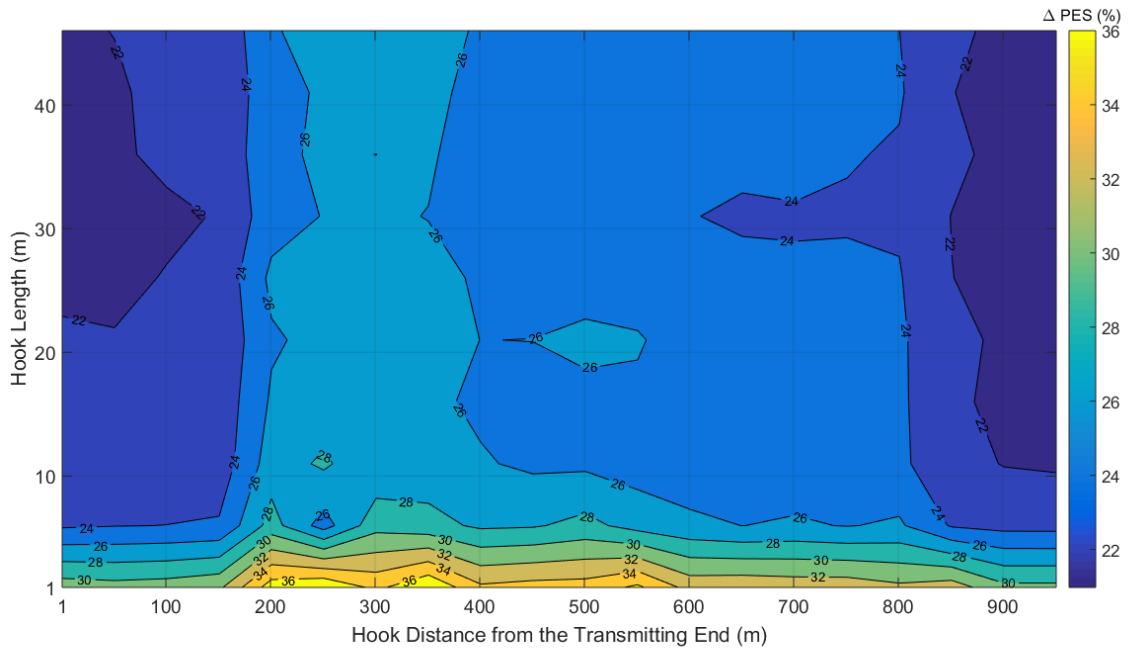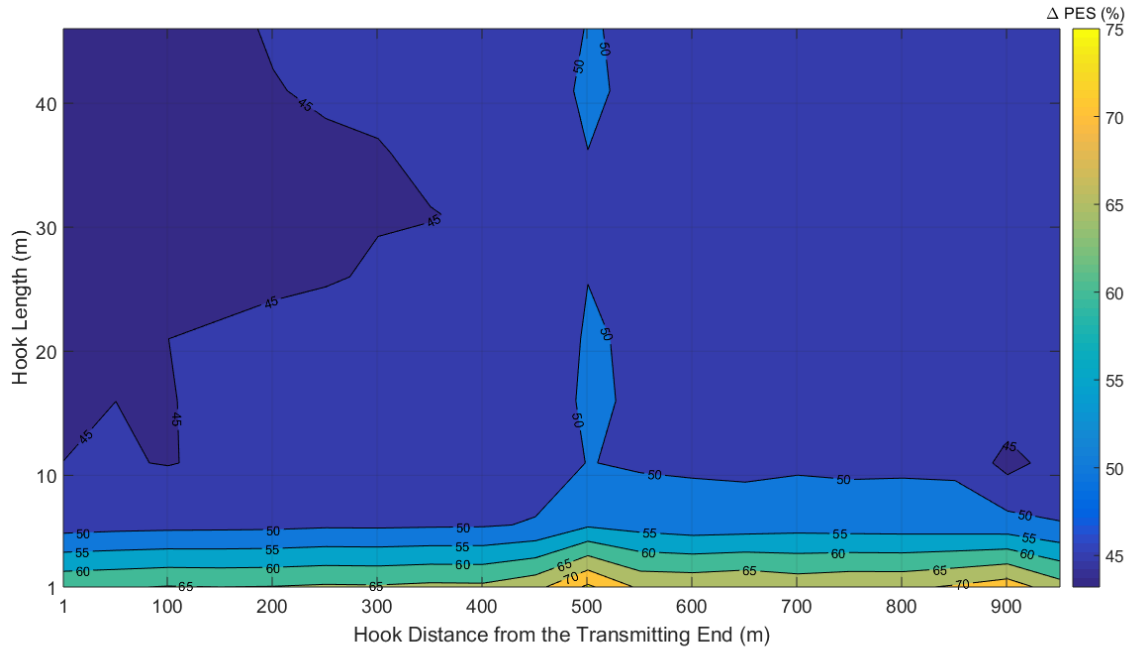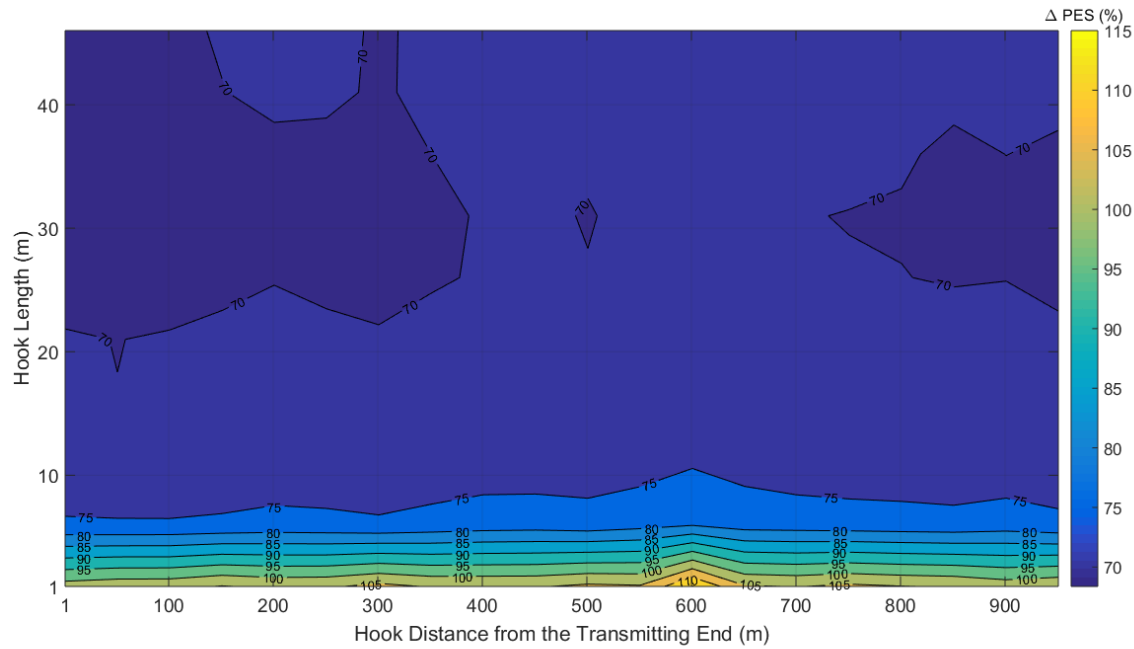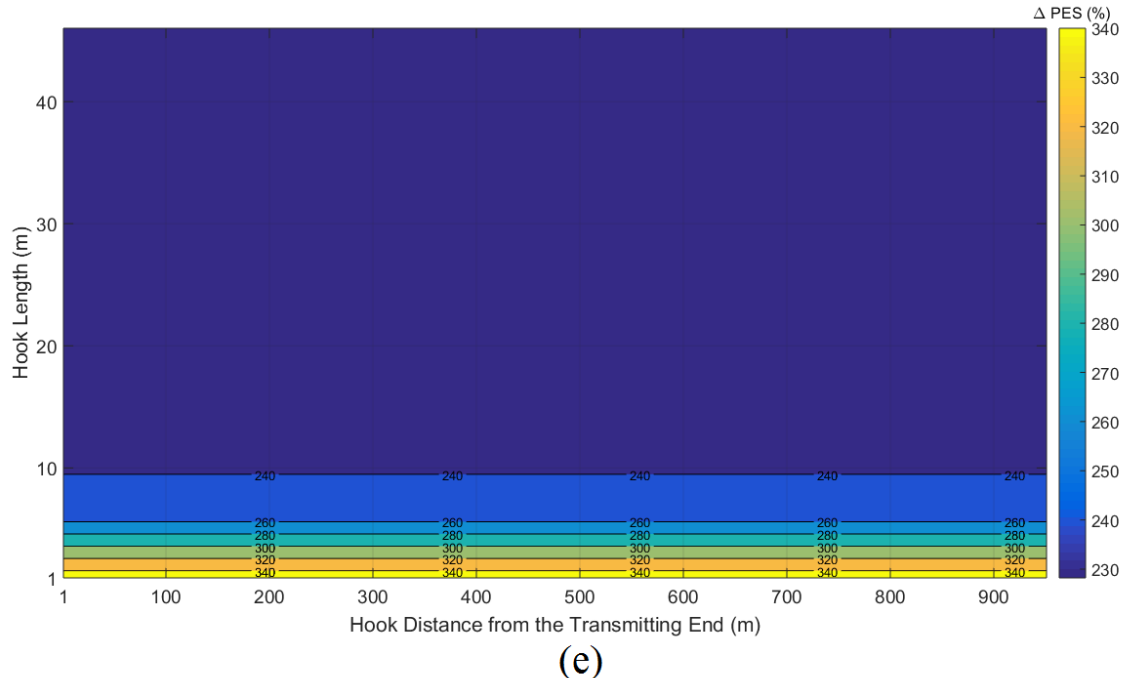
Fig. 3. ΔPES of the indicative OV LV BPL topologies in the 3-88 MHz frequency band for various hook distances from the transmitting end and hook lengths. (a) Urban case A. (b) Urban case B. (c) Suburban case. (d) Rural case. (e) "LOS" case.

Figs. 3(a)-(e) validate the early observations from the Table 2, say:

- The hook detection becomes easier in the cases of OV LV BPL topologies of low number of long branches. "LOS" and rural OV LV BPL topologies allow the safe hook detection as indicated by their high ΔPES values across the entire contour plot.

- The hook distance from the transmitting end influences the performance of HS-DET method only in the cases of OV LV BPL topologies with high number of branches. In these cases, the hook insertion that is treated as a branch from the hybrid model influences the multipath propagation of the original OV LV BPL topology. Depending on the hook length, the presence of the hook may change the channel transfer function and, thus, ΔPES of the modified OV LV BPL topology –see Figs. 3(a)-(c)–. In contrast, modified rural and "LOS" OV LV BPL topologies present little dependence on the hook distance from the transmitting end since the BPL signal distances of the multipath propagation due to the hook insertion remains almost the same for given modified rural and "LOS" OV LV BPL topologies –see Figs. 3(d) and (e)–.

- Regardless of the examined OV LV BPL topology, the performance of HS-DET method mainly depends on the hook length. The detection of the hook style energy theft becomes easier when the hook remains short enough (*i.e.,* shorter than 10 m). In all the cases examined, when the hook exceeds 10 m, the performance of HS-DET decreases. This is evident since longer branches create rare and shallow notches in channel transfer functions that little affect ΔPES. Anyway, in all the cases examined, ΔPES receives significant high values that permit the easy detection.

- In general, when modified OV LV BPL topologies with branches and long hooks are investigated, HS-DET method more easily detects the energy theft of hooks that are situated at the middle of the transmission path rather than near the transmitting and receiving ends. This is clear in contour plots of Figs. 3(a)-(d) through the presence of islands of darker colors near to the transmitting and receiving ends. As the number of branches increases and their length gets shorter, the presence of island of darker colors becomes more intense –see Fig. 3(b)–.

4.2 HS-DET with Measurement Differences

The performance of HS-DET has been investigated in Sec. 4.1 when measurement differences are ignored. Its performance primarily depends on the hook length as well as the examined OV LV BPL topology. The detection of hook style theft becomes easiest when short length hooks are deployed in "LOS" OV LV BPL topologies. It is evident that the existence of measurement differences will deteriorate the performance of HS-DET method. In this subsection, it is examined the degree of performance deterioration of HS-DET method in terms of ΔPES when various CUDs are assumed.

With reference to Fig. 2(b) and Table 2, let assume that the same hook of length L_{bh} is inserted at distance D_h from the transmitting end. In Table 3, $\overline{PES_{or}}$, $\overline{PES_{mod}}$ and $\overline{\Delta PES}$ are reported when $L_{bh} = 5m$ and $D_h = 300m$ are assumed for the five indicative OV LV BPL topologies and different maximum value a_{CUD} of CUD are assumed.

Table 3. PES Metrics of Indicative OV LV BPL Topologies when $L_{bh} = 5m$ and $D_h = 300m$ for different maximum values a_{CUD}

OV LV BPL Topology	$a_{CUD} = 1dB$			$a_{CUD} = 2dB$			$a_{CUD} = 3dB$			$a_{CUD} = 4dB$			$a_{CUD} = 5dB$		
	$\overline{PES_{or}}$ (%)	$\overline{PES_{mod}}$ (%)	$\overline{\Delta PES}$ (%)	$\overline{PES_{or}}$ (%)	$\overline{PES_{mod}}$ (%)	$\overline{\Delta PES}$ (%)	$\overline{PES_{or}}$ (%)	$\overline{PES_{mod}}$ (%)	$\overline{\Delta PES}$ (%)	$\overline{PES_{or}}$ (%)	$\overline{PES_{mod}}$ (%)	$\overline{\Delta PES}$ (%)	$\overline{PES_{or}}$ (%)	$\overline{PES_{mod}}$ (%)	$\overline{\Delta PES}$ (%)
Urban case A	3.94	34.70	30.76	7.84	36.00	28.16	11.39	37.39	26.00	15.14	39.65	24.50	18.95	42.11	23.15
Urban case B	2.60	28.75	26.15	5.19	29.09	23.90	7.61	30.18	22.56	10.18	31.49	21.31	12.73	32.42	19.69
Suburban case	5.83	50.53	44.70	11.58	52.55	40.97	16.70	54.53	37.83	21.98	57.58	35.61	26.97	60.87	33.90
Rural case	9.54	76.36	66.82	18.96	79.36	60.40	26.88	84.78	57.90	34.89	89.60	54.71	42.52	95.23	52.71
"LOS" case	33.57	257.46	223.89	63.36	269.79	206.44	83.95	282.23	198.28	106.31	302.28	195.97	125.20	316.22	191.02

From Table 3, $\overline{PES_{\text{or}}}$ takes values greater than zero when measurement differences are considered. Actually, as the maximum value a_{CUD} increases, so does $\overline{PES_{\text{or}}}$ for given original OV LV BPL topology. With reference to eq. (5), the increase of $\overline{PES_{\text{or}}}$ unveils the anomaly that is added during the computation of coupling transfer functions of the original indicative OV LV BPL topologies due to the existence of measurement differences. At the same time, as the maximum value a_{CUD} increases, so does $\overline{PES_{\text{mod}}}$ for given modified OV LV BPL topology. With reference to eq. (7), $\overline{\Delta PES}$ focuses on the elimination of the impact of the measurement differences through the computation of the difference of $\overline{PES_{\text{or}}}$ and $\overline{PES_{\text{mod}}}$. As it is shown in Table 3, despite the intention of $\overline{\Delta PES}$ to mitigate measurement differences, as the maximum value a_{CUD} increases, $\overline{\Delta PES}$ decreases for given OV LV BPL topology. Although the values of $\overline{\Delta PES}$ decreases remain positive and significantly above zero in all the cases examined, the negative correlation between $\overline{\Delta PES}$ and maximum value a_{CUD} indicates the difficulty in distinguishing energy theft during the application of HS-DET method when measurement differences occur. Anyway, the general behavior of ΔPES, which has been observed in Table 2, concerning its dependence on the examined OV LV BPL topology is also presented during the computation of $\overline{\Delta PES}$ for given maximum value a_{CUD}.

As already been mentioned in Sec. 4.1, HS-DET method should detect any hook style energy theft regardless of the examined OV LV BPL topology and the hook characteristics. Apart from the intrinsic difficulties of HS-DET method presented in Figs. 3(a)-(e), the performance of HS-DET method is here assessed when measurement differences of various maximum values a_{CUD} are considered. To investigate the sensitivity of HS-DET method performance against measurement differences, in Fig. 4(a), $\overline{\Delta PES}$ is plotted versus the hook distance from the transmitting end and the hook length when the OV LV BPL topology of urban case A is assumed and CUD of maximum value a_{CUD} equal to 1dB is considered. In Figs. 4(b)-(e), same plots with Fig. 4(a) are given but for the case of the maximum value a_{CUD} being equal to 2dB, 3dB, 4dB and 5dB, respectively. In Figs. 5(a)-(e), Figs. 6(a)-(e), Figs. 7(a)-(e) and Figs. 8(a)-(e), same contour plots with Figs. 4(a)-(e) are given but for the case of urban case B, suburban case, rural case and "LOS" case, respectively. Here, it should be noticed that the same assumptions concerning the hook distance from the transmitting end span, the hook length span, the range of the hook distance from the transmitting end and the range of the hook length remain the same with Sec. 4.1.

(a)

(b)

(c)

(d)

(e)
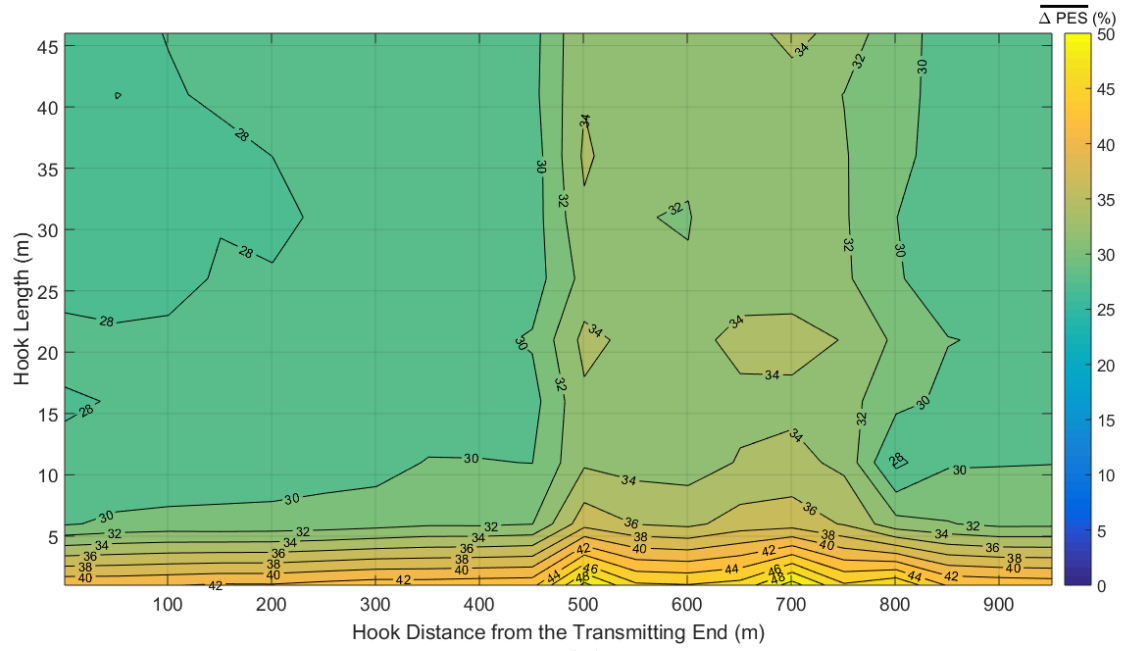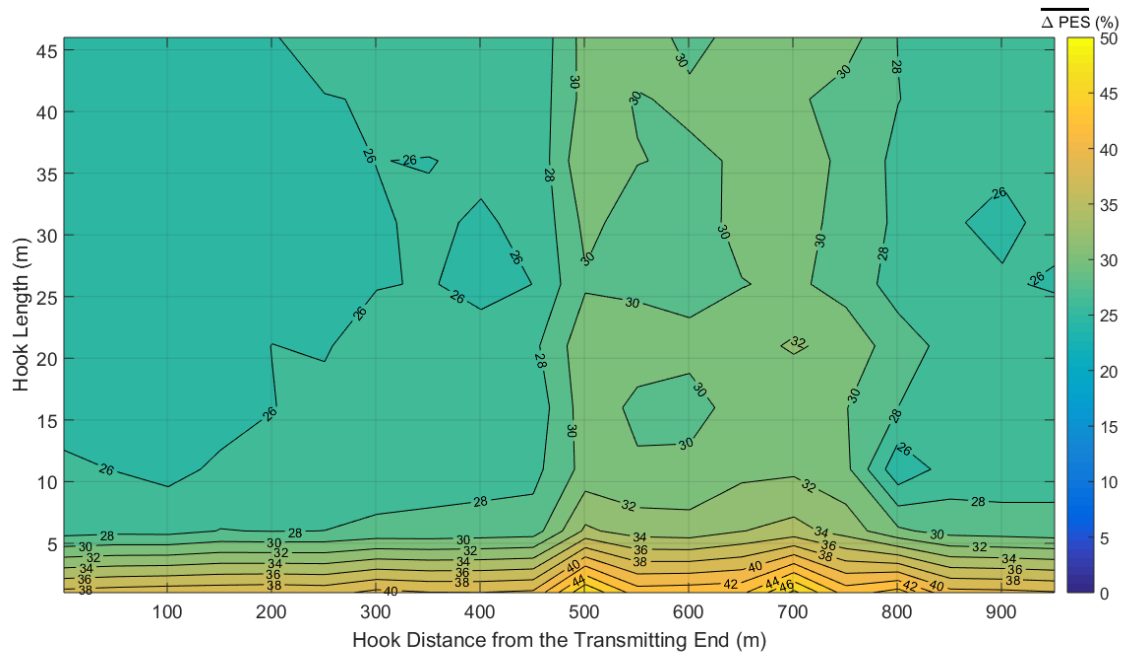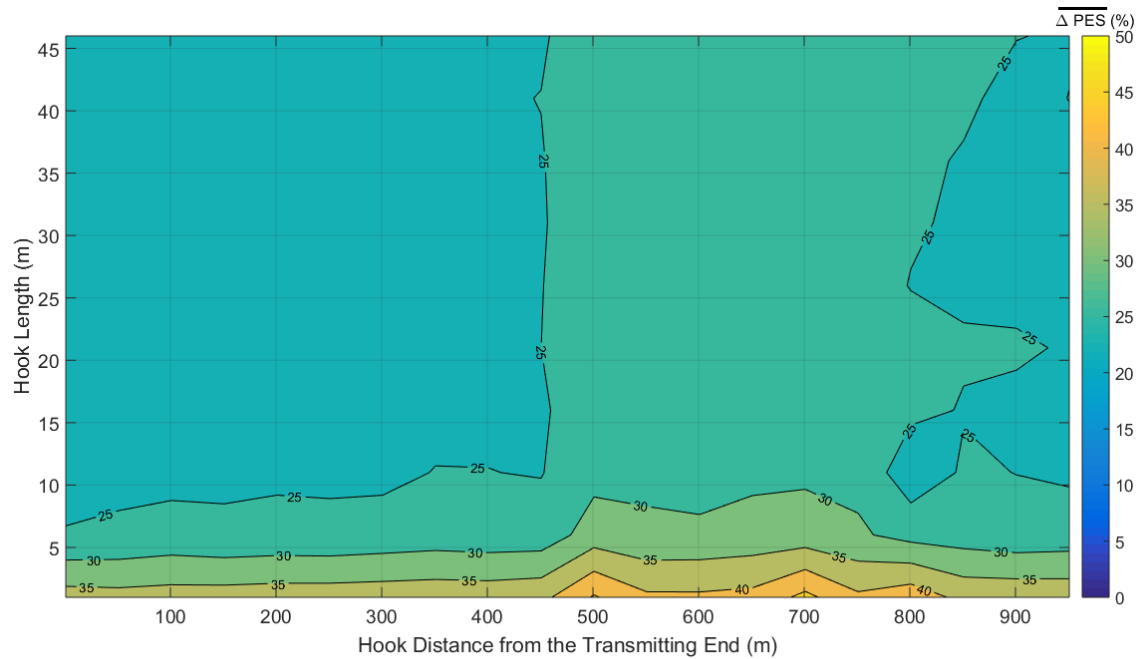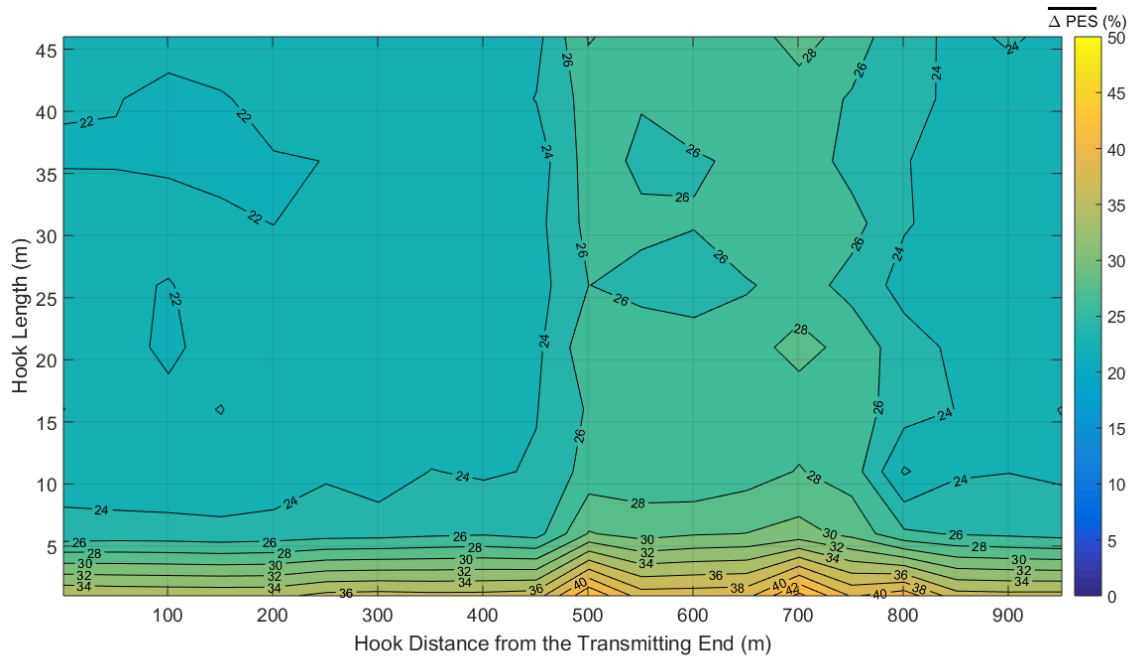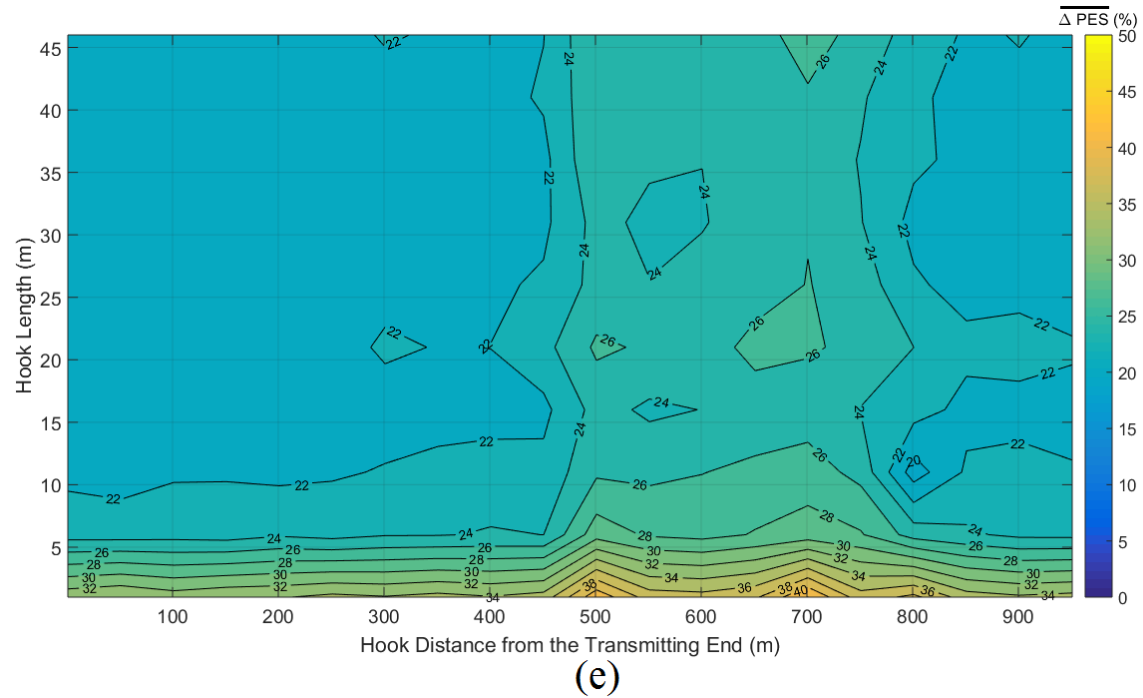
Fig. 4. $\overline{\Delta PES}$ of the urban case A of the indicative OV LV BPL topologies in the 3-88MHz frequency band for various hook distances from the transmitting end and hook lengths when different maximum values a_{CUD} are assumed. (a) $a_{\text{CUD}} = 1\text{dB}$. (b) $a_{\text{CUD}} = 2\text{dB}$. (c) $a_{\text{CUD}} = 3\text{dB}$. (d) $a_{\text{CUD}} = 4\text{dB}$. (e) $a_{\text{CUD}} = 5\text{dB}$.

(a)

(b)

(c)

(d)
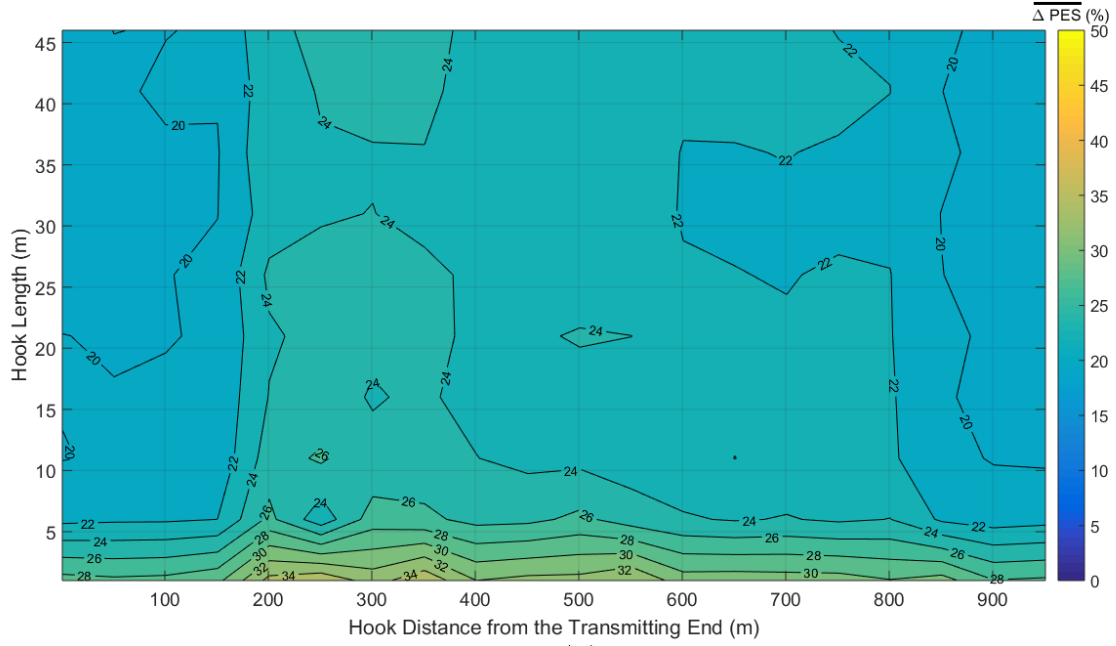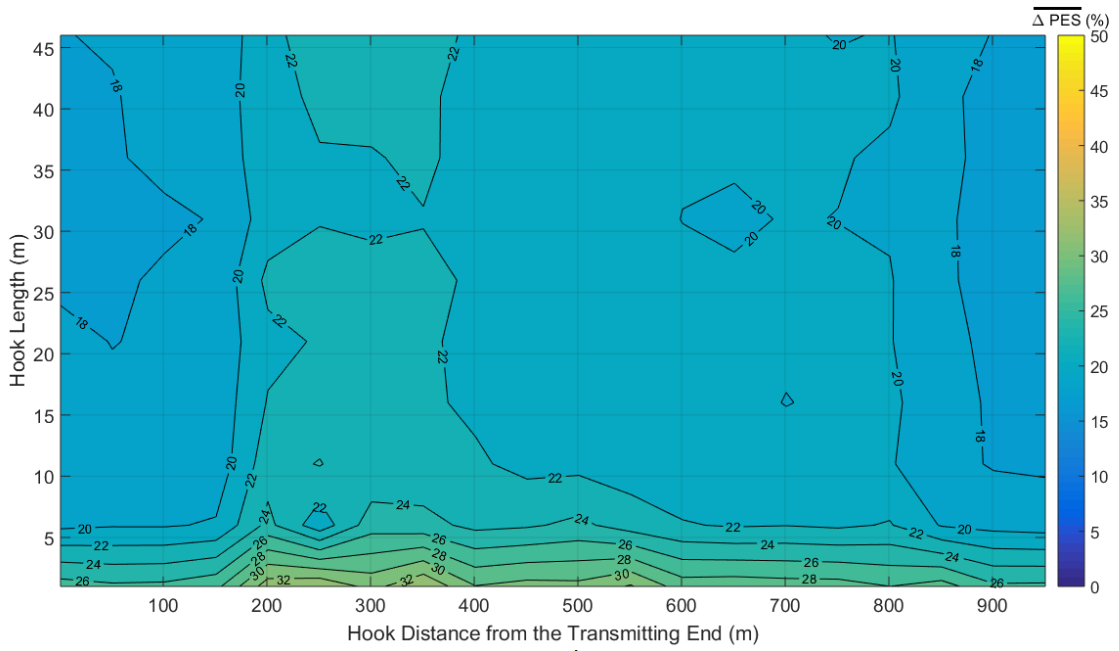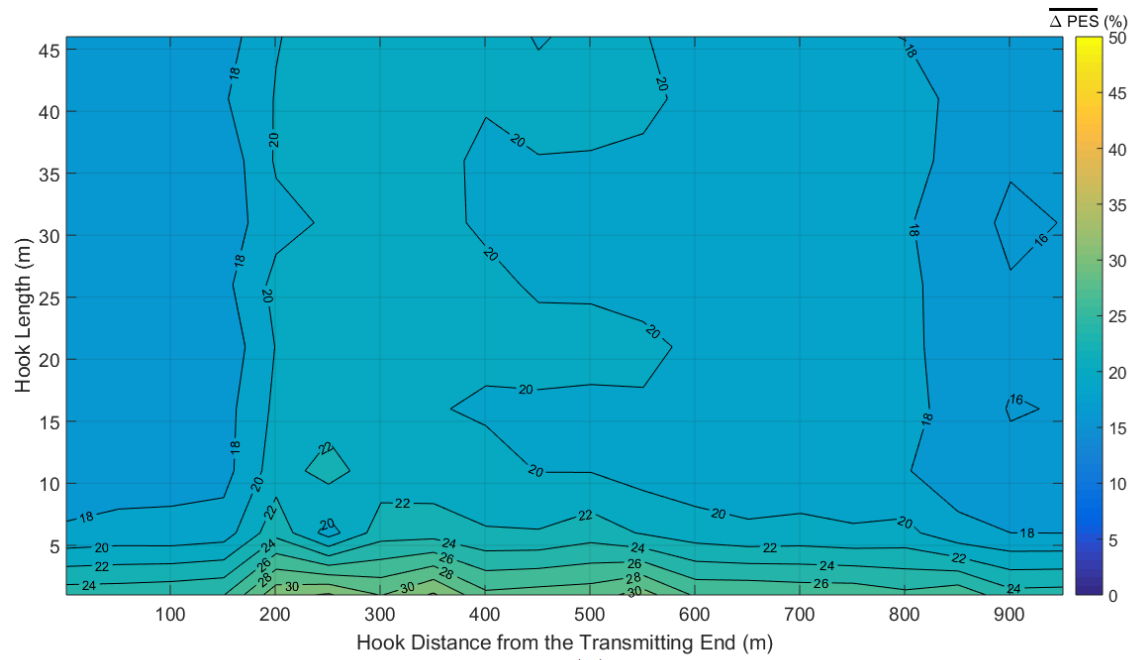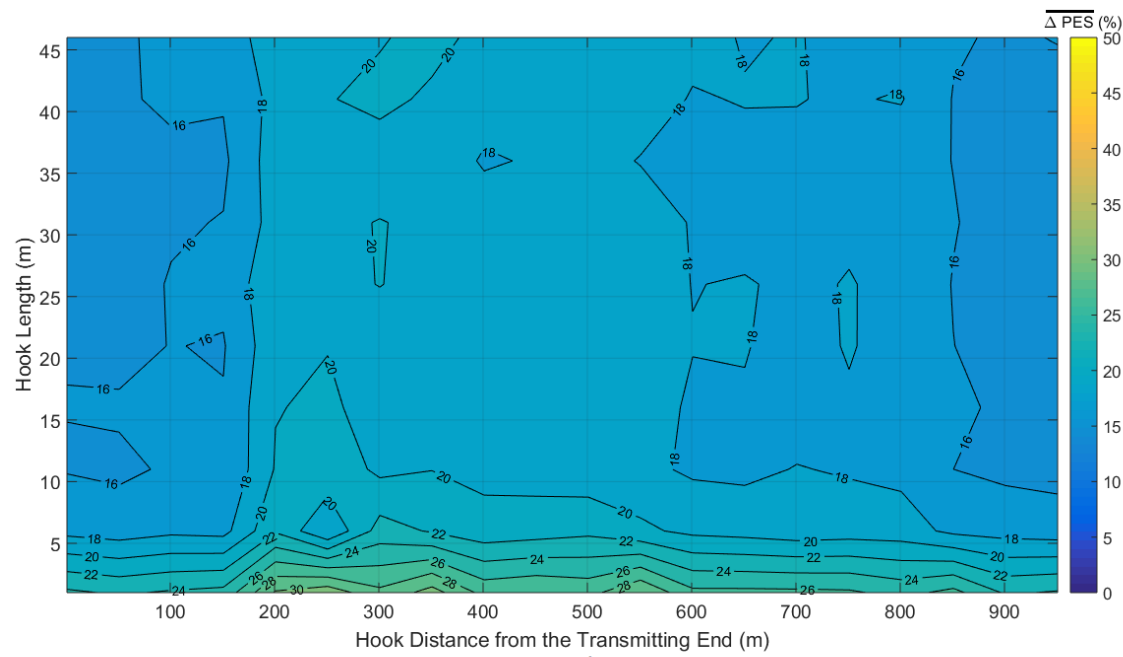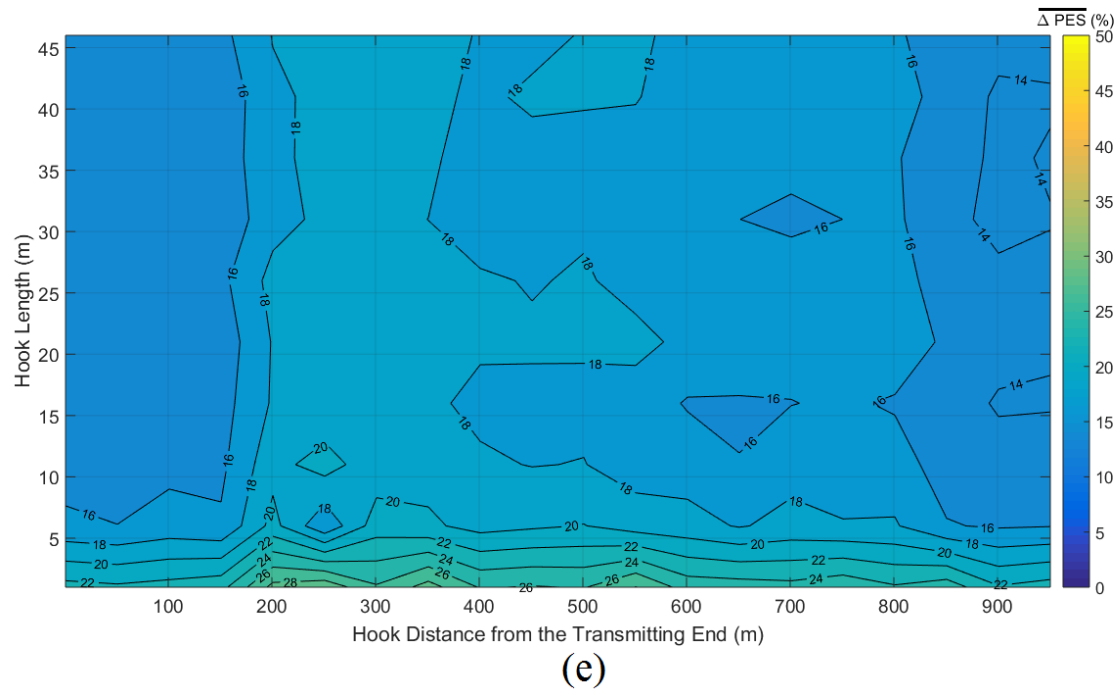
Fig. 5. Same curves with Fig. 4 but for the urban case B.

(a)

(b)

(c)

(d)

(e)
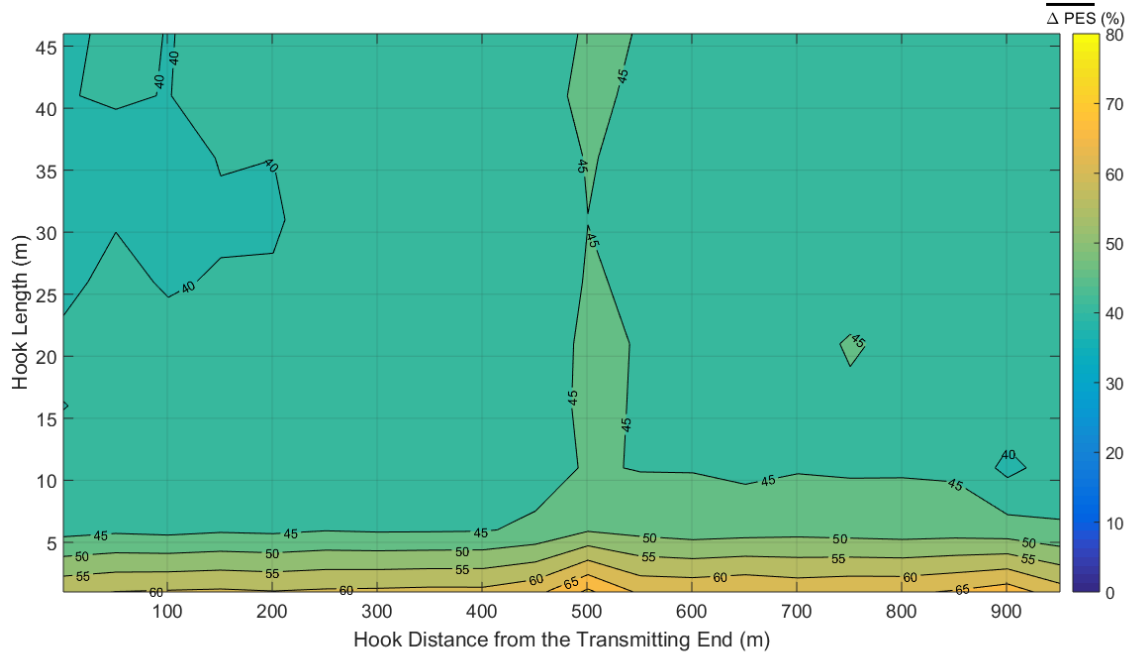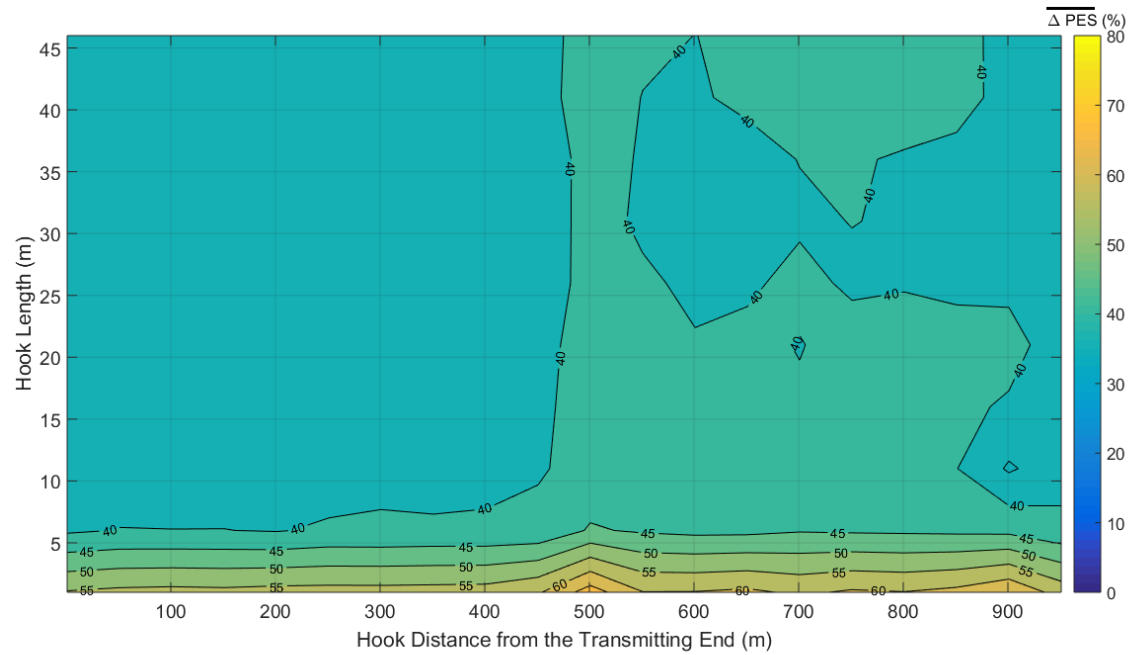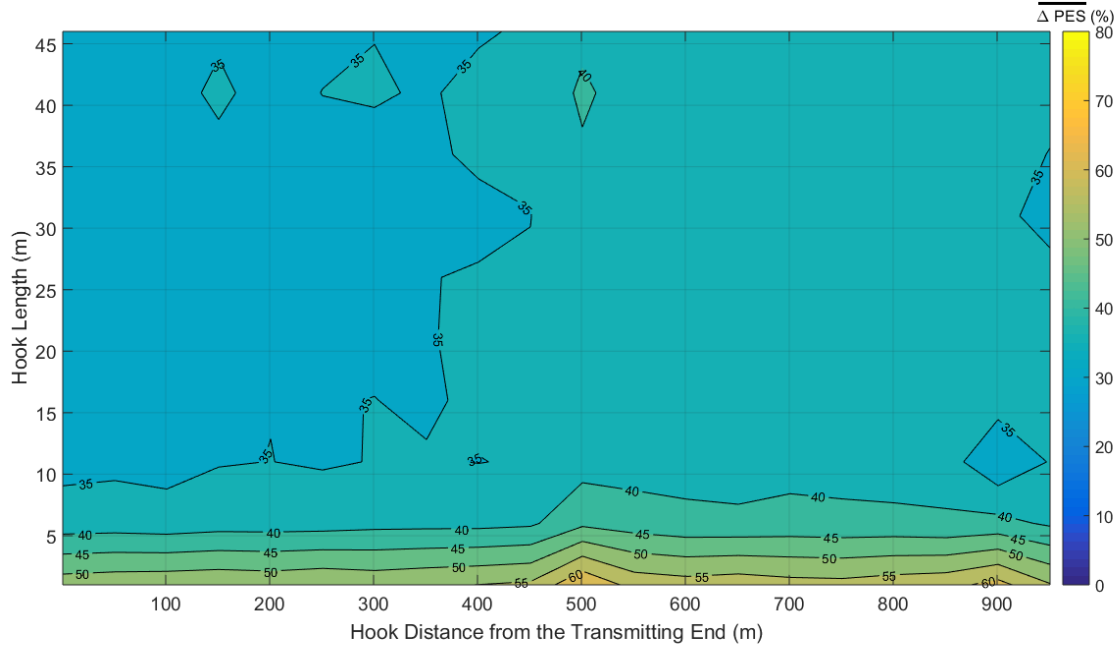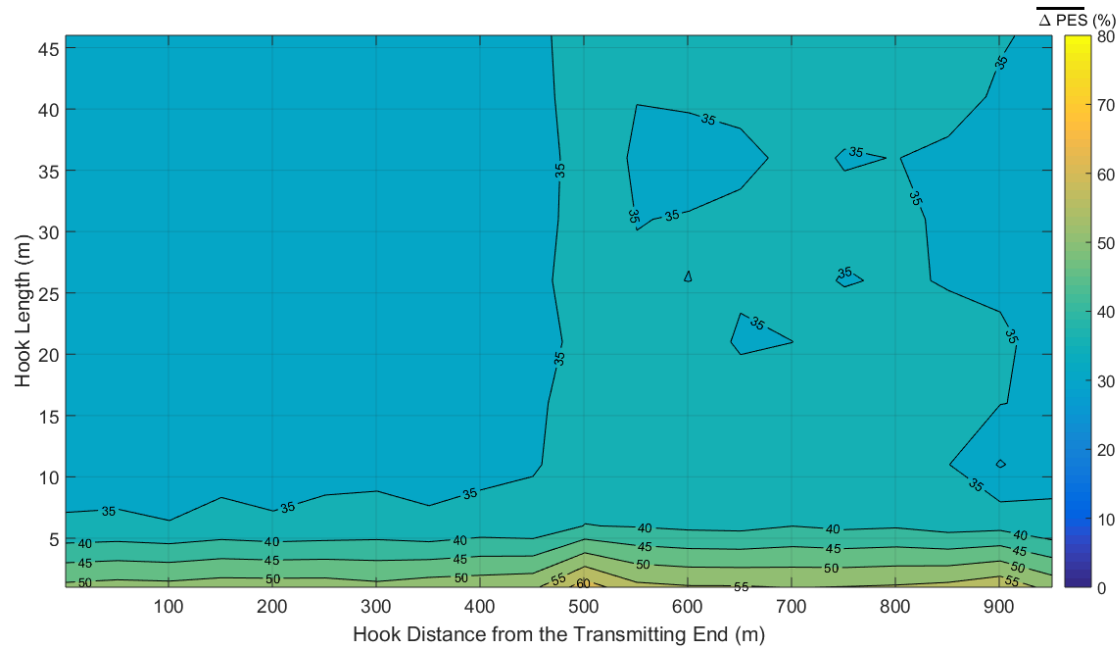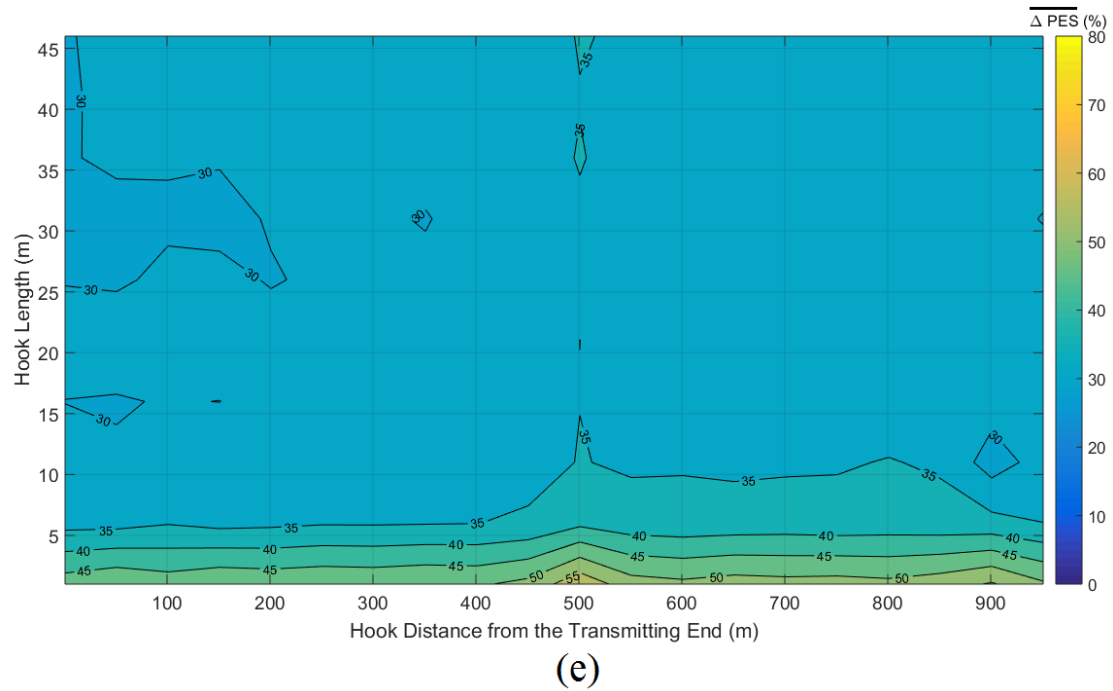
Fig. 6. Same curves with Fig. 4 but for the suburban case.

(a)

(b)

(c)

(d)
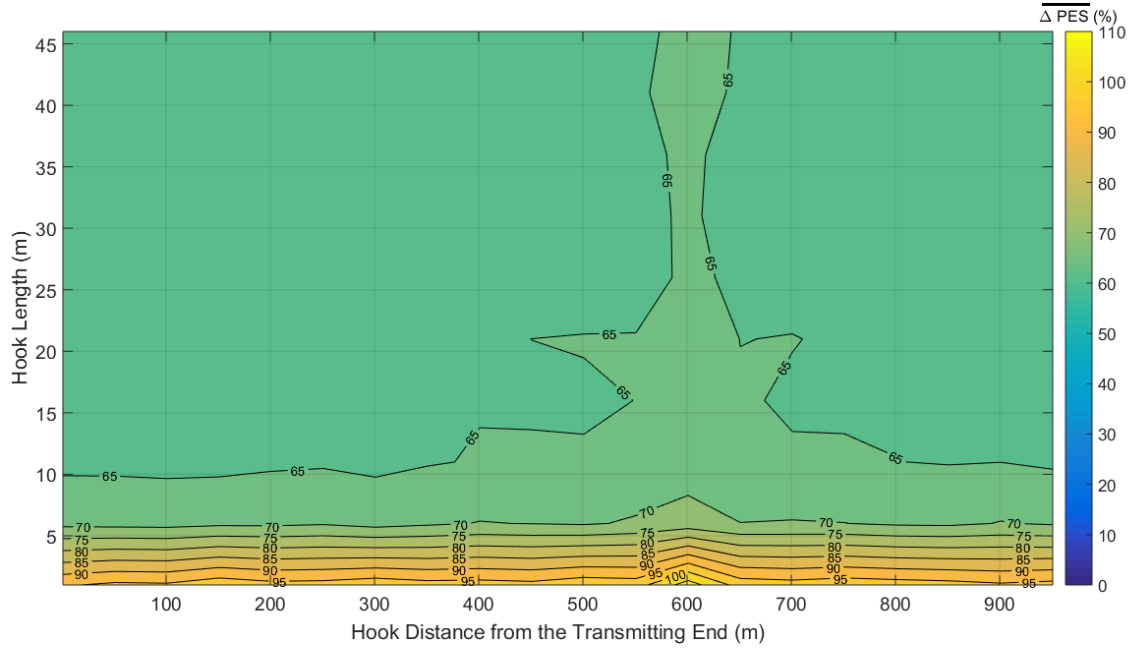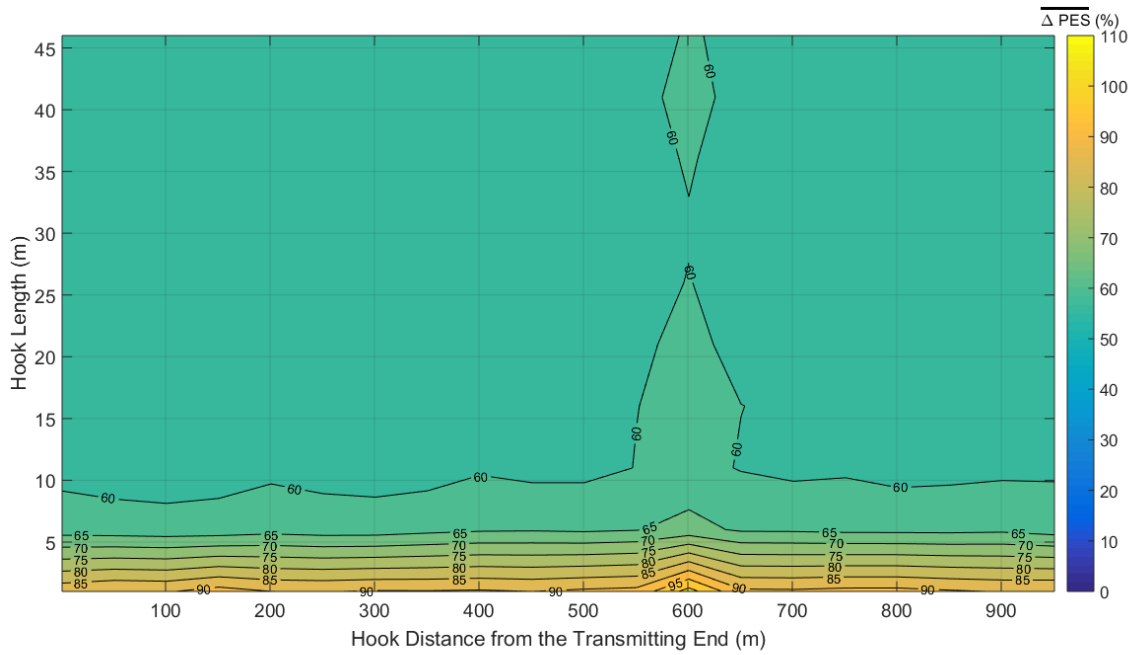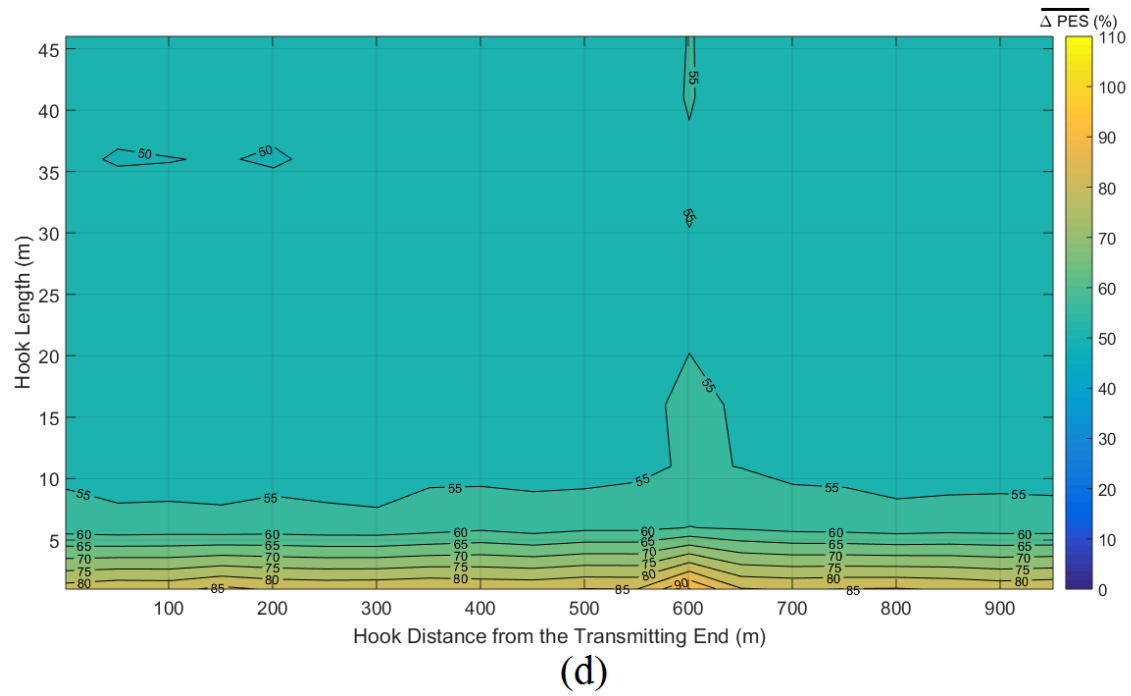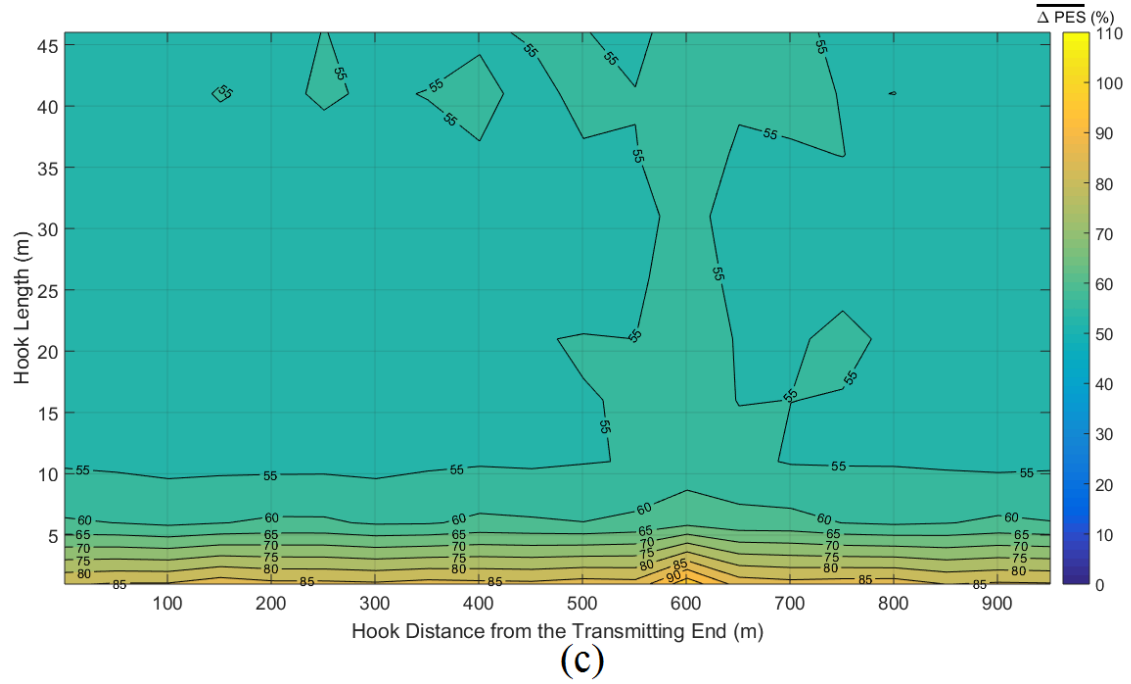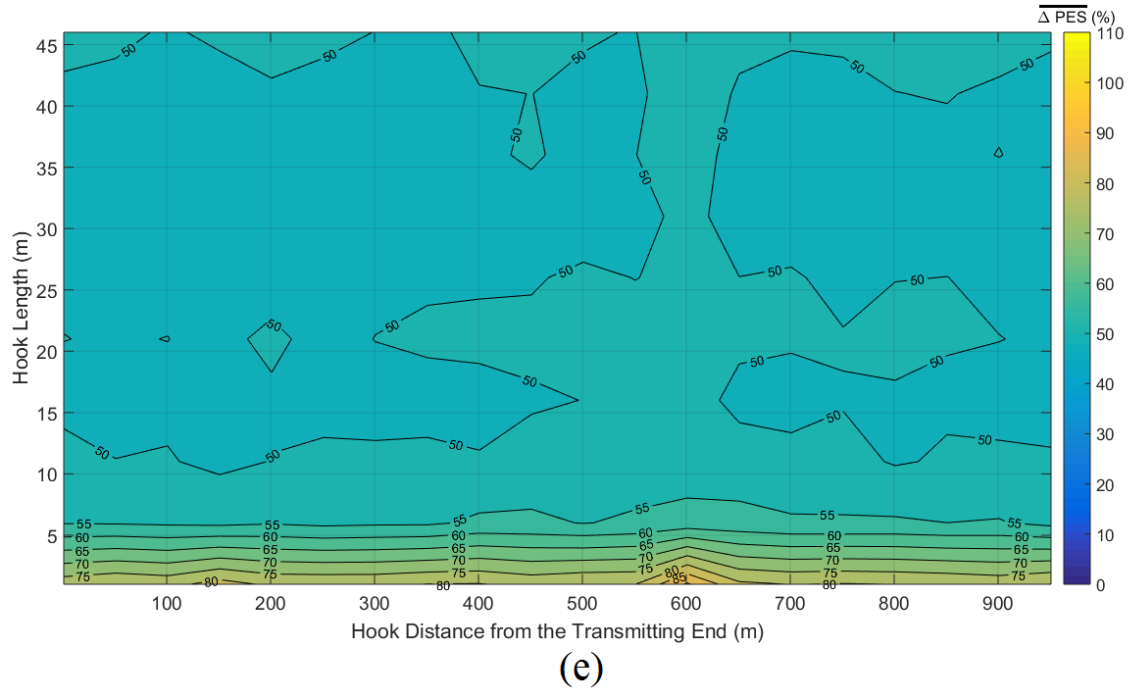
Fig. 7. Same curves with Fig. 4 but for the rural case.

(a)

(b)

(c)

(d)

(e)
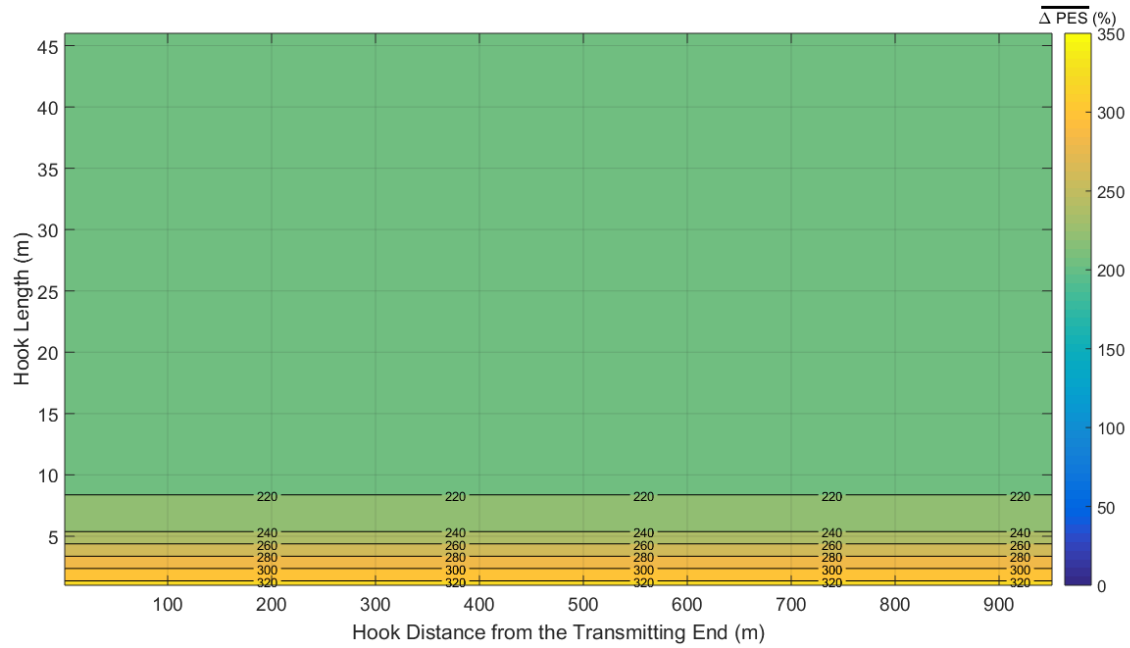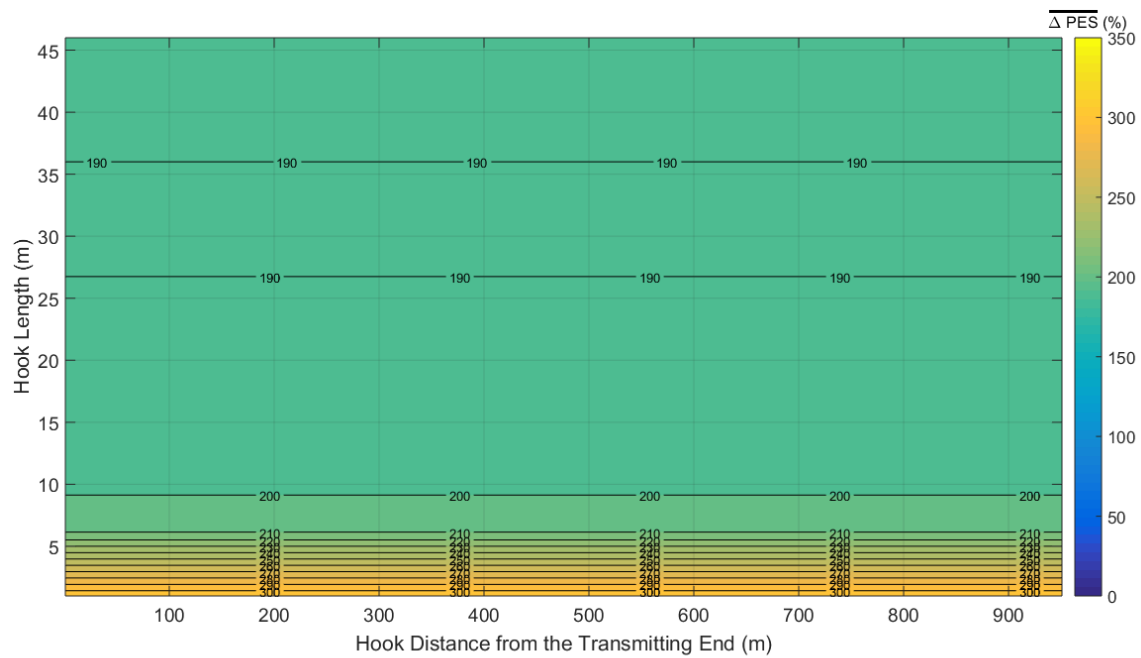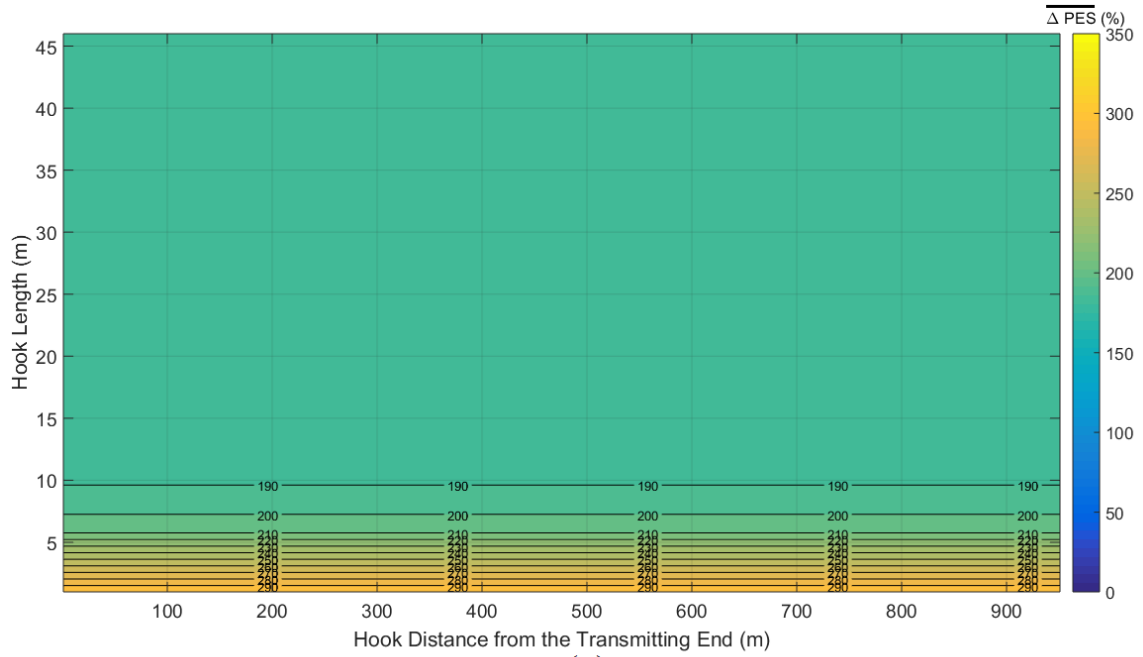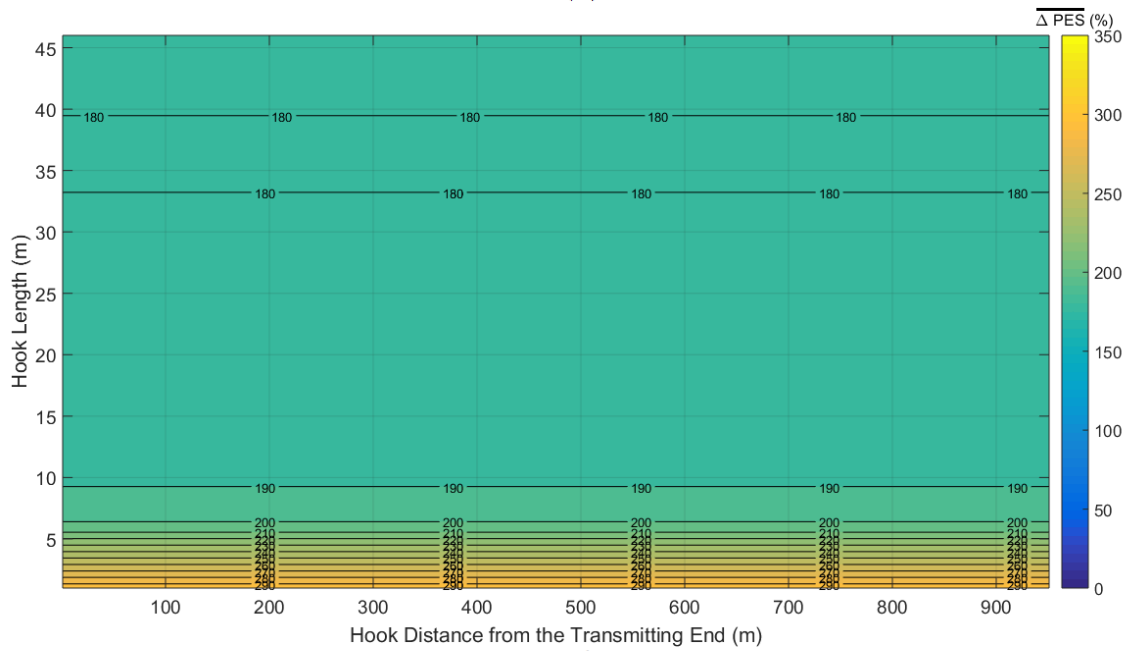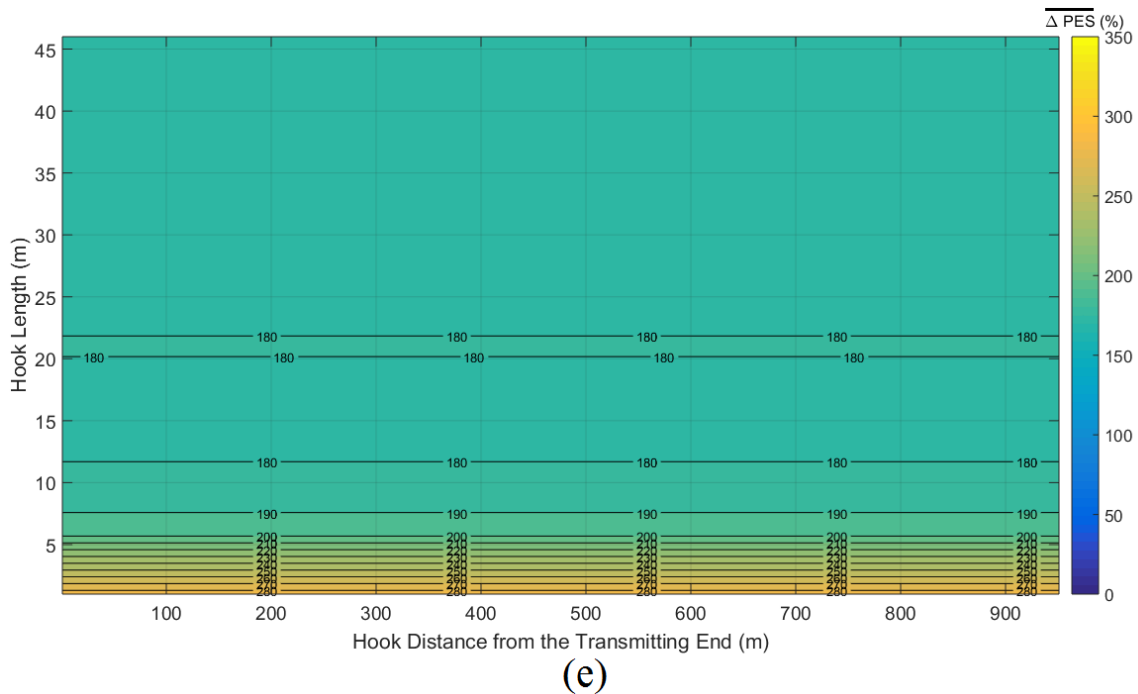
Fig. 8. Same curves with Fig. 4 but for the "LOS" case.

From Figs. 4-8, several interesting conclusions can be deduced concerning the performance of HS-DET method and its behavior when measurement differences of various maximum values a_{CUD} are considered. More specifically:

- In general, measurement differences influence the values of $\overline{\Delta PES}$ regardless of the examined OV LV BPL topology, the hook distance from the transmitting end and the hook length. Hence, the average $\overline{\Delta PES}$ for given contour plot generally decreases with the increase of the maximum value a_{CUD}. This is shown through the adoption of colder colors in contour plots for given OV LV BPL topologies as the maximum value a_{CUD} increases.

- The stochastic nature of measurement differences mainly affects OV LV BPL topologies with branches. Although the general morphology of $\overline{\Delta PES}$ concerning the colored islands remains as the background image of contour plots, the impact of measurement differences on $\overline{\Delta PES}$ acts additively to this image by creating new and frequent colored islands. Conversely, "LOS" topologies are not affected by the measurement differences on the basis of $\overline{\Delta PES}$ since there is no creation of new colored islands in $\overline{\Delta PES}$ contour plots.

- In the OV LV BPL topologies with branches, measurement differences further intensify the island effect of $\overline{\Delta PES}$ at the transmitting and receiving end. In all the cases examined where the island effect occurs the islands remain regardless of the intensity of measurement differences.

- Also been observed in ΔPES, shorter hooks allow their easier identification by HS-DET method. In contrast, when the hooks are longer, ΔPES and $\overline{\Delta PES}$ values become significantly lower than the respective values for hooks with length being equal to 1m for given OV LV BPL topology and maximum value a_{CUD}.

- HS-DET method can safely detect hook style energy thefts that may occur across the OV LV BPL networks. Safe decisions concerning the existence of energy theft or not can be made regardless of the examined OV LV BPL topology, the intensity of the measurement differences and the hook characteristics. ΔPES and $\overline{\Delta PES}$ maintain values greater than zero in all the cases examined. However, the issues that can be addressed regarding the future research are: (i) The existence / definition of the threshold of the maximum value a_{CUD} above which HS-DET method starts to give faulty decisions concerning the energy theft (i.e., if / when ΔPES and $\overline{\Delta PES}$ can receive negative values); (ii) The possibility of the installation of very long hooks in order to mask the hook existence during the application of HS-DET method; and (iii) the use of "smart" hooks that are matched to the characteristic impedances of the lines in order again to camouflage the energy theft.

5. Conclusions

This paper has focused on the detection of the hook style energy theft in the OV LV BPL networks, which is a common type of energy theft in developing countries. Different OV LV BPL topologies, intensities of measurement differences and hook characteristics have been considered in order to assess the performance of the proposed HS-DET method. On the basis of ΔPES and $\overline{\Delta PES}$, several interesting conclusions have been deduced concerning the performance of HS-DET method. Initially, it has been revealed that the hook detection becomes easier in the cases of OV LV BPL topologies of low number of long branches such as "LOS" and rural OV LV BPL topologies. But the performance of HS-DET method mainly depends on the hook length; the detection of the hook style energy theft becomes easier when the hook remains short (*i.e.,* shorter than 10 m). As the influence of measurement differences is discussed, the stochastic nature of measurement differences mainly affects OV LV BPL topologies with branches. Although the general morphology of $\overline{\Delta PES}$ contour plots remains the same, the increase of the CUD maximum value of measurement differences negatively influences the performance of HS-DET method. Anyway, HS-DET method successfully detected the energy theft in all the cases examined regardless of the CUD maximum value of measurement differences. Finally, due to the island effect that has been observed in ΔPES and $\overline{\Delta PES}$ contour plots, HS-DET method more easily detects the energy theft of hooks that are situated at the middle of the transmission path rather than near the transmitting and receiving ends. As the future research concerning the application of HS-DET method is discussed, there are three issues that need further analysis, namely: (i) the existence / definition of the threshold of the maximum value a_{CUD} above which HS-DET method starts to give faulty decisions concerning the energy theft; (ii) the possibility of the installation of very long hooks so that HS-DET method can be jammed; and (iii) the use of "smart" hooks that are matched to the characteristic impedance of lines in order to cover the energy theft.

CONFLICTS OF INTEREST

The author declares that there is no conflict of interests regarding the publication of this paper.

References

[1]   C. H. Lo, and N. Ansari, "CONSUMER: A Novel Hybrid Intrusion Detection System for Distribution Networks in Smart Grid," *IEEE Transactions on Emerging Topics in Computing*, vol. 1, no. 1, pp. 33-44, 2013.

[2]   R. Jiang, R. Lu, Y. Wang, J. Luo, C. Shen, and X. S. Shen, "Energy-theft Detection Issues for Advanced Metering Infrastructure in Smart Grid," *Tsinghua Science and Technology*, vol. 19, no. 2, pp. 105-120, 2014.

[3]   P. Jokar, N. Arianpoo, and V. CM Leung, "Electricity Theft Detection in AMI Using Customers' Consumption Patterns," *IEEE Transactions on Smart Grid*, vol. 7, no. 1, pp. 216-226, 2016.

[4]   S. Salinas, M. Li, and P. Li, "Privacy-preserving Energy Theft Detection in Smart Grids: A P2P Computing Approach," *IEEE Journal on Selected Areas in Communications*, vol. 31, no. 9, pp. 257-267, 2013.

[5]   D. R. Pereira, M. A. Pazoti, L. A. Pereira, D. Rodrigues, C. O. Ramos, A. N. Souza, and J. P. Papa, "Social-Spider Optimization-based Support Vector Machines applied for energy theft detection," *Computers & Electrical Engineering*, vol. 49, pp. 25-38, 2016.

[6]   S. Salinas, M. Ming, and P. Li, "Privacy-preserving Energy Theft Detection in Smart Grids," *Sensor, Mesh and Ad Hoc Communications and Networks (SECON), 2012, in proc. 9th Annual IEEE Communications Society Conference on. IEEE*, pp. 605-613, 2012.

[7]   S. McLaughlin, B. Holbert, S. Zonouz, and R. Berthier, "AMIDS: A Multi-sensor Energy Theft Detection Framework for Advanced Metering Infrastructures," in *Smart Grid Communications (SmartGridComm), in proc of 2012 IEEE Third International Conference on*, pp. 354-359, Nov. 2012.

[8]   P. Antmann, "Reducing Technical and non-Technical Losses in the Power Sector," *Background paper for the WBG Energy Strategy, Tech. Rep.*, Washington, DC, USA: The World Bank, 2009.

[9]   P. McDaniel and S. McLaughlin, "Security and Privacy Challenges in the Smart Grid," *IEEE Security & Privacy*, vol. 7, no. 3, pp. 75-77, 2009.

[10]   Federal Court of Audit, "Operational Audit Report Held in National Agency of Electrical Energy, ANEEL, Brazil", *Rep. no. TC 025.619/2007-2*, Brasília, Brazil, 2007.

[11]   Ministry of Power, India, "Overview of power distribution," *Tech. Rep.*, http://www.powermin.nic.in, 2013.

[12]   C. Bandim, J. Alves, A. Pinto, F. Souza, M. Loureiro, C. Magalhges, and F. Galvez-Durand, "Identification of energy theft and tampered meters using a central observer meter: a mathematical approach," in *Proc. Transmission Distrib. Conf. Exposition*, Sep. 2003.

[13]   A. Ruzzelli, C. Nicolas, A. Schoofs, and G. O'Hare, "Real-time recognition and profiling of appliances through a single electricity sensor," in *Proc. IEEE SECON*, June 2010.

[14] E. L. Quinn, "Privacy and the new energy infrastructure," *Social Science Research Netw.*, pp. 1995–2008, 2009 [Online]. Available: http://ssrn.com/paper=1370731

[15] "Privacy and the smart grid," NIST Guidelines for Smart Grid Cyber Security: vol.2, Aug. 2010 [Online]. Available: http://csrc.nist.gov/publications/nistir/ir7628/nistir-7628_vol1.pdf

[16] K. Sharma and L. M. Saini, "Power-line communications for smart grid: Progress, challenges, opportunities and status," *Elsevier Renewable and Sustainable Energy Reviews,* vol. 67, pp. 704-751, 2017.

[17] T. A. Papadopoulos, A. I. Chrysochos, A. ElSamadouny, N. Al-Dhahir, and G. K. Papagiannis, "MIMO-OFDM narrowband-PLC in distribution systems: Impact of power transformers on achievable data rates,". *Elsevier Electric Power Systems Research*, vol. 151, pp. 251-265, 2017.

[18] E. O. Kontis, T. A. Papadopoulos, A. I. Chrysochos, and G. K. Papagiannis, "Measurement-Based Dynamic Load Modeling Using the Vector Fitting Technique," *IEEE Transactions on Power Systems*, vol. 33, no. 1, pp. 338-351, 2018.

[19] A. G. Lazaropoulos, "Towards Modal Integration of Overhead and Underground Low-Voltage and Medium-Voltage Power Line Communication Channels in the Smart Grid Landscape: Model Expansion, Broadband Signal Transmission Characteristics, and Statistical Performance Metrics (Invited Paper)," *ISRN Signal Processing*, vol. 2012, Article ID 121628, pp. 1-17, 2012. [Online]. Available: http://www.hindawi.com/isrn/sp/2012/121628/

[20] A. G. Lazaropoulos, "Towards broadband over power lines systems integration: Transmission characteristics of underground low-voltage distribution power lines," *Progress in Electromagnetics Research B*, 39, pp. 89-114, 2012. [Online]. Available: http://www.jpier.org/PIERB/pierb39/05.12012409.pdf

[21] A. G. Lazaropoulos and P. G. Cottis, "Transmission characteristics of overhead medium voltage power line communication channels," *IEEE Trans. Power Del.*, vol. 24, no. 3, pp. 1164-1173, Jul. 2009.

[22] A. G. Lazaropoulos and P. G. Cottis, "Capacity of overhead medium voltage power line communication channels," *IEEE Trans. Power Del.*, vol. 25, no. 2, pp. 723-733, Apr. 2010.

[23] A. G. Lazaropoulos and P. G. Cottis, "Broadband transmission via underground medium-voltage power lines-Part I: transmission characteristics," *IEEE Trans. Power Del.*, vol. 25, no. 4, pp. 2414-2424, Oct. 2010.

[24] A. G. Lazaropoulos and P. G. Cottis, "Broadband transmission via underground medium-voltage power lines-Part II: capacity," *IEEE Trans. Power Del.*, vol. 25, no. 4, pp. 2425-2434, Oct. 2010.

[25] A. G. Lazaropoulos, "Broadband transmission characteristics of overhead high-voltage power line communication channels," *Progress in Electromagnetics Research B*, vol. 36, pp. 373-398, 2012. [Online]. Available: http://www.jpier.org/PIERB/pierb36/19.11091408.pdf

[26] A. G. Lazaropoulos, "Green Overhead and Underground Multiple-Input Multiple-Output Medium Voltage Broadband over Power Lines Networks: Energy-Efficient Power Control,"*Springer Journal of Global Optimization*, vol. 2012 / Print ISSN 0925-5001, pp. 1-28, Oct. 2012.

[27] A. G. Lazaropoulos, "Deployment Concepts for Overhead High Voltage Broadband over Power Lines Connections with Two-Hop Repeater System: Capacity

Countermeasures against Aggravated Topologies and High Noise Environments," *Progress in Electromagnetics Research B*, vol. 44, pp. 283-307, 2012. [Online]. Available: http://www.jpier.org/PIERB/pierb44/13.12081104.pdf

[28] A. G. Lazaropoulos, "Broadband transmission and statistical performance properties of overhead high-voltage transmission networks,"*HindawiJournal of Computer Networks and Commun.*, 2012, article ID 875632, 2012. [Online]. Available: http://www.hindawi.com/journals/jcnc/aip/875632/

[29] P. Amirshahi and M. Kavehrad, "High-frequency characteristics of overhead multiconductor power lines for broadband communications," *IEEE J. Sel. Areas Commun.*, vol. 24, no. 7, pp. 1292-1303, Jul. 2006.

[30] T. Calliacoudas and F. Issa, ""Multiconductor transmission lines and cables solver," An efficient simulation tool for plc channel networks development," presented at the *IEEE Int. Conf. Power Line Communications and Its Applications*, Athens, Greece, Mar. 2002.

[31] T. Sartenaer and P. Delogne, "Deterministic modelling of the (Shielded) outdoor powerline channel based on the multiconductor transmission line equations," *IEEE J. Sel. Areas Commun.*, vol. 24, no. 7, pp. 1277-1291, Jul. 2006.

[32] C. R. Paul, *Analysis of Multiconductor Transmission Lines*. New York: Wiley, 1994.

[33] H. Meng, S. Chen, Y. L. Guan, C. L. Law, P. L. So, E. Gunawan, and T. T. Lie, "Modeling of transfer characteristics for the broadband power line communication channel," *IEEE Trans. Power Del.*, vol. 19, no. 3, pp. 1057-1064, Jul. 2004.

[34] B. Li, D. Mansson, and G. Yang, "An efficient method for solving frequency responses of power-line networks," *Progress In Electromagnetics Research B*, Vol. 62, 303-317, 2015. doi:10.2528/PIERB15013008 http://www.jpier.org/pierb/pier.php?paper=15013008

[35] M. Chaaban, K. El KhamlichiDrissi, and D. Poljak, "Analytical model for electromagnetic radiation by bare-wire structures," *Progress In Electromagnetics Research B*, Vol. 45, 395-413, 2012. doi:10.2528/PIERB12091102 http://www.jpier.org/pierb/pier.php?paper=12091102

[36] Y. H. Kim, S. Choi, S. C. Kim, and J. H. Lee, "Capacity of OFDM two-hop relaying systems for medium-voltage power-line access networks," *IEEE Trans. Power Del.*, vol. 27, no. 2, pp. 886-894, Apr. 2012.

[37] A. G. Lazaropoulos, "Measurement Differences, Faults and Instabilities in Intelligent Energy Systems – Part 1: Identification of Overhead High-Voltage Broadband over Power Lines Network Topologies by Applying Topology Identification Methodology (TIM)," *Trends in Renewable Energy*, vol. 2, no. 3, pp. 85 – 112, Oct. 2016. [Online]. Available: http://futureenergysp.com/index.php/tre/article/download/26/32

[38] A. G. Lazaropoulos, "Measurement Differences, Faults and Instabilities in Intelligent Energy Systems – Part 2: Fault and Instability Prediction in Overhead High-Voltage Broadband over Power Lines Networks by Applying Fault and Instability Identification Methodology (FIIM)," *Trends in Renewable Energy*, vol. 2, no. 3, pp. 113 – 142, Oct. 2016. [Online]. Available: http://futureenergysp.com/index.php/tre/article/view/27/33

[39] A. G. Lazaropoulos, "Power Systems Stability through Piecewise Monotonic Data Approximations – Part 2: Adaptive Number of Monotonic Sections and Performance of L1PMA, L2WPMA and L2CXCV in Overhead Medium-Voltage

Broadband over Power Lines Networks," *Trends in Renewable Energy*, vol. 3, no. 1, pp. 33 – 60, Jan. 2017. [Online]. Available: http://futureenergysp.com/index.php/tre/article/view/30/35

[40] A. G. Lazaropoulos, "Power Systems Stability through Piecewise Monotonic Data Approximations – Part 1: Comparative Benchmarking of L1PMA, L2WPMA and L2CXCV in Overhead Medium-Voltage Broadband over Power Lines Networks," *Trends in Renewable Energy*, vol. 3, no. 1, pp. 2 – 32, Jan. 2017. [Online]. Available: http://futureenergysp.com/index.php/tre/article/view/29/34

[41] A. G. Lazaropoulos, "Main Line Fault Localization Methodology in Smart Grid – Part 1: Extended TM2 Method for the Overhead Medium-Voltage Broadband over Power Lines Networks Case," *Trends in Renewable Energy*, vol. 3, no. 3, pp. 2-25, Dec. 2017. [Online]. Available: http://futureenergysp.com/index.php/tre/article/view/36

[42] A. G. Lazaropoulos, "Main Line Fault Localization Methodology in Smart Grid – Part 2: Extended TM2 Method, Measurement Differences and L1 Piecewise Monotonic Data Approximation for the Overhead Medium-Voltage Broadband over Power Lines Networks Case," *Trends in Renewable Energy*, vol. 3, no. 3, pp. 26-61, Dec. 2017. [Online]. Available: http://futureenergysp.com/index.php/tre/article/view/37

[43] A. G. Lazaropoulos, "Main Line Fault Localization Methodology in Smart Grid – Part 3: Main Line Fault Localization Methodology (MLFLM)," *Trends in Renewable Energy*, vol. 3, no. 3, pp. 62-81, Dec. 2017. [Online]. Available: http://futureenergysp.com/index.php/tre/article/view/38

[44] A. G. Lazaropoulos, "Best L1 Piecewise Monotonic Data Approximation in Overhead and Underground Medium-Voltage and Low-Voltage Broadband over Power Lines Networks: Theoretical and Practical Transfer Function Determination," *Hindawi Journal of Computational Engineering*, vol. 2016, Article ID 6762390, 24 pages, 2016. doi:10.1155/2016/6762390. [Online]. Available: https://www.hindawi.com/journals/jcengi/2016/6762390/cta/

[45] A. G. Lazaropoulos, "Smart Energy and Spectral Efficiency (SE) of Distribution Broadband over Power Lines (BPL) Networks – Part 2: L1PMA, L2WPMA and L2CXCV for SE against Measurement Differences in Overhead Medium-Voltage BPL Networks," *Trends in Renewable Energy*, vol. 4, no. 2, pp. 185-212, Aug. 2018. [Online]. Available: http://futureenergysp.com/index.php/tre/article/view/77/pdf

[46] A. G. Lazaropoulos, "Smart Energy and Spectral Efficiency (SE) of Distribution Broadband over Power Lines (BPL) Networks – Part 1: The Impact of Measurement Differences on SE Metrics," *Trends in Renewable Energy*, vol. 4, no. 2, pp. 125-184, Aug. 2018. [Online]. Available: http://futureenergysp.com/index.php/tre/article/view/76/pdf

[47] P. Amirshahi and M. Kavehrad, "Medium voltage overhead powerline broadband communications; Transmission capacity and electromagnetic interference," in *Proc. IEEE Int. Symp. Power Line Commun. Appl.*, Vancouver, BC, Canada, Apr. 2005, pp. 2-6.

[48] M. Tang, and M. Zhai, "Research of transmission parameters of four-conductor cables for power line communication," in *Proc. Int. Conf. on Computer Science and Software Engineering*, Wuhan, China, Dec. 2008, vol. 5, pp. 1306–1309.

[49] M. D'Amore and M. S. Sarto, "A new formulation of lossy ground return parameters for transient analysis of multiconductor dissipative lines," *IEEE Trans. Power Del.*, vol. 12, no. 1, pp. 303-314, Jan. 1997.

[50] M. D'Amore and M. S. Sarto, "Simulation models of a dissipative transmission line above a lossy ground for a wide-frequency range-Part I: Single conductor configuration," *IEEE Trans. Electromagn. Compat.*, vol. 38, no. 2, pp. 127-138, May 1996.

[51] M. D'Amore and M. S. Sarto, "Simulation models of a dissipative transmission line above a lossy ground for a wide-frequency range-Part II: Multi-conductor configuration," *IEEE Trans. Electromagn. Compat.*, vol. 38, no. 2, pp. 139-149, May 1996.

[52] N. Theethayi, "Electromagnetic interference in distributed outdoor electrical systems, with an emphasis on lightning interaction with electrified railway network," Ph.D. dissertation, Uppsala Univ., Uppsala, Sweden, Sep. 2005, [Online]. Available: http://uu.diva-portal.org/smash/get/diva2:166746/FULLTEXT01

[53] A. G. Lazaropoulos, "Wireless Sensor Network Design for Transmission Line Monitoring, Metering and Controlling: Introducing Broadband over Power Lines-enhanced Network Model (BPLeNM)," *ISRN Power Engineering*, vol. 2014, Article ID 894628, 22 pages, 2014. doi:10.1155/2014/894628. [Online]. Available: http://www.hindawi.com/journals/isrn.power.engineering/2014/894628/

[54] A. G. Lazaropoulos, "New Coupling Schemes for Distribution Broadband over Power Lines (BPL) Networks," *Progress in Electromagnetics Research B*, vol. 71, pp. 39-54, 2016. [Online]. Available: http://www.jpier.org/PIERB/pierb71/02.16081503.pdf

[55] A. G. Lazaropoulos, "Broadband Performance Metrics and Regression Approximations of the New Coupling Schemes for Distribution Broadband over Power Lines (BPL) Networks," *Trends in Renewable Energy*, vol. 4, no. 1, pp. 43 – 73, 2018. [Online]. Available: http://www.futureenergysp.com/index.php/tre/article/view/59/pdf

[56] OPERA1, D44: Report presenting the architecture of plc system, the electricity network topologies, the operating modes and the equipment over which PLC access system will be installed, IST Integr. Project No 507667, Dec. 2005.

[57] OPERA1, D5: Pathloss as a function of frequency, distance and network topology for various LV and MV European powerline networks. IST Integrated Project No 507667, Apr. 2005.

[58] A. G. Lazaropoulos, "Factors Influencing Broadband Transmission Characteristics of Underground Low-Voltage Distribution Networks,"*IET Commun.*, vol. 6, no. 17, pp. 2886-2893, Nov. 2012.

[59] J. Anatory, N. Theethayi, and R. Thottappillil, "Power-line communication channel model for interconnected networks-Part II: Multiconductor system," *IEEE Trans. Power Del.*, vol. 24, no. 1, pp. 124-128, Jan. 2009.

[60] J. Anatory, N. Theethayi, R. Thottappillil, M. M. Kissaka, and N. H. Mvungi, "The effects of load impedance, line length, and branches in typical low-voltage channels of the BPLC systems of developing countries: transmission-line analyses," *IEEE Trans. Power Del.*, vol. 24, no. 2, pp. 621-629, Apr. 2009.

[61] A. G. Lazaropoulos, "A Panacea to Inherent BPL Technology Deficiencies by Deploying Broadband over Power Lines (BPL) Connections with Multi-Hop

Repeater Systems," *Bentham Recent Advances in Electrical & Electronic Engineering*, vol. 10, no. 1, pp. 30-46, 2017.

[62] A. G. Lazaropoulos, "Improvement of Power Systems Stability by Applying Topology Identification Methodology (TIM) and Fault and Instability Identification Methodology (FIIM) – Study of the Overhead Medium-Voltage Broadband over Power Lines (OV MV BPL) Networks Case," *Trends in Renewable Energy*, vol. 3, no. 2, pp. 102-128, Apr. 2017. [Online]. Available: http://futureenergysp.com/index.php/tre/article/view/34

Peer-Reviewed Article

Theoretical Design of Energy Generating Gymnasium Pull-down Machine for Green, Renewable and Sustainable Energy Production

M. Musharraf,[1,*] Ifrah Saleem,[2] and Dr. Farhat Iqbal[1]

[1] *Department of Electrical Engineering, University College of Engineering and Technology (UCET), University of Sargodha (UOS), Sargodha, Pakistan 40100*
[2] *University of Lahore (UOL), Lahore, Pakistan 54000*

New technologies are being invented and energy demand is increasing. Growth of population has always been and will remain one of the major causes of energy demand. Science is therefore looking for new major and minor energy resources to keep world in progress. The main focus of energy engineering and technology in the field of energy generation is to harvest energy by any mean from any source. A theoretical research is introduced in this paper which will contribute its reasonable share in the field of renewable and green energy sector. This energy generating system is named as energy generating gymnasium system (EGGS). The core idea behind this energy harvesting system is that, the human being is also a source of renewable energy and it is possible to harness electrical energy from people by the use of EGGS. Human energy is wasted when excessive calories of body are burnt during exercise in gymnasiums to achieve the desired fitness. EGGS will provide an opportunity to return expended energy in the form of electrical energy from gymnasium equipment and cardiovascular machines. This electrical energy will be cheap and also green since it will not emit any carbon dioxide (CO_2) gas during the process. This system can increase the potential of renewable energy area and the electrical energy generated from EGGS can be sold back to the national utility via micro grids (MG). The proposed system will be very beneficial for such countries that are facing energy crises as well as the third world countries. Authors have discussed a gymnasium machine named as "Pull-down machine" and proposed a theoretical modification to make it as an energy generating gymnasium machine (EGGM) in the presented research.

Keywords: EGGS; EGGM; Gymnasium; Renewable energy; Cable and pulley; Pull-down machine; Micro grid

1. Introduction

The world around us is changing significantly and the use of technology has become one of the major drivers for economic and social development. Rapid advancement in engineering and Information Technology (IT) all over the world has transformed not only the way people think, but also the way people act. Most of the technologies require electricity for their proper operation and consequently the share of electricity is increasing

rapidly than total primary energy generation/supply. World total final consumption (TFC) by fuel was 9,384 metric tons oil equivalents (MTOE) in 2015 and by 2040 it will be 10,706 MTOE [1]. World net electricity generation increases by 45%, rising from 23.4 trillion kilowatt hours (kWh) in 2015 to 34.0 trillion kWh in 2040 [2]. World net electricity generation increases 69% by 2040, from 21.6 trillion kilowatt hours (kWh) in 2012 to 25.8 trillion kWh in 2020 and 36.5 trillion kWh in 2040.

The great outdoor (TGO) gymnasium company in United Kingdom (UK) has been generating electrical energy through playing and exercise by using energy generating gymnasium equipment (EGGE) and has installed green energy generating fitness machines at Sir George Monoux College, Trafalgar Square, and the Green Heart in Hull city [3, 4]. TGO Company has launched outdoor gymnasium machines, which offer a cardiac workout and generate electricity, and has upgraded the Cross Trainer, Recumbent Bike, Spinning Bike, and Hand Bike to green energy gymnasium equipment that generates on average 50-100 watts each depending on the fitness of the user [3]. A generator is connected to these machines in such a way as the circular rotation of the front wheel rotates the coils of wires inside the generator between the poles of the magnets [5]. These machines generate electricity from their rotating parts, which lead the authors towards an idea of extracting energy from gymnasium machines that do not exhibit rotating motion but have linear moving parts.

This research presents a possibility of electricity generation from linear motion of Pull-down machine whenever the user applies force on it by expending energy. Solar energy is converted into chemical energy by plants and this chemical energy is stored in human body by consuming plants as shown in Fig 1.The conversion of this stored chemical energy in human body into the electrical energy is the focus of this research. Solar radiation is an ultimate source for generating renewable, sustainable, and environmentally friendly energies. There are various ways of harvesting and using solar energy for fulfilling the energy needs of the modern society. Solar energy arrives at planet earth through radiation and photosynthesis is the process to bring and spreads solar energy into the living system through food chain and food web. Plants and algae like cyanobacteria convert light energy into chemical energy through photosynthesis naturally, which can be later released and used as an energy source by these organisms to fuel their activities. The converted chemical energy is stored in the form of carbohydrates such as sugars, which are synthesized from CO_2 and water. The process of photosynthesis not only generates fuel but it also releases
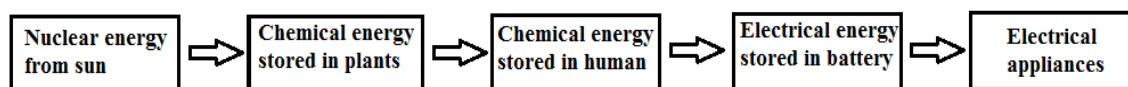
Figure 1. Human body converts solar nuclear energy into electrical energy

oxygen as a by-product. The benefits of mimicking the process of photosynthesis can benefit living organisms on earth twofold. There are producers and energy converter in this natural cycle in which producers make food (glucose) by using water and sun light. Human consumes this food and chemical energy of this food, which is converted into mechanical energy whenever some useful work is done, and this mechanical energy can be converted into electrical energy with the help of the energy generating gymnasium machines (EGGM). Energy generating gymnasiums will be the places in future where

electrical energy can be harvested from renewable (non-conventional) energy resources (human beings).

2. Classification of Energy Resources

Generally, the energy resources have been classified as "conventional and renewable energy resources (non-conventional)".

2.1 Conventional Energy Resources

These energy resources includes fossil oil, natural gas, coal and some metals like uranium and plutonium. Conventional energy resources remain fixed in nature. According to world energy council [6], *Fossil oil* remained the world's leading fuel, accounting for 32.9% of global energy consumption and roughly 63% of oil consumption comes from the transport sector. *Natural gas* is the second largest energy source in power generation, representing 22% of generated power globally. *Coal* still provides around 40% of the world's electricity and Asia presents the biggest market for coal and currently accounts for 66% of global coal consumption. Kazakhstan is the world's leading producer of *uranium.* Global uranium production increased by 40% between 2004 and 2013.

2.2 Renewable Energy Resources

These are resources of energy which regenerate themselves naturally after specific time interval and will never come to an end. *Hydro power* is the leading renewable source for electricity generation globally, supplying 71% of all renewable electricity at the end of 2015 and undeveloped potential is approximately 10,000 Tara watt hour per year (TWh/y) worldwide [6]. Global *wind* power generation capacity reached 432 Giga watt (GW) in 2015, around 7% of total global power generation capacity (420 GW onshore, 12 GW offshore). Global installed capacity for *solar*-powered electricity has seen an exponential growth, reaching around 227 GW at the end of 2015, producing 1% of all electricity used globally. Global output of *Geothermal* is estimated to be 75 TWh for heat and 75 TWh for power, but is concentrated on geologic plate boundaries [6].

Adenosine Triphosphate (ATP) is a source of energy which is stored in human muscles and available for muscles movements. Hence any movement that is last longer than a few seconds more ATP is produced in human body. Presented research suggests that ATP possessed by human body is a source of renewable energy and may be converted into electrical energy. ATP is regenerated by addition of a phosphate group to adenosine di-phosphate (ADP) in human body [7, 8]. Energy is required when the phosphate bond is formed with ADP which

Figure 2. Energy released for cell metabolism

results in ATP and this ATP stores in human body. When phosphate group is removed the ATP breaks apart and releases its energy and becomes ADP, the ATP – ADP cycle is a revolving door [9]. ADP utilizes energy and gains an extra "p" and is recharged back to ATP [10]. Cell's energy currency-ATP, is a bigger molecule consisting of five smaller

units *i.e.*, adenine, ribose, and three phosphate groups which are shown in Fig 2. Catabolic reactions in human cell provide energy to phosphorylate ADP into ATP. In a catabolic reaction large molecules are broken down into small ones and release energy. ATP cycle is synchronized with transfer of energy from catabolic to anabolic pathways [11]. ATP contains more energy than ADP because it has more bonds. Energy is necessary to produce
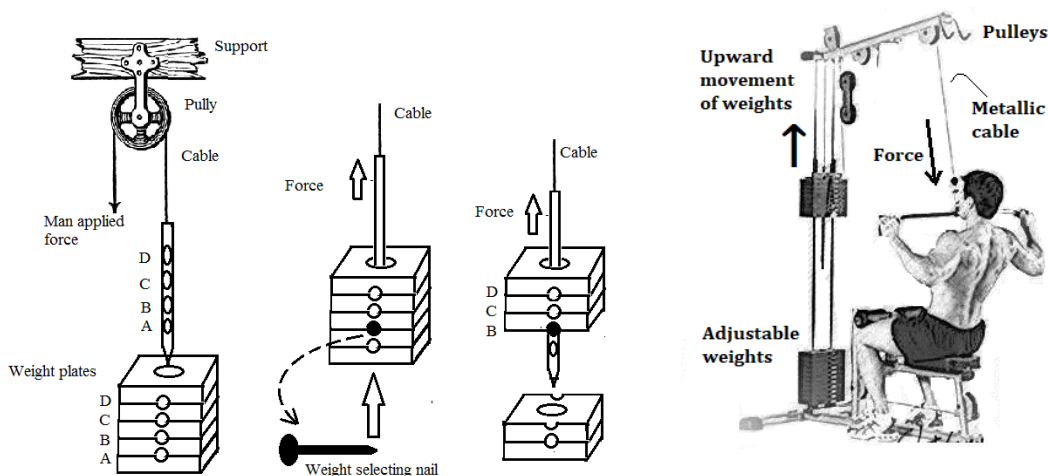
Figure 3. Working principle of pull-down machine

physical movement, maintain body temperature and metabolic activities. Human body has three systems to produce ATP [12].

1) ATP-PC (phosphocreatine System) - High power short duration
2) Glycolytic system - Moderate power/ moderate duration
3) Oxidative system - Low power/ long duration

First two are anaerobic systems; it means oxygen is not required to produce ATP. Last one oxidative system is aerobic which requires oxygen for ATP production. In ATP-PC system, movements last about 5 to 15 seconds, such as power movements, jumps and throwing ball, which can be done by the ATP stored in the muscles [13]. ATP-PC system produces energy very quickly but not over a long duration. Next energy domain shifted to glycolytic system, in this system ATP is generated by a process called as Glycolysis in which rapid break down of carbohydrates into glucose occurs. The generated amount of Glucose constantly circulates in the human blood. Glycolytic system produces energy quickly however again not for a long duration. Oxidative system involves the use of oxygen, fats, carbohydrates and sometimes proteins for resynthesizing ATP. This system produces far more ATP than either of the energy systems however it produces the ATP much more slowly.

3. Proposed Work

Energy demand is ascending day by day and humankind is exploring new ideas and resources from where they can extract any form of energy. Biomass energy is created by the combustion or biochemical conversion of an organic matter to be used for fuel. Some of organic materials used as a source for biomass energy include wood, sawdust, grasses, corn, sugarcane, and farm waste (cow manure). The processes for converting biomass into

energy are numerous, which are: combustion process, co-firing process, thermal conversion, gasification, pyrolysis, chemical conversion, biomass oil, fermentation process, and torrefaction. This research will discuss a method in order to harvest energy from biomass. In the proposed method, human will act as a device or machine for converting biomass energy into electrical energy. The device which converts one form of energy into another form of energy is called a transducer, so human could be considered as a transducer.

A person gains calories from food and performs activities of daily life, however excess of calories, unbalanced diet and extra fats make him unhealthy. Gymnasiums are the place where different types of machines are available to perform exercises like running, weight lifting, and muscles building in order to burn the excess of calories and fats. There are specified machines to perform exercise of a particular portion of human body *e.g.,* cable preacher curl, close grip bar curl, barbell curl, and dumbbells lifting are some exercises for biceps. Chest exercises include barbell bench press, flat bench dumbbell press, low inclined barbell bench press, seated machine bench press, etc. As the demand of energy is increasing day by day, it is essential to invent new ways and techniques to produce energy within a small area which may be a gymnasium or home. Most of cardiovascular machines in gymnasiums are made of cables and pulleys and these machines are the main focus of this research, because these machines can contribute in harvesting energy. During exercise, persons apply force on machines and expend energy to do some work. This expenditure of energy may be converted in other form of energy *e.g.*, in the form of electrical energy. It is possible to construct gymnasium machines that can convert and store expended energy by the users into electrical energy throughout the exercise [14, 15].

3.1 Working Principle of "Pull-down" Machine

Pull-down machine consists simply of weights, pulley, and a metallic cable rolled over pulleys. One end of the cable is attached to adjustable weights via a metallic rod and the other end is free to apply force by the user in order to lift the weights in upward direction. Pull-down machine is also known as "cable and pulleys" which is a multipurpose machine used to exercise for multi joints, biceps, triceps, shoulder, and legs. The working principle of the pull-down machine is mentioned in Fig 3, in which weights are selected by inserting a pin into specific cavity *i.e.,* A, B, C, or D. If the pin entered into the cavity 'B', three upper most weights will be selected and lifted up for the purpose of exercise.

3.2 Pull-down Machine as an Energy Generating Device

The novelty of presented research is to explore the theoretical possibility to make "Pull-down" as an energy generating machine by

Figure 4. (a) Force on electrons under magnetic field in a conductor (b) Two conductor connected in parallel moving under the influence of magnetic field

modifying the structure of this machine. This machine can be made as an energy generating machine by installing a generator in it directly [16]. This research paper will propose a new

way of alteration in order to convert a pull-down machine into an energy generating machine. According to the Faraday's law of electromagnetic induction, it states that "electro motive force (e.m.f)/ voltage is induced in a conductor when it is moved under the influence of magnetic field and cut the magnetic lines or whenever a conductor is placed under changing magnetic field (flux), the voltage is induced in it". The magnitude of induced voltage is directly proportional to the rate of change of magnetic flux. The mathematical form of Faraday's law for a conductor which is moving under the influence of magnetic field is:

$$e_{ind} = \left| \frac{d\phi}{dt} \right| \tag{3.1}$$

where e_{ind} is induced voltage and $\frac{d\phi}{dt}$ is the rate of change of magnetic flux linkage. Voltage induced due to motion of conductor is known as motional e.m.f. Authors used the basic principles of physics & electronics to prove mathematically that electrical energy can be generated from the weights of pull-down machine.

3.3 Induced Voltage on a Conductor Moving in a Magnetic Field

When a piece of wire with proper orientation is moved with velocity "V" through a magnetic field "B", according to Faraday's law of electro-magnetic induction, voltage will be induced in it and the amount of this voltage will be equal to the rate of change of magnetic flux. The expression for induced voltage in a piece of wire is given below:

$$e_{ind} = (V \times B) \bullet L \tag{3.2}$$

The angle between vectors V & B is 90° and the angle between "L" & "V×B" is zero. The direction of resultant vector of cross product is upward, therefore the voltage on the conductor will be built up with positive at the top and negative at the bottom as represented in Fig 4(a).

$$e_{ind} = (VBsin\theta)Lcos\theta$$
$$e_{ind} = (VBsin90)Lcos0$$
$$e_{ind} = VBL \tag{3.3a}$$

The above expression of induced voltage can be derived by Faraday's law. Let the conductor travel a distance of "$V.dt$" in a very short interval of time "dt" and gain a new position which is shown by dotted lines in Fig 4(a). The magnetic flux "$d\phi$" cut by conductor during time "dt" will be equal to the product of area swept by the conductor and the magnetic flux density "B".
$d\phi = (Area\ swept\ by\ conductor)B$
$\Rightarrow d\phi = (L.V.\ dt)B$
The rate of cut/change of magnetic flux will become:

$$\frac{d\phi}{dt} = VBL \tag{3.3b}$$

Conductor is moving perpendicular to the magnetic field, therefor magnetic force acting on a single negative charge (electron) will be in downward direction. Therefore, the charge will be separated in the conductor because the upper end will become positively charged and the lower end will become negatively charged, resulting in a potential difference. The

"ϕ" is the magnetic field and "B" is the magnetic field density which is magnetic flux per unit area. Electric field lines travel from the positive end to the negative end are represented by "E", the force on electron due to E is "F_E", "q" is the charge on electron and the magnetic force on electron is "F_B". Maximum potential difference occurs at the equilibrium state when both forces are equal. Conductor is moving perpendicular to the magnetic field so $\theta = 90^o$ and forces on a charge particle are given below:

$$F_B = qVBsin\theta = qVB \tag{3.4}$$

$$F_E = qE \tag{3.5}$$

At equilibrium state, F_E becomes equal to F_B:

$$E = VB \tag{3.6}$$

Potential difference induced at end points will be:
$V_{ab} = V_b - V_a = EL$

$$V_{ab} = VBL \tag{3.7}$$

Above expression is the *motional e.m.f* , which will be induced in a single conductor. If there are 2 conductors connected in parallel as shown in Fig 4(b), the induced voltage at its ends "a_2" & "b_2" will also be "*VBL*". However current produced due to induced e.m.f will increase by two times. Similarly, for "N" conductors, the induced current will increase by "N" times, but the voltage will remain constant.

3.4 Modification in Weights of Pull-down Machine

Weights of the machine are supposed to be winded with a laminated copper wire. Winding will be made in such a way that the conductors of copper will remain perpendicular to the applied magnetic field. Winding on each weight will be in the form of
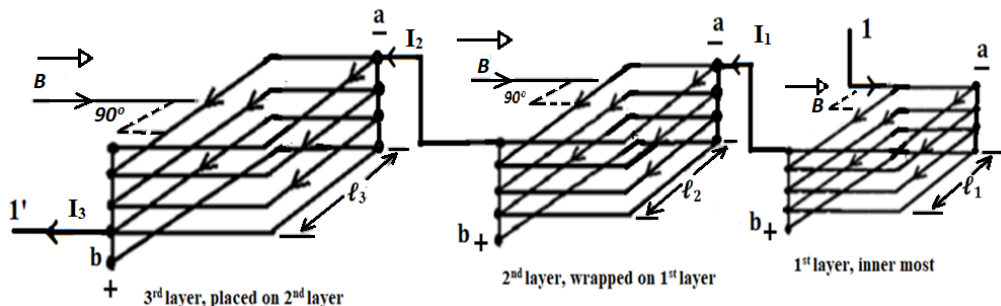
Figure 5. Induced current in 3 layers (parallel combination) windings on a single weight
layers *e.g.,* the 1st layer of winding will be on the weight surface, when all surfaces of the weight are covered, and then a 2nd layer will be made on the surface of the 1st layer. After completion of the 2nd layer, the 3rd layer of turns will be wrapped on the second layer and so on. All three layers should be connected in series so that voltage induced by all layers

will add up cumulatively. Suppose a single weight (upper most) says as "w_1" having the inner most layer of conductors in which 4 conductors are on left and 4 conductors are on right side, so there are total of 8 conductors connected in parallel with each other. Let "w_1" have 3 layers and every layer consists of 8 parallel connected conductors.

There will be different lengths of conductors for each layer such as $\ell_3 > \ell_2 > \ell_1$ because these conductors are wrapped in the form of layers and all the layers are connected in series as shown in Fig 5. It is obvious that there are 8 numbers of conductors for each layer, however practically these numbers of conductors can vary for each layer. For the 1st layer, 8 laminated conductors are connected in parallel circuit arrangement ($N_1 = 8$) therefor the total perpendicular length of the conductor will become $8l_1$. Similarly if the 2nd layer has N_2 perpendicular conductors with total perpendicular length of N_2l_2 and the 3rd layer will have total of N_3l_3 perpendicular length to the magnetic field. All conductors of each layer will be short circuited at point "a" & "b" so that conductors will be in parallel circuit arrangement. In parallel circuit arrangement, there will be the same voltage on each conductor within a layer *e.g.*, all conductors of the 1st layer will have the same induced voltage however the current will be added up. Total induced current taken from 3 layers will be:

$$I_{W1} = I_1 + I_2 + I_3 \qquad (3.8)$$

3.5 Magnetic Field

An electro magnet or a permanent magnet will be used for magnetic field. Electro-magnet will be made by winding copper wire on a soft iron core and two ends of winding will be connected to a permanent D.C supply. Magnetic poles are placed around the weights of the machine as presented in Fig 6. Magnetic field lines travel from the North pole to the South pole, and they become perpendicular to the length of conductors which are present at the left and right sides of weights.

3.6 Induced Voltage

When these winded weights of the machine are lifted up by the user, the conductors which are perpendicular to the magnetic field will cut the magnetic field. According to Faraday's Law, electro-magnetic induction e.m.f

Figure 6. Pull-down machine as an energy generating machine having copper winding in on each weight

will be induced in these conductors. Upward movement of weights is due to the external force applied by person and downward movement is due to gravity. As long as the exercise of lifting weights continues, the induction of e.m.f will also continue and reverse its polarity according to the direction of motion (upward or downward). Fig. 6 shows that 3 weights are selected to perform exercise. Two ends of winding of the upper most weight, the 2nd weight, and the 3rd weight are marked as 1 & 1', 2 & 2'; and 3 & 3', respectively. During upward motion of the weight, it is assumed that left ends of winding of all weights will become positive and right ends of windings will become negative. When weights move

freely under the influence of gravity in downward direction, the polarity marks on the ends of windings will be reversed.

3.7 Calculations of Induced e.m.f

Let "ϕ" be the magnetic field and "B" is the magnetic field density which is magnetic flux per unit area (B = ϕ/A). F_{ext} is the external force which is applied by the user on the weights to lift them up with velocity "V" in upward direction. In order to calculate "e_l" that is the induced voltage from w_l, it is necessary to add up induced voltages from all the layers of w_l. The motional e.m.f induced in the 1st and 2nd layers is given below:

$$e_{L1} = N_1 \ell_1 VB \tag{3.9a}$$

$$e_{L2} = N_2 \ell_2 VB \tag{3.9b}$$

As it is mentioned in Fig 5 that all layers are connected in series therefor the induced voltage of all layers will be added up. Suppose that w_l contains "m" number of layers that are connected in series, and then the total induced voltage between the two ends 1 &1' will be:

$$e_1 = \sum_{i=1}^{m} (N_i . \ell_i . B . V) \tag{3.10}$$

3.8 Electrical Current

Practically winding on weights has some resistance "R" in it. If "I_{w1}" is the total output current flowing from interval A to B (Fig 6) from "w_l" and total induced motional e.m.f in w_l is "e_l" [17]:

$$I_{w1} = \frac{e_1}{R} \tag{3.11}$$

3.9 Mechanical Input Power

When torque is applied on the pulley by external force, the pulley rotates. As applied force is increased torque in pulley will also increase. The amount of mechanical power supplied by the user is converted to the electrical form that is given by the following equation:

$$P_{in} = Force \times Velocity = FV \tag{3.12}$$

With respect to angular velocity of pulley, the power supplied is
$P_{in} = (Torque\ in\ pulley)(Angular\ velocity\ of\ pulley)$

$$P_{in} = \tau . \omega \tag{3.13}\ [6]$$

By comparing equation (3.12) & (3.13) gives rise to:

$$F.V = \tau.\omega \tag{3.14}$$

If "r" is the radius of pulley, equation (3.14) is changed by multiplying "r" on both sides:

$$r(F.V) = \tau.r\omega \tag{3.15}$$

In circular motion, the relation between linear and angular velocity is V= r. ω, so equation (3.15) becomes:

$$r.F = \tau \tag{3.16}$$

This is the amount of torque which induces e.m.f in a pull-down machine.

3.10 Electrical output power

If "R" is the resistance of winding of selected weight, the output electrical power from a single weight (say w_1) will be:

$$P_{out} = e_t\,I_{w1} - I_{w1}{}^2 R \tag{3.17}$$

Electrical output power will always be less than the mechanical input power due to friction, heat, and electrical losses.

4. Scope of EGGS

The concept of energy generating gymnasium system (EGGS) has a great scope in developing countries where youths are becoming more fitness conscious [18]. Solar and wind power generation are the most famous renewable energy resource among the energy consumers. In this research, authors are describing another energy generating source which is definitely renewable, and this energy source is human itself [14]. The fundamental idea of EGGS is shown in Fig 7, in this system the energy generating gymnasium machines (EGGMs) are figured as M_1 to M_4. These EGGMs supply power to A.C and D.C appliances within the gymnasium building. EGGS will be very beneficial for those people who are running the gymnasium business. The gymnasium owners could be able to cut down the electricity expenses and get free energy (electrical energy) from the users who come in gymnasium for exercise. So, the owners would be able to get double benefits. One is receiving money in the form of fee and second one is to enjoy free energy. Normally, a gymnasium runs 16 hours per day. However, for a crowded area, a gymnasium may be opened for 24 hours a day. So, the output of all the gymnasium machines will give a bulk amount of electrical energy. The excessive electrical energy can be sold back to the utility [19]. Smart grid system which is evolving for the power delivery in the 21st century enables the customer to sell excess of electric energy from distributed energy sources (DES) back to the utility via micro grid (MG). MG is a small grouping of interconnected power generation and control technologies, which can operate within or independent of a central grid and increasing system reliability. By enabling the integration of distributed generation (DG) such as wind and solar, these systems can be more flexible than traditional grids.

EGGS will be taken as a new distributed power generating source in the field of renewable energy resources.

5. Conclusions

In the proposed theoretical model, it is concluded that the expended energy by people during exercise in gymnasium in order to burn their calories to achieve their desired fitness level can be converted and stored in batteries in the form of electrical energy. EGGS are very beneficial for the gymnasium owners, because this system would make the gymnasium independent in the energy production. The energy harvested from EGGM will be green, clean, eco-friendly, and renewable. Distributed EGGS in all over the world will definitely play an important role in business and pay its share in renewable and sustainable energy resources.

6. Summary

The main idea behind the research is to make electricity from men power and then store this electrical energy in D.C batteries. Presented research theoretically suggests that the energy spent in gymnasium should be converted into electrical energy, for this purpose gymnasium machines are modified into EGGM by using copper windings and magnets. Whenever these machines are operated, the human exerted energy is then utilized to charge batteries. Excess of energy could be sold back to the national utility through MG. Man takes his energy from food which is stored in human body in the form of ATP. During different types of exercises ATP-ADP conversion is also presented.
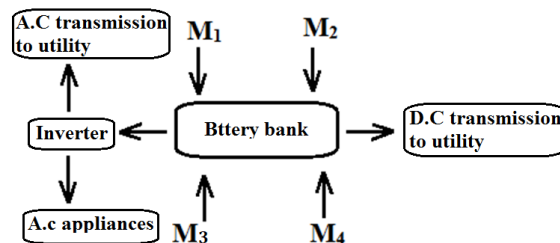
Figure 7. Block diagram of EGGS

Acknowledgement

CONFLICTS OF INTEREST

The authors declare that there is no conflict of interests regarding the publication of this paper.

REFERENCES

[1]   International Energy Agency. (2017). Key world energy statistics. https://www.iea.org/publications/freepublications/publication/KeyWorld2017.pdf (last accessed on October 7, 2018).

[2]   U.S. Energy Information Administration (EIA). (2017). International Energy Outlook 2017. https://www.eia.gov/outlooks/ieo/pdf/0484(2017).pdf (last accessed on October 7, 2018).

[3]   The Great Outdoor Gym Company. (2018). Green Energy. http://www.tgogc.com/Green-Energy.html (last accessed on October 7, 2018)

[4]   The Great Outdoor Gym Company. (2018). Lumi Plus. http://www.tgogc.com/Products/TGO-Energy-Play...-Coming-Soon/Lumi-Plus.Html?cPath=7_175 (last accessed on October 7, 2018).

[5]   Strzelecki, R., Jarnut, M., and Benysek, G. (2007). Exercise bike powered electric generator for fitness club appliances. In: *Proc., Power Electronics and Applications, 2007 European Conference on*, IEEE, pp: 1-8.

[6]   World Energy Council. (2016). World Energy Resources 2016. https://www.worldenergy.org/wp-content/uploads/2016/10/World-Energy-Resources-Full-report-2016.10.03.pdf (last accessed on October 7, 2018).

[7]   Verma, P. S., V. K. Agarwal, and P. S. Verma. (2007). *Cell biology, genetics, molecular biology, evolution and ecology*. S. chand & Company Limited.

[8]   Herman, I.P. (2016). *Physics of the Human body*. Springer.

[9]   Manoj, K.M. (2007). Mitochondrial oxidative phosphorylation: Debunking the concepts of electron transport chain, proton pumps, chemiosmosis and rotary ATP synthesis, *arxiv preprint arxiv: 1703.05826*.

[10]   DuPlesis, S.S, Agarwal, A. Mohanty, G., and Vander Lind, M. (2015). Oxidative phosphorylation versus glycolysis: What fuel do spermatozoa use? *Asian journal of andrology*, 17(2), 230.

[11]   Martin, W.F, Thauer, R.K. (2017). Energy in ancient metabolism. *Cell*, 168(6), 953-955.

[12]   Lodish, H. Berk, A. Matsudaria, P. Kaiser, C.A, Krieger, M. Scott, M.P, Zipursky, S.L, Darnell. (2004) *Molecular cell biology* (5th ed). New York.NY:W.H. Freeman.

[13]   Gustin, P.B. (2001). Energy system interaction and relative contribution during maximal exercise. *Sports medicine*, 31(10), 725-741.

[14]   Bidwai, M.S, Jaykar, M.A. and Shinde, M.S. (2017). Gym Power Station: Turning Workout into Electricity. *International Research Journal of Engineering and Technology (IRJET)*. 4(03), 424-426.

[15]   Borchate, S., Gaikwad, A., Jadhav, A., Dhage, P. (2017) Design of Treadmill to Generate Electricity by using Mechanical Energy. *International Conference on Ideas, Impact and Innovation in Mechanical Engineering (ICIIIME 2017)* 5 (04), 498-505.

[16]   Bonde, V.S., Khatake, B.V., Zambare, D.V., Patel, V.D., Kadam, N.V. (2018). Electric Power Generation from Gym Equipment with Polarity Checker and Changer Circuit. *International Journal for Scientific Research & Development*, 5(02), 992-995.

[17]   Chapman, S.J. (2005). *Electric Machinery Fundamentals* (4th ed). New York, NY: McGraw-hill.

[18] Gaurav, H., Nikhurpa, K.S., Chaudhary, D., Feroz, W. (2015). Energy harvesting through smart gym. In Proceedings of *National Conference on "Emerging Trends in Electronics & Communication" (ETEC-2015), 1(02), 37-42.*

[19] Kumar, M., Mundada, G.S. (2017). Energy Harvesting from Gym Equipments. *International Journal of Innovative Research in Electrical, Electronics, Instrumentation and Control Engineering.* 5 (07), 127-131. DOI 10.17148/IJIREEICE.2017.5721

Special Cases during the Detection of the Hook Style Energy Theft in Overhead Low-Voltage Power Grids through HS-DET Method – Part 1: High Measurement Differences, Very Long Hook Technique and "Smart" Hooks

Athanasios G. Lazaropoulos[*]

School of Electrical and Computer Engineering / National Technical University of Athens / 9 Iroon Polytechniou Street / Zografou, GR 15780

On the basis of [1], this pair of companion papers investigates the possibility of jamming the method of the detection of the hook style energy theft (HS-DET method) that can be used for the detection of the hook style energy theft in the overhead low-voltage (OV LV) power grids. The three main suspicious issues that have been identified in [1] are further investigated in this paper. The robustness of the HS-DET method against these issues is assessed by using percent error sum (PES) submetrics, appropriate contour plots and a new proposed robustness PES submetric against the hook style energy theft of HS-DET method.

1. Introduction

A portfolio of Broadband over Power Lines (BPL) applications, such as Topology Identification Methodology (TIM) [2], Fault and Instability Identification Methodology (FIIM) [3], methodology to preserve power system stability [4], [5] and main line fault localization methodology (MLFLM) [6]-[8], have already been discussed. In earlier published literature [1], the hook style energy theft detection method (HS-DET method) has been proposed and added in the aforementioned broadband application portfolio thus contributing towards a more accurate and more reliable monitoring, metering and controlling of distribution power grids.

HS-DET method is based on the hybrid model [9]-[26] while HS-DET method output is expressed in terms of appropriate percent error sum (PES) submetrics and contour plots. As the hybrid model is concerned, it consists of two interconnected modules, namely: (i) the bottom-up approach module; and (ii) the top-down approach module. The channel attenuation, that is one of the provided outputs of the hybrid method for given OV LV BPL topology and BPL operation frequency range, is further processed by the HS-DET method so that PES metrics can be produced. Depending on the values of the PES metrics, the decision regarding the existence of hook style energy theft in

60

overhead low-voltage (OV LV) BPL networks can be made. On the basis of PES metrics, the impact of different hook characteristics, OV LV BPL topologies and different intensities of measurement differences can be expressed in terms of appropriate contour plots [1].

In accordance with [1] and if all the other problematic cases, which concern the operation of the OV LV power grid and described in [2]-[8], are excluded, HS-DET method can safely detect hook style energy thefts that may occur across the OV LV BPL networks. As indicated in [1], safe decisions concerning the existence of energy theft or not can be made regardless of the examined OV LV BPL topology, the intensity of the measurement differences and the hook characteristics. However, three critical issues have been recognized during the numerical result section of [1] that may jam HS-DET method and need further examination in order to assess the extent of jamming that may create. With reference to [1], these three special cases are: (i) the existence / definition of the threshold of the intensity of measurement differences that may occur / be produced by external sources above which HS-DET method starts to give faulty decisions concerning the existence of hook style energy theft; (ii) the possibility of the installation of very long hooks in order to mask the hook existence during the application of HS-DET method, which is anyway a broadband technique; and (iii) the use of "smart" hooks that are matched to the characteristic impedances of the lines in order again to cover the energy theft. In the following sections, the mitigation efficiency of HS-DET against these three special cases will be assessed either in theoretical or in numerical terms via theoretical analysis, PES metrics and contour plots.

The rest of this paper is organized as follows: In Section 2, a brief synopsis of HS-DET method and its PES metrics is given. Also, the theoretical basis is presented in order to cope with the three examined special cases. In Section 3, numerical results and discussion are provided, aiming at practically evaluating the extent of jamming to HS-DET method that may create the three examined special cases as well as the possibility of masking the hook style energy theft exists. Section 4 concludes this paper.

2. HS-DET Method Synopsis

2.1 Measurement Differences

As already been mentioned in [1], the measurement differences that are used during the BPL simulations describe the significant differences that may occur between experimental measurements and theoretical results. Anyway, the mathematical consideration of the measurement differences remains a well-defined straightforward process, since the total measurement difference can be conveniently assumed to follow continuous uniform distribution (CUD) with minimum value $-a_{\mathrm{CUD}}$ and maximum value a_{CUD} [2], [6]-[8], [27]. On the basis of the CUD measurement difference $e\{\cdot\}$, the measured coupling scheme transfer function $\overline{H^{\mathrm{c}}}\{\cdot\}$ for given coupling scheme can be determined by

$$\overline{H^{\mathrm{c}}}(f_i) = H^{\mathrm{c}}(f_i) + e(f_i), \ i=1,\dots,u \tag{1}$$

where $H^{\mathrm{c}}\{\cdot\}$ is the theoretical coupling scheme transfer function, $f_{i}, i=1,\dots,u$ denotes the measurement frequency, u is the number of subchannels in the examined frequency range and $e(f_i)$ synopsizes the total measurement difference in dB at frequency f_i. Note that the theoretical coupling scheme transfer function is among the outputs of the hybrid method

and depends on the examined MTL configuration, OV LV BPL topology and the applied coupling scheme [9], [12], [15], [17]-[19], [28], [29].

2.2 Impact of the Hook Insertion

With reference to Fig. 2(b) of [1], each hook is characterized by: (i) its length L_{bh}; and (ii) its distance $D_h = L_h + \sum_{i=1}^{k-1}(L_i)$ from the transmitting end. To facilitate the application of the hybrid method, the hook termination is assumed to be: (a) open circuit; (b) fully interconnected with the distribution lines (*i.e.,* hook derivation points at the same distance from the transmitting end on all the three phases); and (c) horizontal. The aforementioned three assumptions concerning the hook insertion permit its handling as branch from the hybrid method.

Apart from the hook characteristics and hook assumptions, a set of settings regarding the OV LV BPL topology operation should be taken under consideration as usually. More specifically, the topological characteristics of the indicative OV LV BPL topologies of Table 1 of [1] as well as a set of assumptions concerning the transmission and propagation of the BPL signal and the circuital parameters that are detailed in [9], [10]-[17], [19], [21], [30]-[34] are again assumed in this paper.

Obviously, the hook insertion modifies the original OV LV BPL topology to the respective modified one thus influencing the determination of coupling scheme transfer functions. With reference to eq. (1) and [1], $H_{or}^C\{\cdot\}$ and $H_{mod}^C\{\cdot\}$ are the original and modified theoretical coupling scheme channel transfer functions, respectively, while $\overline{H_{or}^C}\{\cdot\}$ and $\overline{H_{mod}^C}\{\cdot\}$ are the original and modified measured coupling scheme channel transfer functions, respectively. Note that it is assumed that the measured coupling scheme transfer function of original and modified end-to-end OV LV BPL topologies suffers from the same total measurement differences.

2.3 PES Submetrics of HS-DET Method and Special Cases

PES submetrics define the cornerstone metrics of HS-DET method. However, PES submetrics are not the first time that are used by BPL applications since they have already been used in TIM [2], FIIM [3], power system stability methodology [4], [5] and MLFLM [6]-[8] in order to assess the approximation accuracy of the original and modified coupling scheme transfer functions. With reference to eq. (1) and Sec. 2.2, the PES submetrics that are used in this paper are:

$$\overline{PES}_{or} = 100\% \cdot \frac{\sum_{i=1}^{u}\left|\overline{H_{or}^C}(f_i) - H_{or}^C(f_i)\right|}{\sum_{i=1}^{u}\left|H_{or}^C(f_i)\right|} \tag{2}$$

$$\overline{PES}_{mod} = 100\% \cdot \frac{\sum_{i=1}^{u}\left|\overline{H_{mod}^C}(f_i) - H_{or}^C(f_i)\right|}{\sum_{i=1}^{u}\left|H_{or}^C(f_i)\right|} \tag{3}$$

where $\overline{PES}_{or}$ and $\overline{PES}_{mod}$ assess the accuracy of the original measured coupling scheme channel transfer function and modified measured coupling scheme channel transfer functions, respectively, in relation with the original theoretical coupling scheme channel transfer function. With reference to eqs. (2) and (3), the main PES submetric of HS-DET method is the difference between the original measured coupling scheme channel transfer function and modified measured coupling scheme channel transfer functions, say

$$\overline{\Delta PES} = \overline{PES}_{mod} - \overline{PES}_{or} \tag{4}$$

On the basis of $\overline{\Delta PES}$, appropriate contour plots can be plotted so that the detection ability of the HS-DET method can be assessed with respect to the hook length and the distance from the transmitting end [1].

In accordance with [1] and if all the other problematic cases, which concern the operation of the OV LV power grid and described in [2]-[8], are excluded, HS-DET method can safely detect hook style energy thefts through $\overline{\varDelta PES}$. Actually, the definition of $\overline{\varDelta PES}$ implies that the larger part of measurement differences can be mutually mitigated. Since the role of measurement differences is typically eliminated, values of $\overline{\varDelta PES}$ above zero imply that modified measured coupling scheme channel transfer function is more different than the original measured coupling scheme channel transfer function with respect to the original theoretical coupling scheme channel transfer function. Greater values of $\overline{\varDelta PES}$ mean greater differences between the modified and the original OV LV BPL topology and, thus, a safer decision regarding the existence of an energy theft can be secured.

Although the vast majority of the serious problematic cases can be detected through the aforementioned set of BPL broadband applications, small differences can occur during the computation of the coupling transfer functions due to secondary reasons such as temperature, wind, humidity, etc. These small differences can cause false energy theft alarm. Hence, a threshold for $\overline{\varDelta PES}$ should be assumed so that the likelihood of false energy theft alarm due to secondary reasons can be reduced without jeopardizing the performance of HS-DET method. Since the measurement differences can be satisfactorily mitigated due to the definition of $\overline{\varDelta PES}$, a fixed percentage for all the examined OV LV BPL topologies can act as a proper $\overline{\varDelta PES}$ threshold (see Sec.3).

Although the theoretical framework of HS-DET method is well-defined and the assessment of the previous findings have been made in [1], three special cases have been identified that may foment the operation of HS-DET method. More specifically:

- *High measurement differences that may intentionally / unintentionally be produced can jam HS-DET method.* As already been mentioned, due to the definition of $\overline{\varDelta PES}$, $\overline{\varDelta PES}$ is almost invulnerable to the measurement differences since the larger part of them has already been mitigated. Hence, it is expected that even if high maximum values a_{CUD} are adopted, HS-DET method can still detect the energy theft through the positive values of $\overline{\varDelta PES}$ (but even safer above the $\overline{\varDelta PES}$ threshold). However, the robustness of the decision, that mainly depends on the intensity of measurement differences, should be computed; say, the degree of certainty. Robustness of the decision concerning the existence of energy theft is given by

$$\overline{Rob} = 100\% \cdot \frac{\overline{\varDelta PES}}{PES_{or}} \tag{5}$$

  This additional PES submetric that assesses the quality of the decision concerning the existence of energy theft demands high values. High values of $\overline{Rob}$ allow high margins of certainty.

- *The installation of very long hooks in order to mask the hook existence during the application of HS-DET method.* By misinterpreting the trends of Figs. 3-8 of [1], it can be mentioned that since $\overline{\varDelta PES}$ negatively depends on the hook length, very long hooks could jam HS-DET method. However, this assertion is not valid since MTL configurations such as of OV LV BPL topologies are analyzed on the basis of TL theory. This is going to be validated in Sec. 3.2.

3. Numerical Results and Discussion

The numerical results of this Section focus on assessing the performance of HS-DET method to successfully detect the potential energy theft when high measurement differences, which may intentionally / unintentionally be produced, and the installation of very long hooks or "smart" hooks occur. All these three special cases try to jam HS-DET method. For that reason, the robustness of decisions of HS-DET method is also evaluated.

3.1 High Measurement Differences and HS-DET Method Jamming

The influence of measurement differences of maximum value a_{CUD} up to 5 dB has been thoroughly discussed in [1] while the influence of measurement differences of maximum value a_{CUD} above 5 dB is here evaluated. For maximum values a_{CUD} below 5 dB, it has been verified that the stochastic nature of measurement differences mainly affects OV LV BPL topologies with branches. Also, on the basis of $\overline{\Delta PES}$ contour plots, the increase of the CUD maximum value of measurement differences negatively influences the performance of HS-DET method since a general reduction of $\overline{\Delta PES}$ values of contour plots is observed with the increase of maximum value a_{CUD}. However, HS-DET method successfully detected the energy theft in all the cases examined regardless of the CUD maximum value of measurement differences since $\overline{\Delta PES}$ values have been always greater than 0%. In this paper, the influence of high measurement differences (*i.e.,* measurement differences of maximum value a_{CUD} above 5 dB) is evaluated in this paper. In accordance with Sec. 2.3, the performance of HS-DET method against high measurement differences will be assessed in terms of $\overline{\Delta PES}$, $\overline{PES_{or}}$ and $\overline{Rob}$.

With reference to Fig. 2(b) of [1] and the indicative original OV LV BPL topologies as reported in Table 1 of [1], let assume that a hook of length L_{bh} is inserted at distance D_h from the transmitting end. In Fig. 1(a), $\overline{\Delta PES}$ is plotted with respect to the maximum value a_{CUD} when $L_{bh} = 5\text{m}$ and $D_h = 300\text{m}$ are assumed for the five indicative original OV LV BPL topologies. In Figs. 1(b) and 1(c), same curves with Fig. 1(a) are given but for $\overline{PES_{or}}$ and $\overline{Rob}$, respectively.
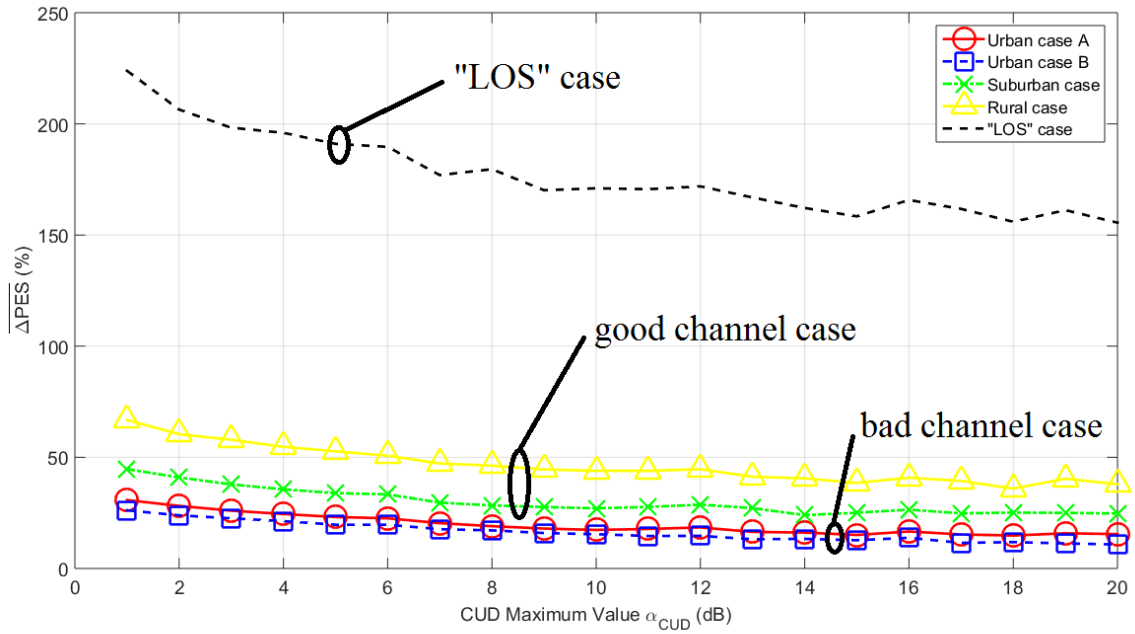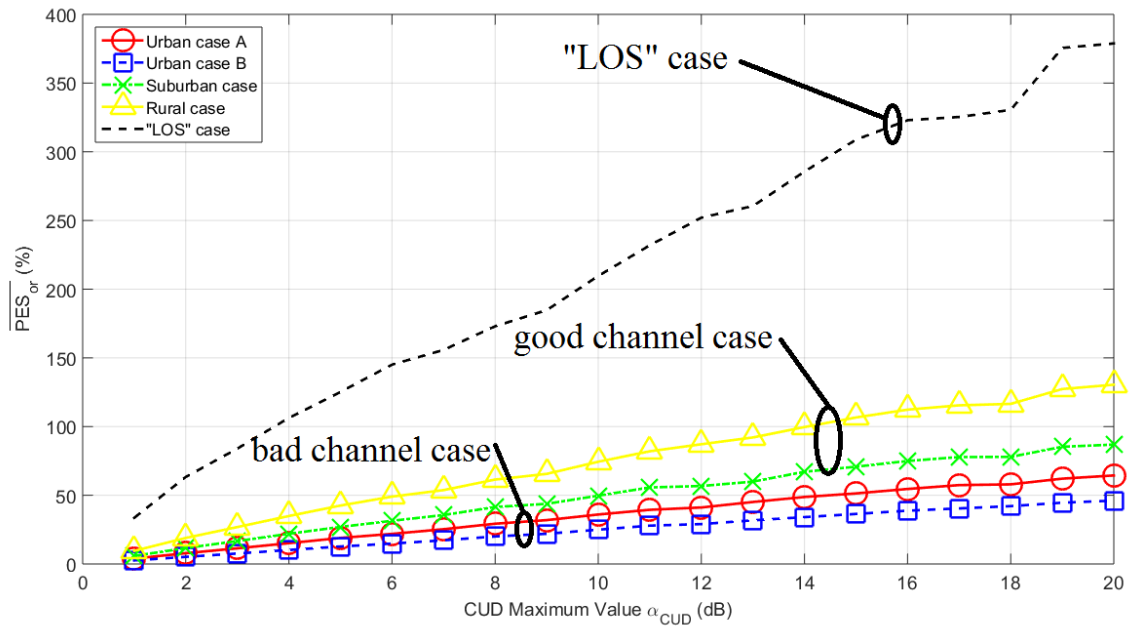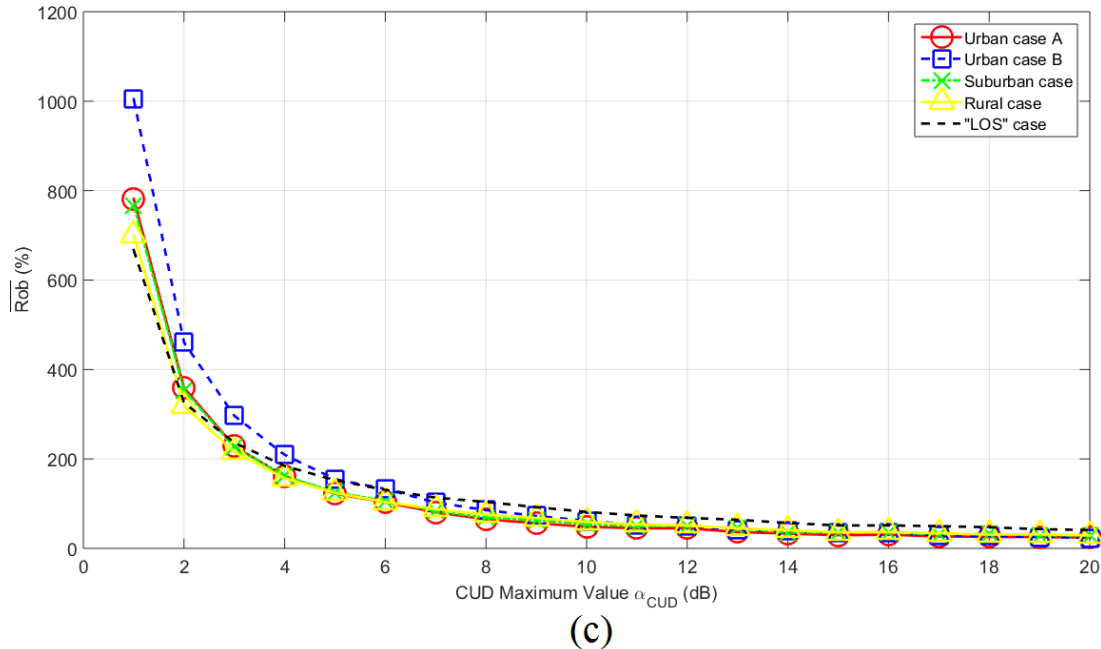
(a)

(b)

(c)

Fig. 1. PES submetrics of HS-DET method for the five original indicative OV LV BPL topologies of [1] when hook length of 5 m, hook distance from the transmitting end of 300 m and open-circuit hook termination are assumed for various maximum values a_{CUD}. (a) $\overline{\Delta PES}$. (b) $\overline{PES_{or}}$. (c) $\overline{Rob}$.

From Figs. 1(a) and 1(b), it is evident that $\overline{\Delta PES}$ and $\overline{PES_{or}}$ present similar results that clarify the impact of high measurement differences on the HS-DET method. Actually, three categories of OV LV BPL topologies can be defined, say:

- *"LOS" case*: Even if measurement differences of high maximum value a_{CUD} are considered, their impact on the performance of HS-DET method is anemic. In all the cases examined, $\overline{\Delta PES}$ remains over 150% thus indicating the easy detection of energy theft in OV LV BPL "LOS" case. Although $\overline{PES_{or}}$ of "LOS" case presents the highest values in comparison with the respective values of the other examined modified OV LV BPL topologies, HS-DET method can successfully mitigate the measurement differences and give a secure decision concerning the existence of energy theft.

- *Good channel case*: Good channel case consists of the suburban and rural modified OV LV BPL topologies. Although $\overline{\Delta PES}$ is significantly lower than the respective value of the "LOS" case, its value remains high enough to secure a decision concerning the existence of energy theft regardless of the maximum value a_{CUD}.

- *Bad channel case*: On the basis of $\overline{\Delta PES}$ of urban case A and B, this is the most difficult decision concerning the existence of power theft. $\overline{\Delta PES}$ receives low values but always positive. It is obvious that an arbitrary $\overline{\Delta PES}$ threshold concerning the strict decision about the existence of power theft can be estimated by the urban case B $\overline{\Delta PES}$ when the maximum value a_{CUD} of measurement differences is assumed to be equal to 20dB.

Note that in all the cases examined, $\overline{PES_{or}}$ is an increasing function with reference to the maximum value a_{CUD}. This is due to the fact the asymmetry between the modified and

the respective original OV LV BPL topology increases as more intense measurement differences are added.

Now, as the robustness of the decisions concerning the existence of energy theft is concerned, their robustness is examined in Fig. 1(c). As indicated in Fig. 1(c), the robustness mainly depends on the maximum value a_{CUD} rather than the examined OV LV BPL topology. High measurement differences create uncertainty that foments the robustness of the decisions. Very high measurement differences, which exceed 10 dB, obviously create great uncertainty that is reflected on low values of robustness. Similarly to the $\overline{\Delta PES}$ threshold, an arbitrary $\overline{Rob}$ threshold can also be defined by the $\overline{Rob}$ of the urban case B when maximum value a_{CUD} of measurement differences is assumed to be equal to 20 dB.

In numerical terms and in order to define the $\overline{\Delta PES}$ and $\overline{Rob}$ thresholds, $\overline{\Delta PES}$ and $\overline{Rob}$ values of the modified OV LV BPL topologies of Figs 1(a)-(c) are reported in Table 1 when maximum value a_{CUD} of measurement differences is assumed to be equal to 20 dB.

Table 1. $\overline{\Delta PES}$ and $\overline{Rob}$ of Indicative OV LV BPL Topologies when $L_{\text{bh}} = 5\text{m}$ and $D_{\text{h}} = 300\text{m}$ (open-circuit hook termination) for maximum values a_{CUD} equal to 20 dB

	Modified OV LV BPL Topology				
	Urban case A	Urban case B	Suburban case	Rural case	"LOS" case
$\overline{\Delta PES}$ (%)	15.47	10.80	24.73	37.90	155.55
$\overline{Rob}$ (%)	24.01	23.42	28.46	29.05	41.06

From Table 1, it is evident that HS-DET method can safely detect the energy theft even if the worst scenarios concerning the examined OV LV BPL topology and measurement differences are assumed. Also, a strict version of $\overline{\Delta PES}$ and $\overline{Rob}$ thresholds can be assumed to be equal to 10% and 20%, respectively. Finally, as it has been already recognized by Figs. 1(a)-(c), urban case B and "LOS" case define the worst and the best case regarding the energy theft detection in OV LV BPL networks when high measurement differences are assumed.

In order to understand the potential reader the strict version of $\overline{\Delta PES}$ and $\overline{Rob}$ thresholds as well as the safety that is provided, the impact of measurement differences during the computation of $\overline{\Delta PES}$, $\overline{PES_{\text{or}}}$ and $\overline{Rob}$ of the original indicative OV LV BPL topologies is given in the Appendix. Instead of a modified OV LV BPL topology with a hook, it is assumed that the modified OV LV BPL topology is the indicative OV LV BPL topology. It is proven there that the assumed $\overline{\Delta PES}$ and $\overline{Rob}$ thresholds are high enough in order not to active a fault energy theft alarm because of high measurement differences.

The high measurement differences, which are assumed in this paper, can be either intentionally or unintentionally occur. However, the HS-DET method is robust enough and can act as countermeasure technique in order to mitigate these measurement differences. If all the other problematic cases, which concern the operation of the OV LV power grid and described in [2]-[8], are excluded, HS-DET method can safely detect hook style energy thefts even though measurement differences up to 20 dB are assumed

due to the countermeasure character against measurement differences of HS-DET method (see the Appendix).

However, intentional measurement differences can be combined with other techniques in order to mask a potential hook style energy theft. In the following subsections, the installation of very long hooks (see Sec.3.2) and the use of "smart" hooks (see Sec.3.3) that are matched to the characteristic impedances of the lines are examined in order to jam HS-DET method when intentional measurement differences are produced.

3.2 Very Long Hooks and HS-DET Method Jamming

The influence of measurement differences of maximum value a_{CUD} above 5 dB has been presented in Sec.3.1. The installation of very long hooks is considered as one of the potential techniques against the energy theft detection. In this subsection, the detection performance of HS-DET method is investigated when the technique of very long hooks is adopted and measurement differences occur.

To examine, the detection performance of HS-DET method, in Fig. 2(a), $\overline{\Delta PES}$ is plotted versus the hook distance from the transmitting end and the hook length when the OV LV BPL topology of urban case A is assumed, very long hooks are considered (*i.e.,* 50 m, 100 m, 200 m, 500 m, 1000 m, 2000 m and 5000 m) and maximum value a_{CUD} of 1 dB is applied. In Figs. 2(b)-(d), same contour plots with Fig. 2(a) are given but for maximum value a_{CUD} of 5 dB, 10 dB and 20 dB, respectively. In Figs. 3, 4, 5 and 6, same plots with Fig. 2 are given but for the case of the urban case B, suburban case, rural case and "LOS" case, respectively. In accordance with [1], the hook distance from the transmitting end span is assumed to be equal to 50 m while the range of the hook distance from the transmitting end is from 1 m to 951 m for all the examined contour plots of this paper.

(a)
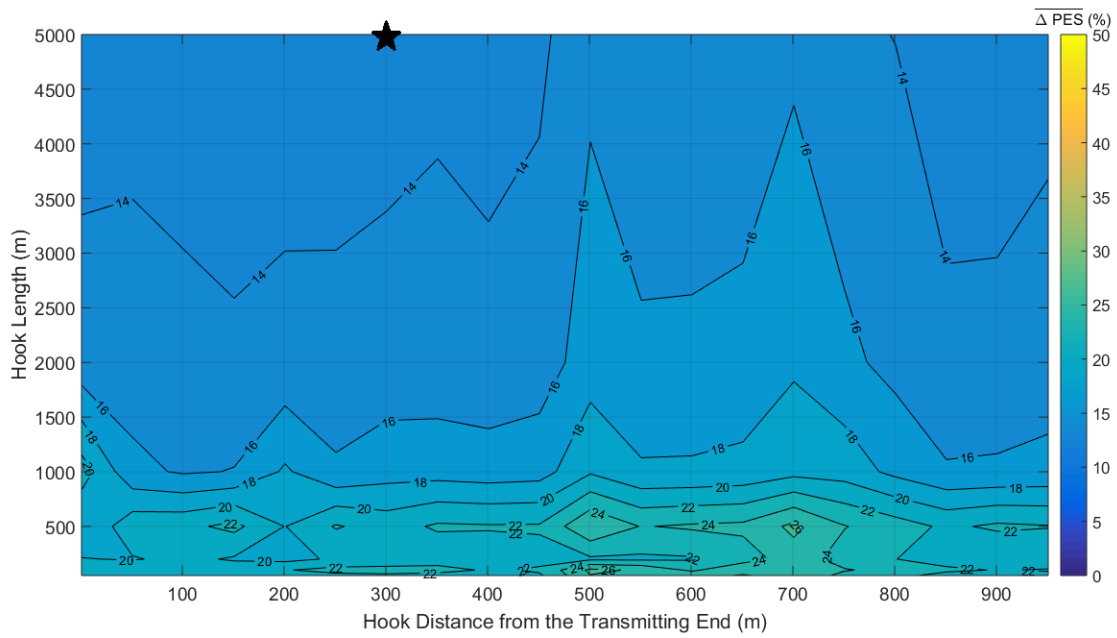
(b)
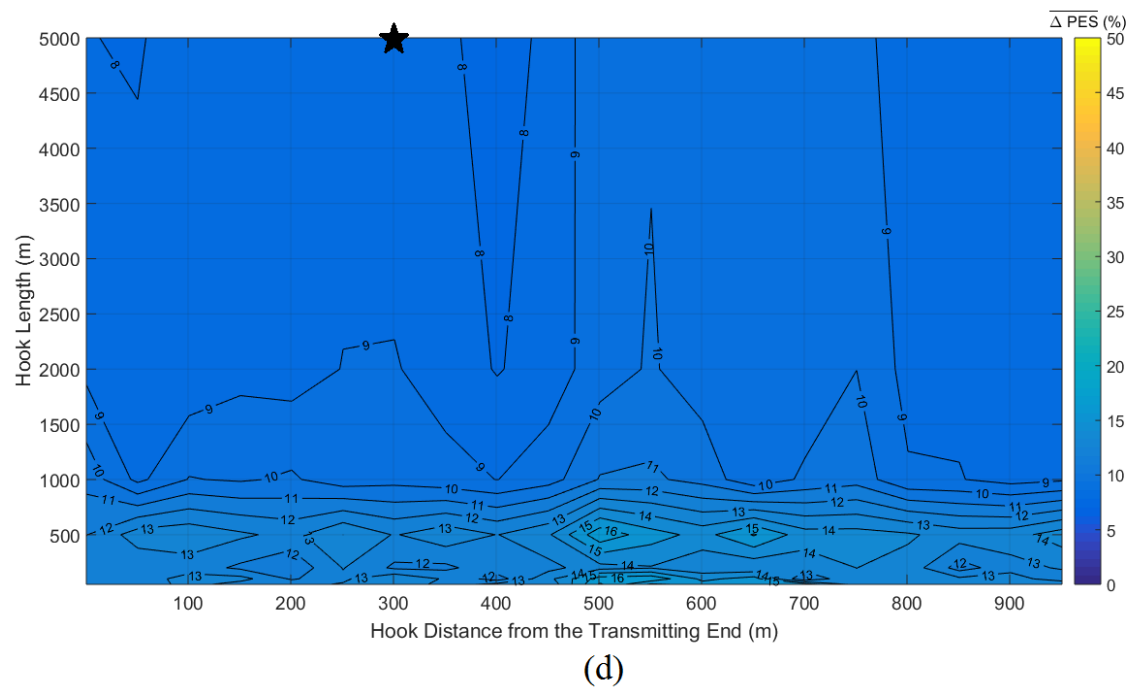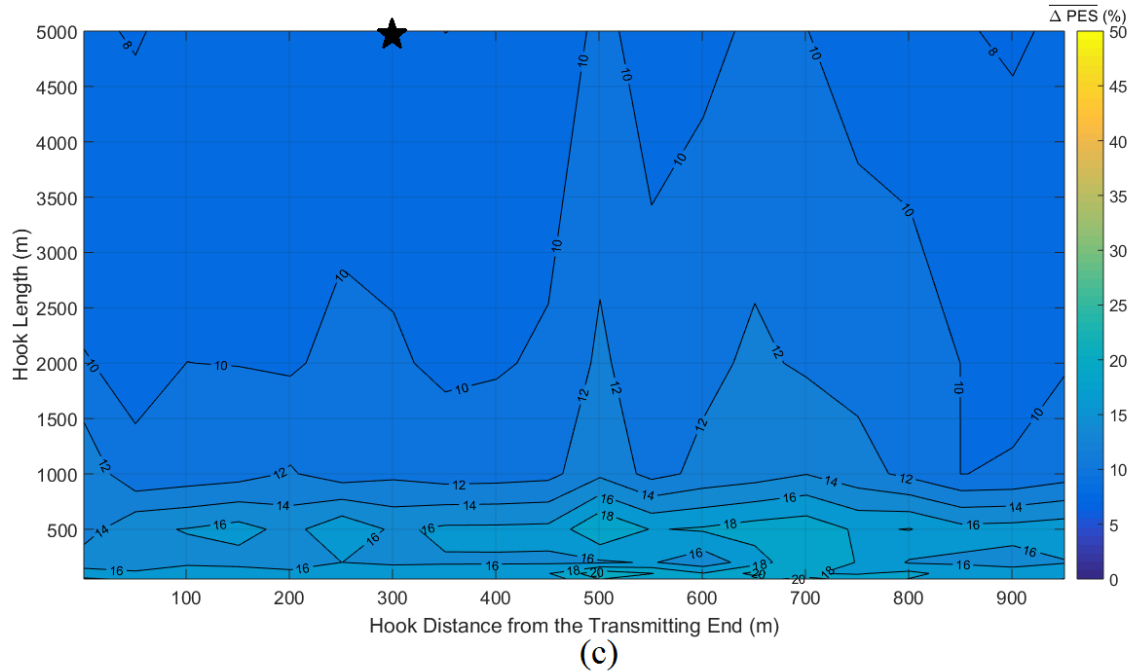
(c)

(d)

Fig. 2. $\overline{\Delta PES}$ of the urban case A of the indicative OV LV BPL topologies in the 3-88 MHz frequency band for various hook distances from the transmitting end and very long hook lengths when high maximum values a_{CUD} are assumed. (a) $a_{CUD} = 1dB$. (b) $a_{CUD} = 5dB$. (c) $a_{CUD} = 10dB$. (d) $a_{CUD} = 20dB$.
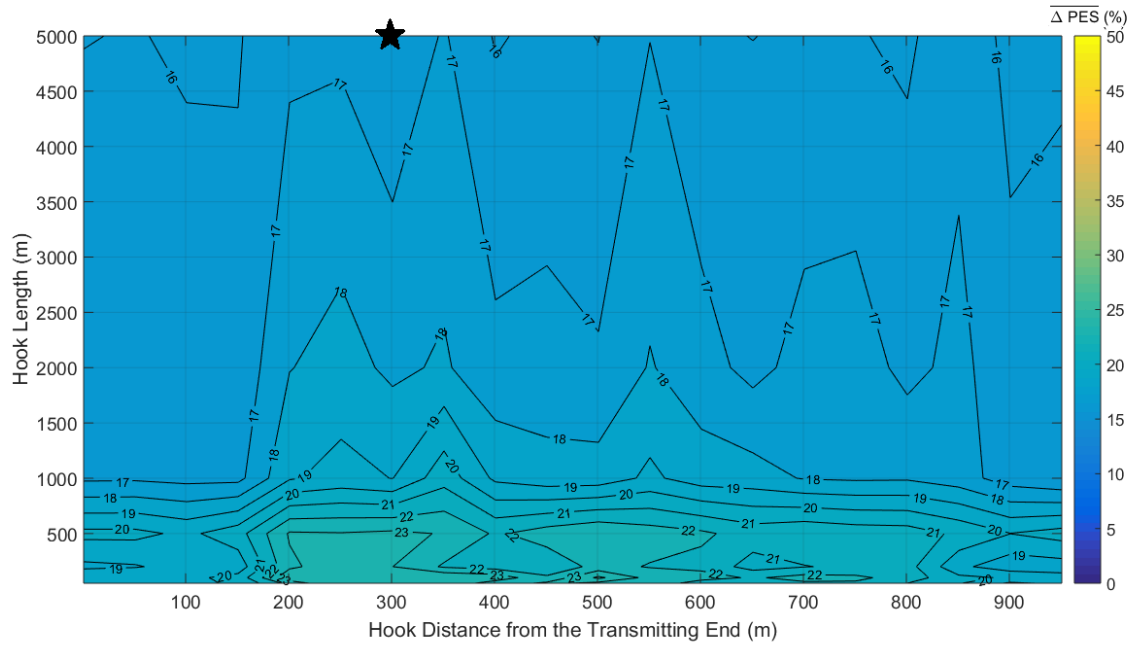
(a)
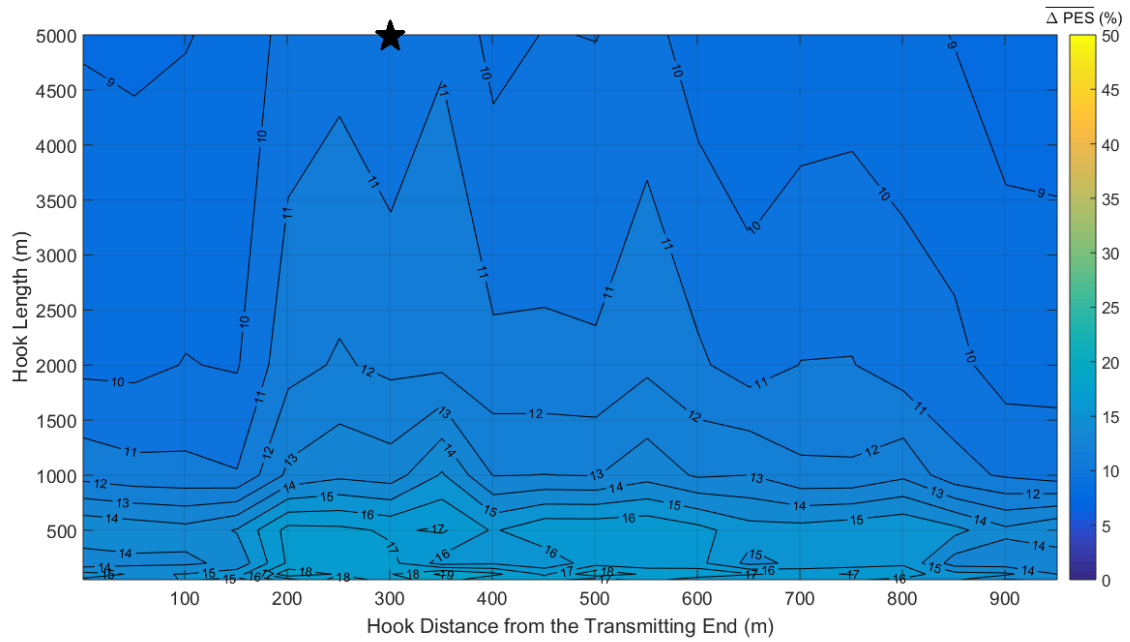
(b)
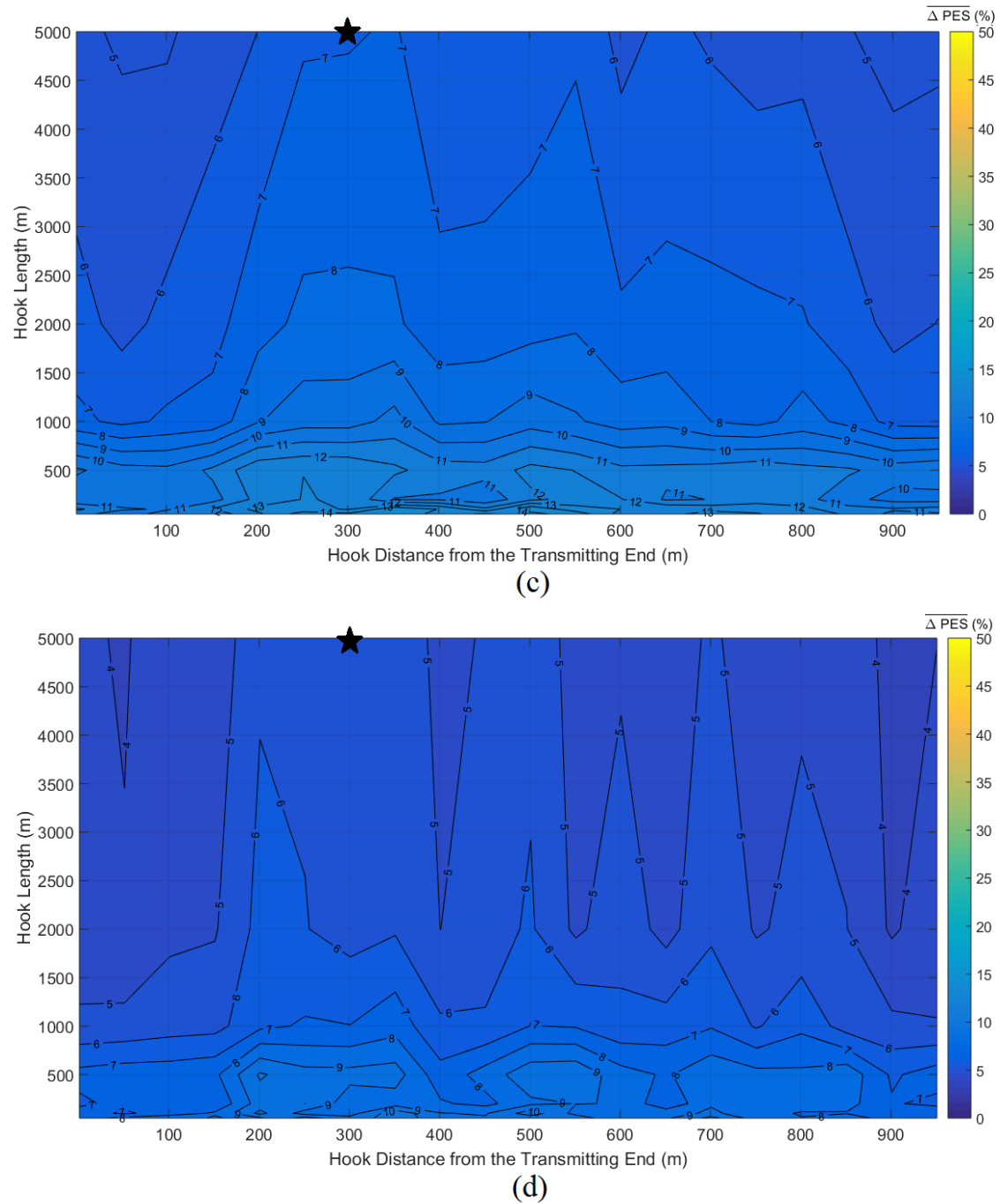
(c)

(d)

Fig. 3. Same curves with Fig. 2 but for the urban case B.

(a)

(b)

(d)
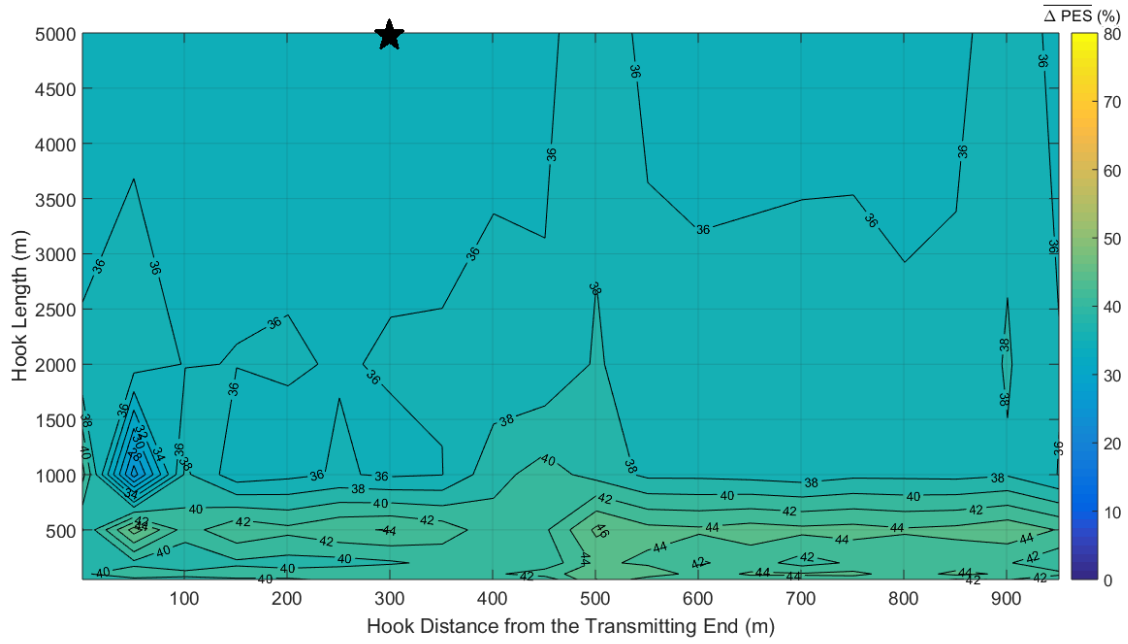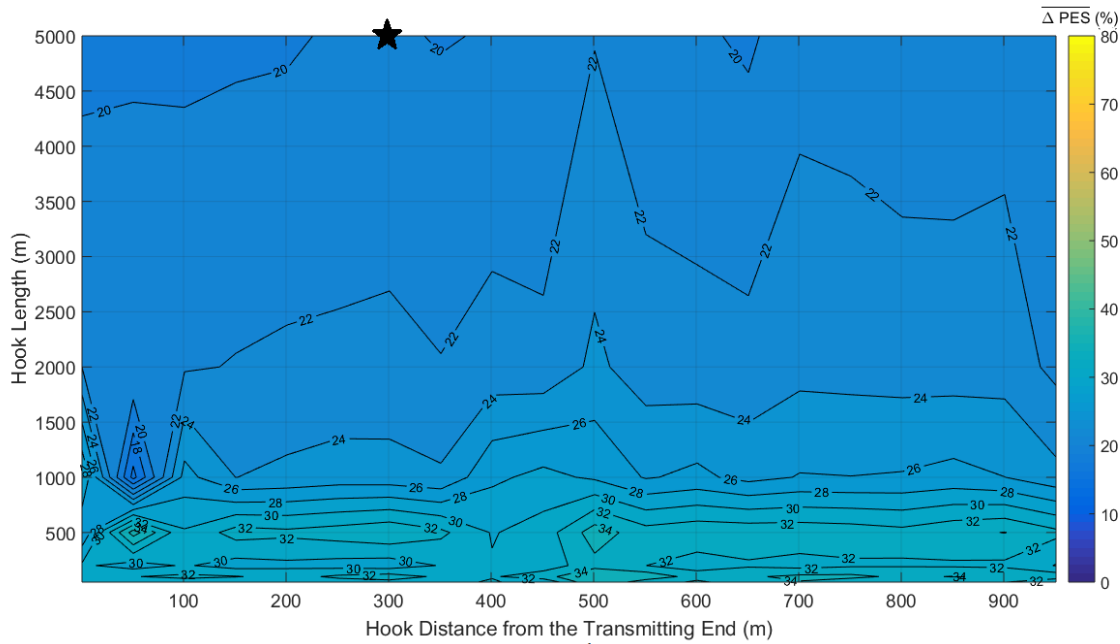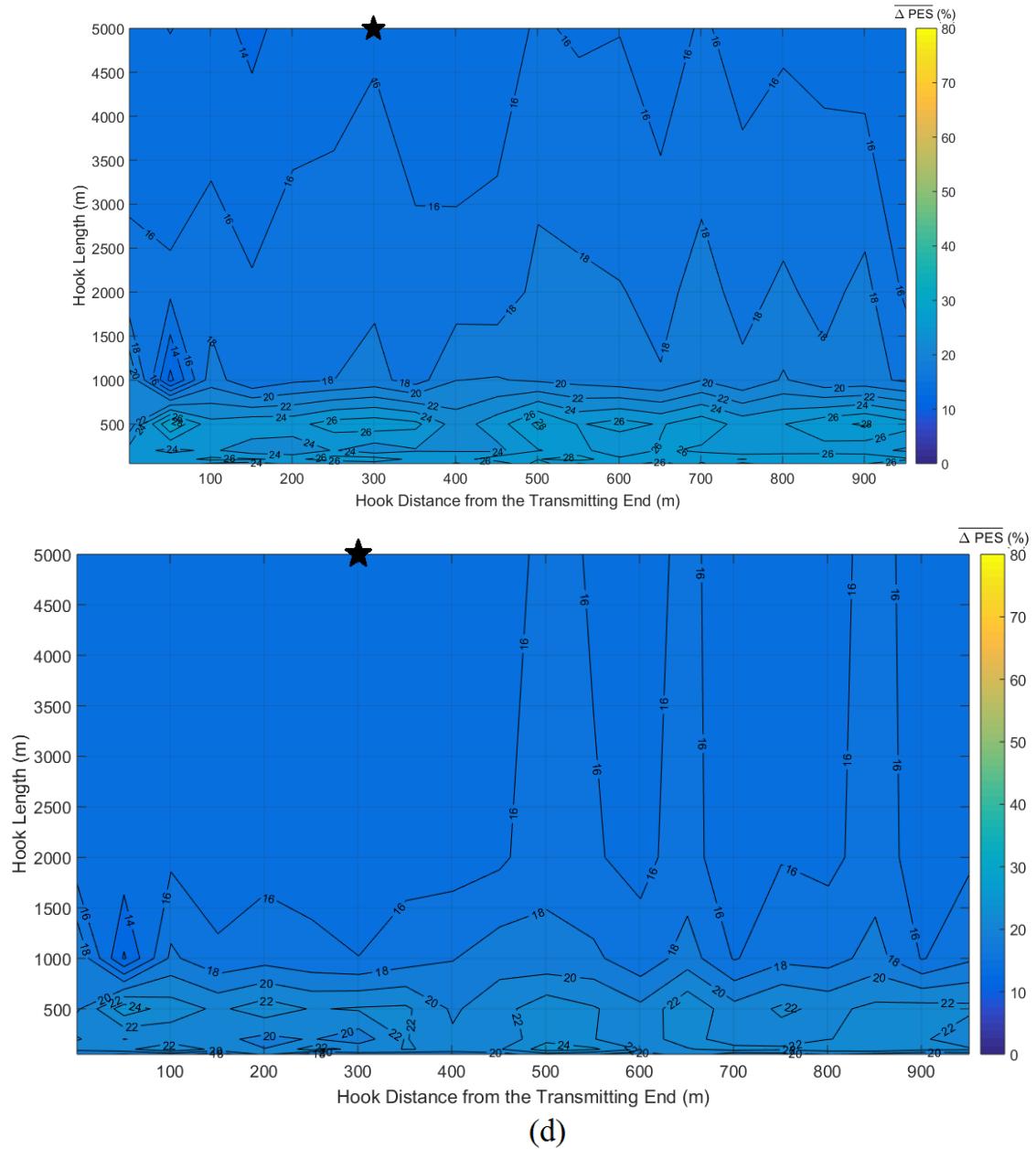
Fig. 4. Same curves with Fig. 2 but for the suburban case.

(a)

(b)

(c)

(d)

Fig. 5. Same curves with Fig. 2 but for the rural case.

(a)

(b)

(c)

(d)
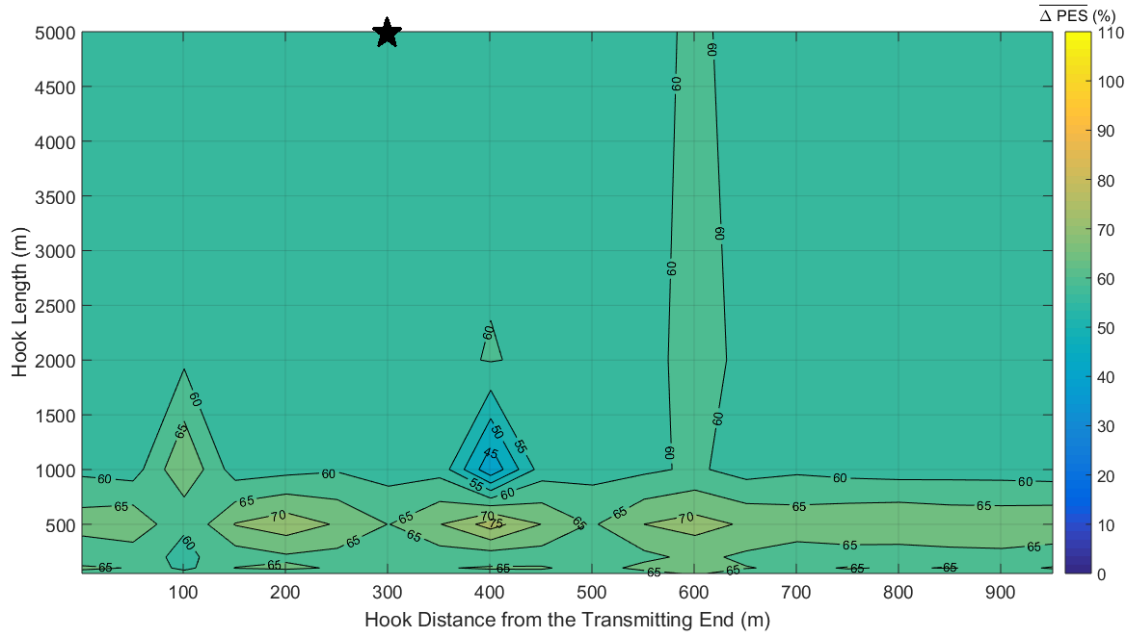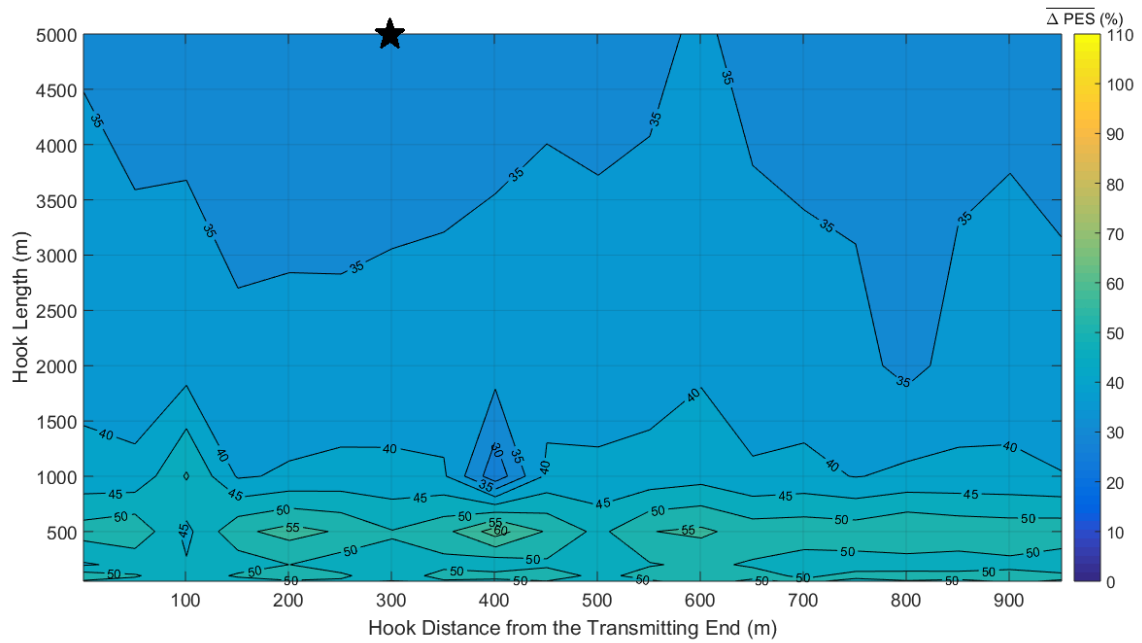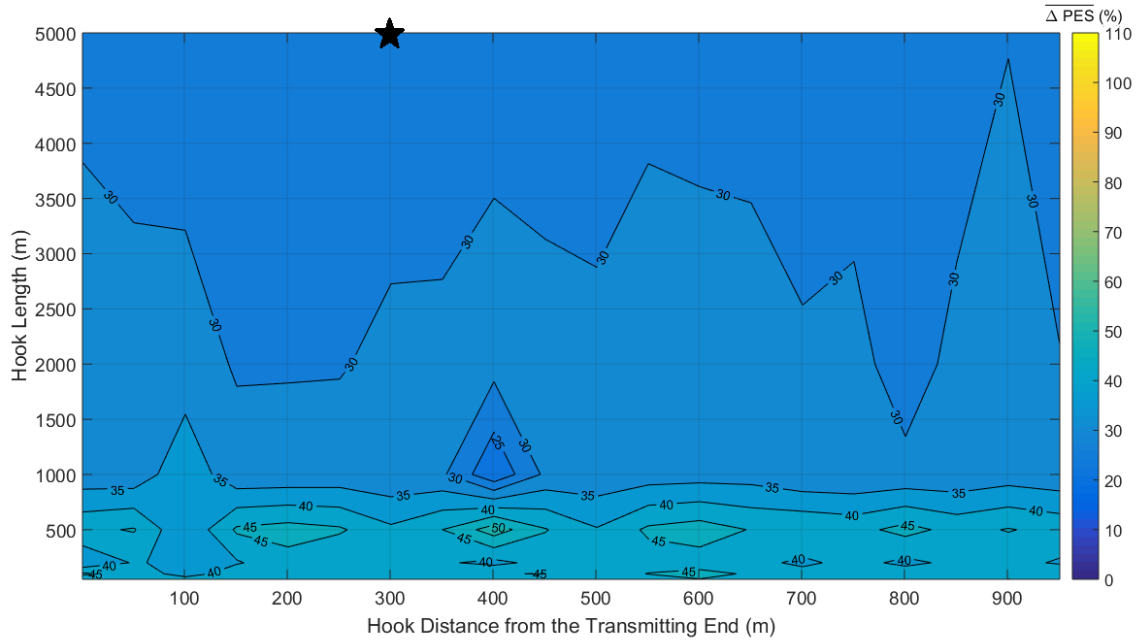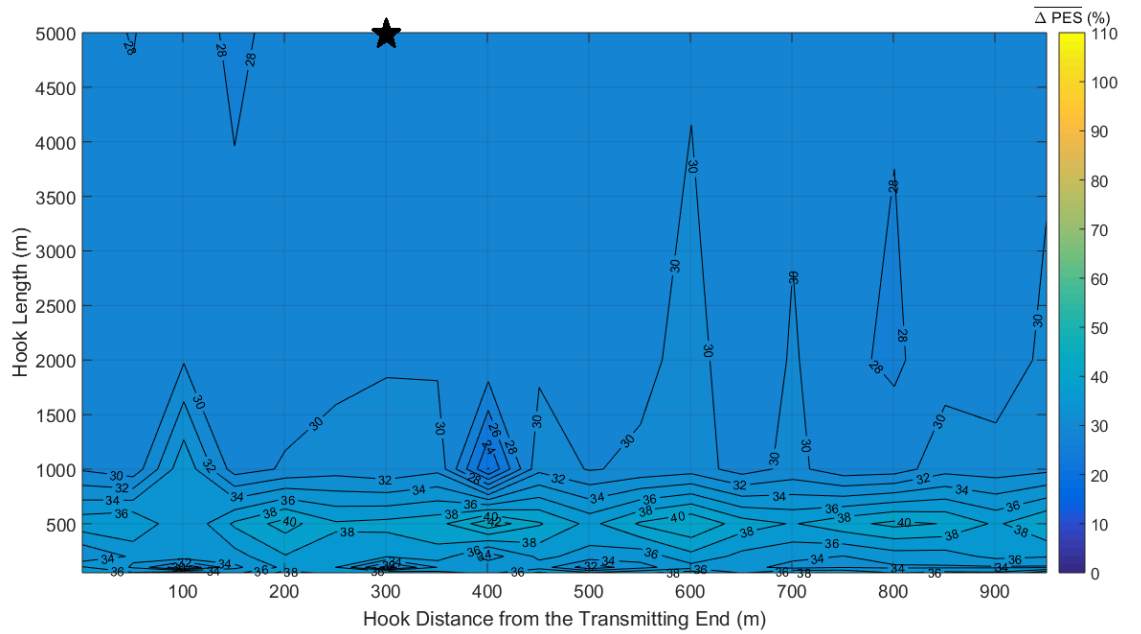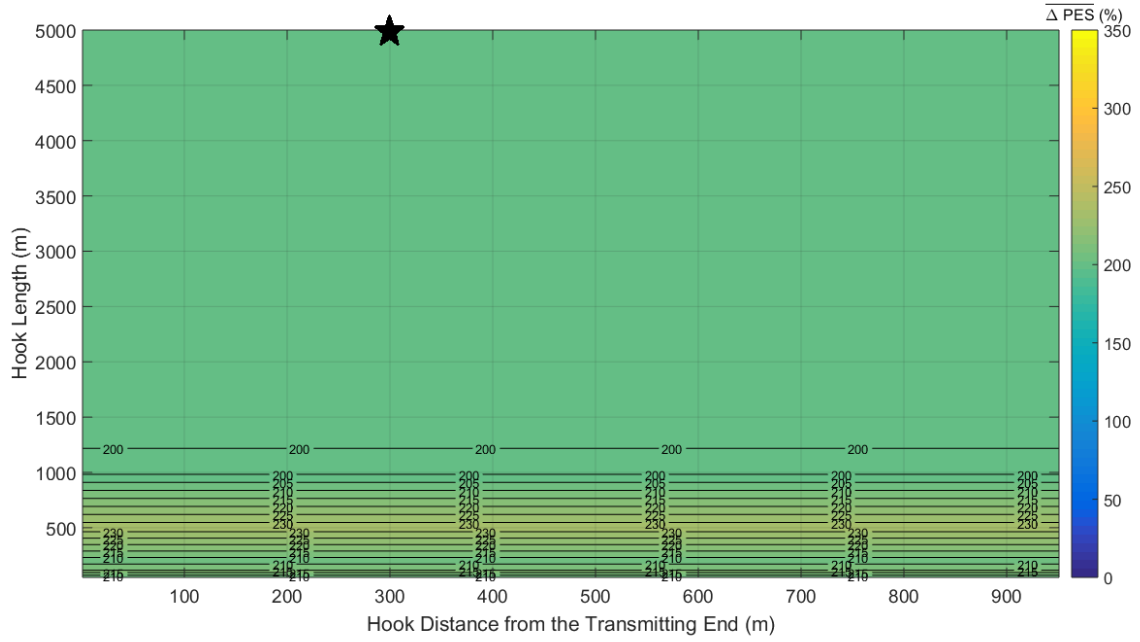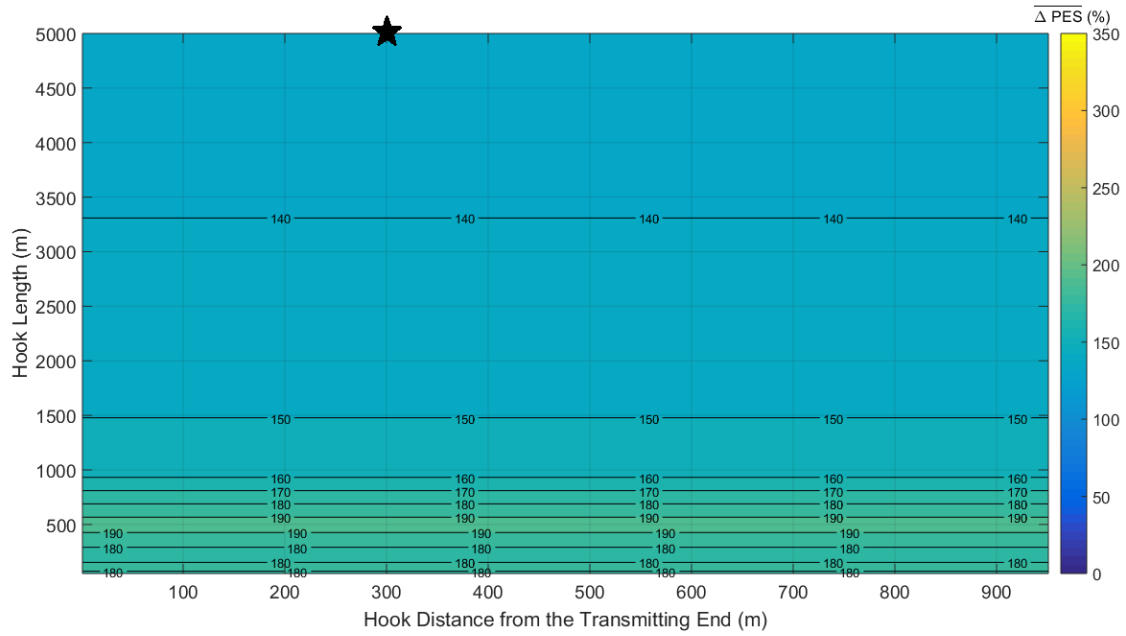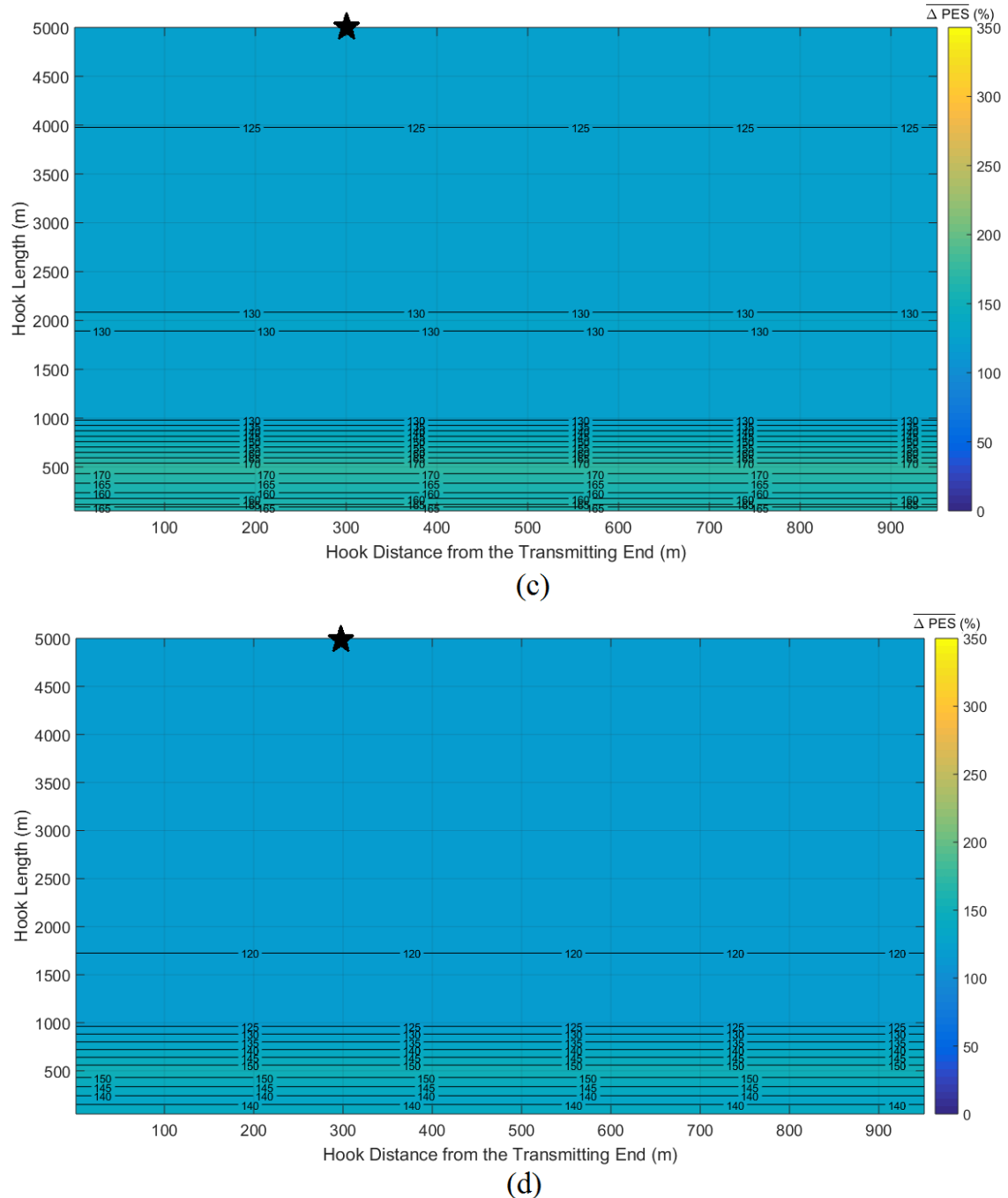
Fig. 6. Same curves with Fig. 2 but for the "LOS" case.

From Figs. 2-6, several interesting conclusions concerning the technique of the very long hooks that aims at jamming HS-DET method can be reported, namely:

- As in [1] and already reported in Table 1, high measurement differences significantly influence the values of $\overline{\Delta PES}$ regardless of the examined OV LV BPL topology, the hook distance from the transmitting end and the hook length. Contour plots of colder colors occur as the maximum value of measurement differences increases implying that the combination of any energy theft technique

with high measurement differences renders the detection of the energy theft more difficult.

- When very long hooks are applied, $\overline{\Delta PES}$ receives significantly lower values in comparison with $\overline{\Delta PES}$ values of short hooks. Since long hooks are treated by the hybrid model as branches, long branches create shallow and rare notches in coupling transfer functions. In accordance with TL theory, while the hooks are characterized by very high length, their input impedance tends to be matched. Therefore, these pseudo-matched terminations can indeed challenge HS-DET method through their lower $\overline{\Delta PES}$ values of their modified OV LV BPL topologies in comparison with the respective topologies of short length hook and open-circuit termination. Hence, hook lengths that tend to infinity create little $\overline{\Delta PES}$ difference in comparison with the hook lengths of 5000 m since they anyway resemble to a matched termination.

- When very long hooks are installed, the main difficulty of HS-DET method concerning the detection of the energy theft is focused on the multi-branched OV LV BPL topologies. Actually, when very long hooks are installed in urban OV LV BPL topologies (e.g., urban case A and B) and are combined with high measurement differences, $\overline{\Delta PES}$ values of these modified urban cases can become lower than the strict $\overline{\Delta PES}$ threshold of 10% of HS-DET method in some cases. For example, $\overline{\Delta PES}$ islands of 9%, 5% and 4% appear in $\overline{\Delta PES}$ contour plots of the modified urban case B when maximum value a_{CUD} is assumed to be equal to 5 dB, 10 dB and 20 dB, respectively. Anyway, the energy theft can be detected by HS-DET method through its loose $\overline{\Delta PES}$ threshold of 0%.

- The most emphatic performance difference of HS-DET method when very long branches are deployed can be revealed by comparing Fig. 8(a) of [1] and Fig. 6(a) of this paper. $\overline{\Delta PES}$ differences up to 100% can be spotted when a very long hook is hung at the MTL configuration of the "LOS" OV LV BPL topology.

- Although the energy theft through very long hooks can make its detection less easy by HS-DET method, its practicality is under question. Issues concerning the power delivery quality, the power attenuation as well as the size of the energy theft installation make the adoption of this technique practically less possible.

On the basis of the matched terminations that can jam HS-DET method in the extent discussed before, an interesting trade-off between the hook length and the hook smartness can be defined. Say, instead of using very long hooks that resemble matched terminations but they are easily detectable, smart hooks that can be configured to be matched to the characteristic impedance of the examined OV LV BPL topology can be used.

3.3 Smart Hooks and HS-DET Method Jamming

Although the installation of additional equipment on the power grid is easily detectable by the authorized maintenance personnel and the energy theft cannot live life long, smart hooks can be camouflaged due to their smaller size in comparison with the very long hooks technique thus saving sufficient time until their detection. Actually, smart hooks can be hooks of relatively short length that are matched to the characteristic impedance in the 3-88 MHz frequency band of BPL operation.

As been observed in Figs. 2-6, HS-DET method can detect any hook style energy theft that is based on the concept of matched terminations. Regardless of the technique that is used to accomplish matched terminations (*i.e.,* either via very long hooks or via smart hooks), HS-DET method can detect the energy theft: (i) in the majority of the cases through its strict $\overline{\mathit{\Delta PES}}$ threshold; and (ii) in the cases of the aggravated urban OV LV BPL topologies that suffer from intentional / unintentional measurement differences through the loose $\overline{\mathit{\Delta PES}}$ threshold.

It is expected that the smart hooks will present the same $\overline{\mathit{\Delta PES}}$ behavior with the cases examined in Figs. 2-6 where hook lengths of 5000 m occur for given OV LV BPL topology. Indeed, similarly to Sec.3.1, let assume that a smart hook (*i.e.,* matched termination) of length L_{bh} is inserted at distance D_h from the transmitting end. In Fig. 7(a), $\overline{\mathit{\Delta PES}}$ is plotted with respect to the maximum value a_{CUD} when $L_{bh} = 5m$ and $D_h = 300m$ are assumed for the five indicative original OV LV BPL topologies. In Figs. 7(b) and 7(c), same curves with Fig. 7(a) are given but for $\overline{PES_{or}}$ and $\overline{Rob}$, respectively.
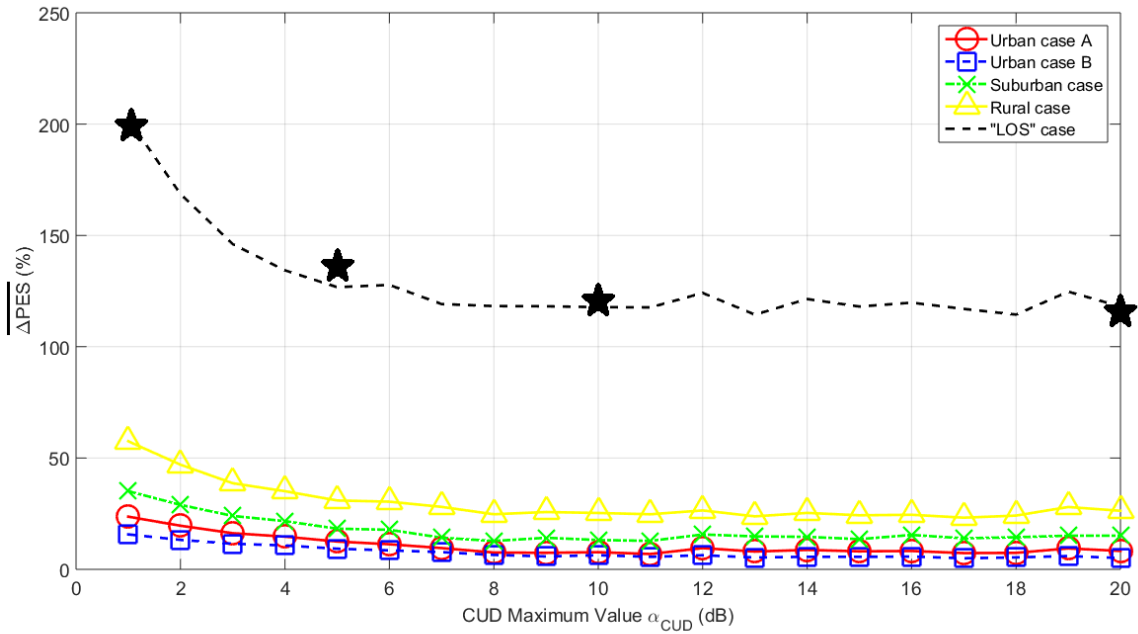
(a)
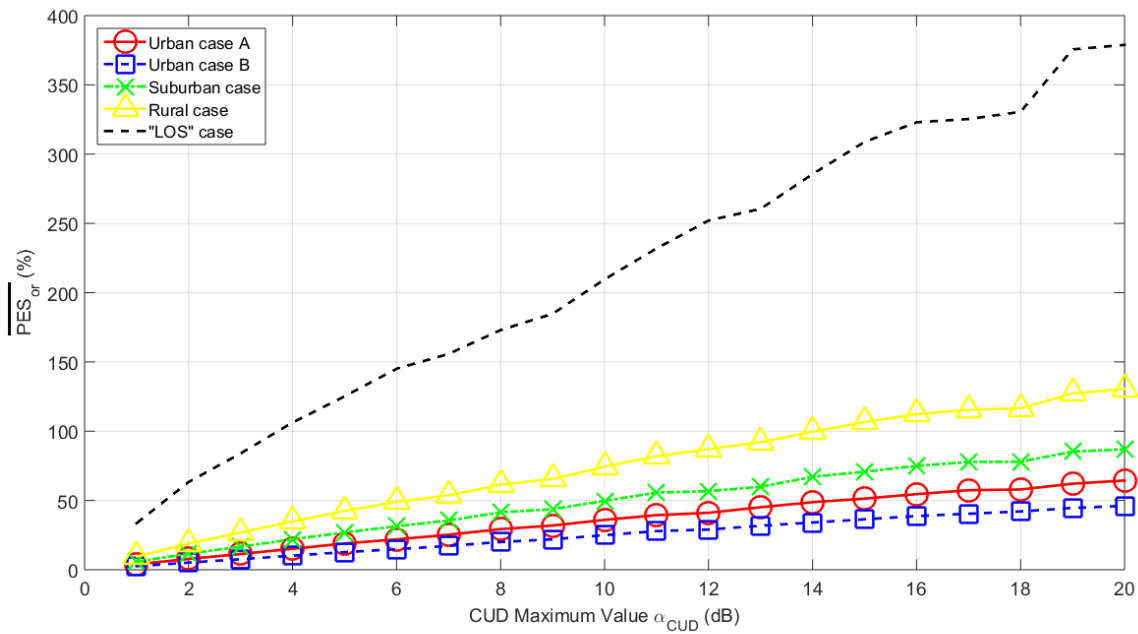
(b)
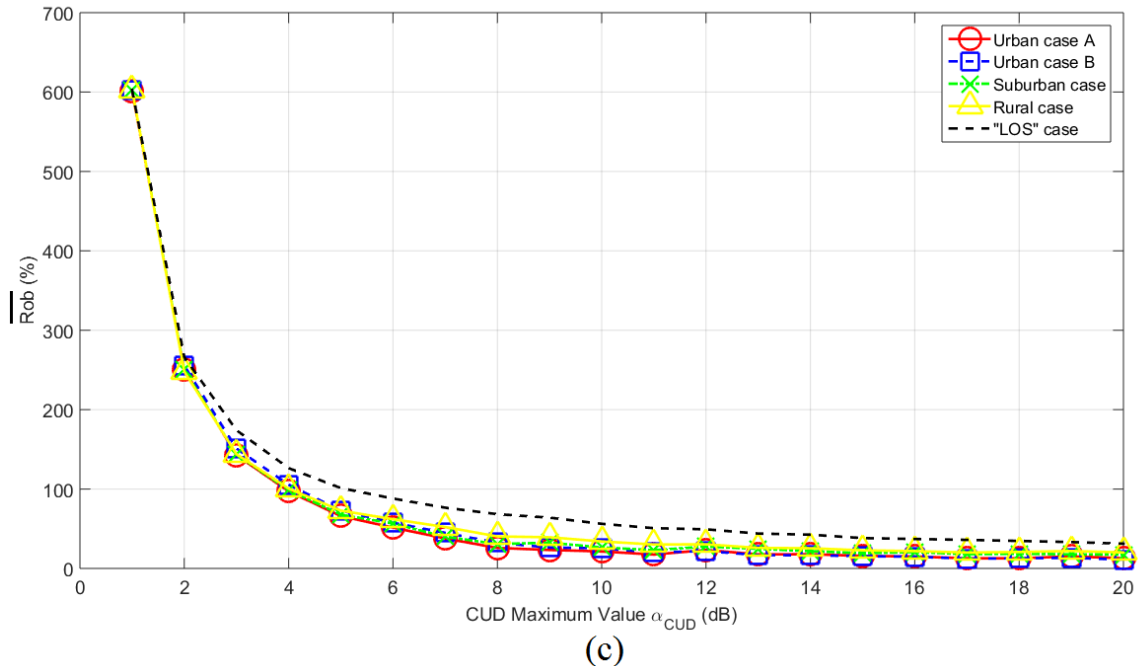
Fig. 7. PES submetrics of HS-DET method for the five original indicative OV LV BPL topologies of [1] when hook length of 5 m, hook distance from the transmitting end of 300 m and matched hook termination are assumed for various maximum values a_{CUD}. (a) $\overline{\Delta PES}$. (b) $\overline{PES_{or}}$. (c) $\overline{Rob}$.

By comparing Figs. 1(a)-(c) with the respective Figs. 7(a)-(c), the three categories of OV LV BPL topologies concerning their behavior of $\overline{\Delta PES}$ and $\overline{PES_{or}}$ is also observed during the installation of smart hooks. Similarly to the open-circuit hooks, HS-DET method can more easily detect the energy theft via smart hooks first in "LOS" case, second in good channel case and third in bad channel case. The only difference by comparing curves of given OV LV BPL topology is that $\overline{\Delta PES}$ values of smart hooks are significantly lower than the respective ones of open-circuit short hooks.

By comparing Fig. 1(c) and Fig. 7(c), $\overline{Rob}$ curves of the examined OV LV BPL topologies almost coincide for given energy theft technique. But the $\overline{Rob}$ values of the smart hook technique are above the half of the respective ones of the open-circuit short length hooks. This result indicates the difficulty of HS-DET method to detect the energy theft when smart hooks can be applied.

As the comparison between smart hook technique and very long hook technique is regards, by comparing Figs. 2-6 with Fig. 7(a), it is obvious that $\overline{\Delta PES}$ behavior of smart hooks present similarities with the behavior of very long hooks. For given OV LV BPL topology, $\overline{\Delta PES}$ behavior of Fig. 7(a) that describes the smart hook technique can be safely approximated by the respective black stars $\overline{\Delta PES}$ values of Figs. 2-6 that anyway describe the very long hook technique. Indeed, the black stars of Figs. 6(a)-(d), which describe the impact of very long hook technique on $\overline{\Delta PES}$ of "LOS" case, have been transferred to Fig. 7(a) where the impact of smart hook technique on $\overline{\Delta PES}$ of "LOS" case is also described. The almost coincidence of black stars and the black dashed line indicates the $\overline{\Delta PES}$ agreement of these two energy theft techniques that is anyway expected due to their matched termination objective.

In numerical terms and on the basis of the $\overline{\Delta PES}$ and $\overline{Rob}$ thresholds of Sec.3.1, $\overline{\Delta PES}$ and $\overline{Rob}$ values of the modified OV LV BPL topologies of Figs 7(a)-(c) are reported in Table 2 when maximum value a_{CUD} of measurement differences is assumed to be equal to 20dB.

Table 2. $\overline{\Delta PES}$ and $\overline{Rob}$ of Indicative OV LV BPL Topologies when $L_{bh} = 5m$ and $D_h = 300m$ (matched hook termination) for maximum values a_{CUD} equal to 20dB

	Modified OV LV BPL Topology				
	Urban case A	Urban case B	Suburban case	Rural case	"LOS" case
$\overline{\Delta PES}$ (%)	8.29	5.09	15.11	26.30	118.08
$\overline{Rob}$ (%)	12.86	11.04	17.39	20.16	31.17

Comparing $\overline{\Delta PES}$ values of Table 2 with the respective values of Table 1, $\overline{\Delta PES}$ and $\overline{Rob}$ values of smart hooks are almost the half in comparison with the respective ones of open-circuit hook of the same hook length in the OV LV BPL topologies of the "LOS" and good channel cases. $\overline{\Delta PES}$ and $\overline{Rob}$ differences remain important even in the OV LV BPL topologies of the bad channel case. Anyway, in all the cases examined $\overline{\Delta PES}$ values are always above 0% and, hence, HS-DET method can successfully detect the energy theft in all the cases. Again, the matched terminations are proven to be a challenge for the HS-DET method in comparison with the open-circuit terminations.

Already been mentioned in the case of the very long hooks, the detection of the energy theft by the HS-DET is accomplished through the strict $\overline{\Delta PES}$ and $\overline{Rob}$ thresholds in the OV LV BPL topologies of "LOS" and good channel cases while the loose $\overline{\Delta PES}$ and $\overline{Rob}$ thresholds need to be adopted for the OV LV BPL topologies of the bad channel case. In accordance with the analysis made in this paper, it is evident that the strict $\overline{\Delta PES}$ and $\overline{Rob}$ thresholds guarantee a safer decision concerning the existence of a hook style energy theft in contrast with the loose $\overline{\Delta PES}$ and $\overline{Rob}$ thresholds.

In addition, measurement differences influence the values of $\overline{\Delta PES}$ even in smart hook case regardless of the examined OV LV BPL topology further deteriorating the quality of decisions regarding the existence of the energy theft. In fact, with reference to Fig. 7(a), when measurement differences are not so severe (i.e., the maximum value a_{CUD} is below 6dB), the detection of the energy theft by HS-DET method can be made through the strict $\overline{\Delta PES}$ threshold in all the OV LV BPL topologies examined.

Finally, it has been proven that the combined operation of smart hooks with high measurement differences can significantly complicate the decision of HS-DET method concerning the existence of energy theft but the implementation of this combined operation is not an easy task. From one side, the use of very sophisticated technology is required so that a smart hook can be implemented while from the other side the use of appropriate jammers that can create measurement differences of such maximum values is questionable. Anyway, even if the aforementioned prerequisites can be achieved, HS-DET method can detect the energy theft even in the most challenging cases of the aggravated urban OV LV BPL topologies through the adoption of the loose $\overline{\Delta PES}$ threshold.

Concluding this paper and synopsizing the findings of this paper in relation with three special cases of [1], HS-DET method succeeds in detecting hook style energy thefts that may occur across the OV LV BPL networks even if high measurement differences occur and specialized jamming techniques, which focus on the exploitation of the matched terminations, are applied. In fact, through the definition of two types of $\overline{\Delta PES}$ threshold (*i.e.,* strict and loose $\overline{\Delta PES}$ threshold), the quality of decision concerning the existence of a hook style energy theft can be evaluated. As the installation of very long hooks is examined in order to mask the energy theft, certain crucial disadvantages have been spotted, namely: (i) the quality of the power delivery; (ii) the apparent size of the energy theft equipment; (iii) the need for very long hooks (above 2000 m-5000 m) so that the behavior of the hook can be appeared as hook with matched termination and create $\overline{\Delta PES}$ values that are below the strict $\overline{\Delta PES}$ threshold; and (iv) even if very high measurement differences can be produced intentionally, HS-DET method detects the energy theft through the loose $\overline{\Delta PES}$ threshold. As the installation of smart hooks is examined in order to jam the HS-DET method, several disadvantages have been reported, namely: (i) the need for sophisticated technology so that a smart hook can be implemented; and (ii) even if very high measurement differences can be produced intentionally, HS-DET method detects the energy theft through the loose $\overline{\Delta PES}$ threshold.

After the analysis of this paper, the future research consists of three sophisticated cases that need further investigation concerning the behavior of HS-DET method, namely: (i) The existence of different CUD measurement differences of the same maximum value a_{CUD} in eqs. (2) and (3). This scenario examines the possibility of not recording the last measurement of $\overline{PES_{or}}$ of eq. (2) and only $\overline{PES_{mod}}$ of eq. (3) is available at the moment of the hook installation; (ii) The installation of second smart hook in order to further jam HS-DET method. In this case, the first smart hook will perform the energy theft while the second smart hook will act as a mask; and (iii) The impact of the assumption of full interconnection during the computation. This issue has to do with the operation of the hybrid method and the assumption made concerning the connection to all three phases and the neutral. All the aforementioned three sophisticated aim at jamming HS-DET method while the hook style energy theft detection performance of the HS-DET method regarding these three cases is further investigated in [35].

4. Conclusions

This paper has focused on the performance of HS-DET method when the three special cases of [1] are addressed. As the first special case is examined, there is no threshold of CUD maximum values a_{CUD} of measurement differences below 20 dB that HS-DET method could not detect the hook style energy theft. Even if high CUD measurement differences occur, HS-DET method can detect the energy theft through its strict $\overline{\Delta PES}$ threshold of 10% in the vast majority of the OV LV BPL topologies examined while the loose $\overline{\Delta PES}$ threshold of HS-DET method of 0% allows the energy theft in the remaining OV LV BPL topologies (*e.g.,* urban OV LV BPL topologies when very high measurement differences occur). As the second special case is examined, the installation of very long hooks in order to mask the hook existence during the application of HS-DET method can indeed make the energy theft detection less easy by HS-DET

method but again in all the cases HS-DET method through its strict and loose $\overline{\Delta PES}$ thresholds. The $\overline{\Delta PES}$ behavior of very long hooks (*i.e.,* hook lengths above 5000 m) resembles to the matched termination $\overline{\Delta PES}$ behavior. However, the main disadvantage of this energy theft technique is its practicability that is questionable due to its size. As the third special case is examined, the $\overline{\Delta PES}$ behavior of "smart" hooks resembles to the respective behavior of very long hooks. Although this energy theft technique imposes difficulties to HS-DET method especially when these "smart" hooks are installed in urban OV LV BPL topologies, in all the cases HS-DET method through its strict and loose $\overline{\Delta PES}$ thresholds can detect the energy theft. The main disadvantage of the "smart" hook energy theft technique is its sophisticated technology. In order to evaluate HS-DET method during extreme scenarios of hook style energy theft, three questions need further examination and future research: (i) The existence of different CUD measurement differences of the same maximum value a_{CUD} during the last transfer function recording and the hook insertion moment; (ii) The installation of second smart hook in order to mask the presence of the first one; and (iii) The impact of the assumption of full interconnection during the computations by HS-DET method.

Appendix – Can High Measurement Differences Trigger the Hook Style Energy Theft Alarm of HS-DET Method

The impact of measurement differences on $\overline{\Delta PES}$, $\overline{PES_{or}}$ and $\overline{Rob}$ of the original indicative OV LV BPL topologies is examined in this Appendix. For this purpose, during the computation of the aforementioned PES submetrics from eqs (2)-(5), the modified measured coupling scheme channel transfer function $\overline{H^C_{mod}}\{\cdot\}$ is assumed to be equal to the original measured coupling scheme channel transfer function $\overline{H^C_{or}}\{\cdot\}$. With reference to eqs. (2) and (3), $\overline{PES_{mod}}$ becomes equal to $\overline{PES_{or}}$ when the aforementioned assumption occurs. Taking under consideration the last observation, the following conclusions can be deduced concerning $\overline{\Delta PES}$, $\overline{PES_{or}}$ and $\overline{Rob}$, say:

- $\overline{\Delta PES}$: With reference to eq. (4), $\overline{\Delta PES}$ becomes equal to zero. Therefore, either the loose $\overline{\Delta PES}$ threshold (i.e., $\overline{\Delta PES}$ above 0%) or the strict $\overline{\Delta PES}$ threshold (i.e., $\overline{\Delta PES}$ above 10%) cannot be exceeded by the measurement differences.
- $\overline{PES_{or}}$: With reference to eq. (2), $\overline{PES_{or}}$ is independent of the modified measured coupling scheme channel transfer function since it depends only on the original measured and original theoretical coupling scheme channel transfer function. $\overline{PES_{or}}$ is already plotted in Fig.1(b).
- $\overline{Rob}$: With reference to eq. (5), $\overline{Rob}$ is equal to 0% since $\overline{\Delta PES}$ is equal to 0%. Again, either the loose $\overline{Rob}$ threshold (i.e., $\overline{Rob}$ above 0%) or the strict $\overline{Rob}$ threshold (i.e., $\overline{Rob}$ above 20%) cannot be exceeded by the measurement differences.

Concluding this Appendix, when there is no hook style energy theft the measurement differences cannot trigger the energy theft alarm. This result is an important safety characteristic of the HS-DET method.

CONFLICTS OF INTEREST

The author declares that there is no conflict of interests regarding the publication of this paper.

References

[1]   A. G. Lazaropoulos, "Detection of Energy Theft in Overhead Low-Voltage Power Grids – The Hook Style Energy Theft in the Smart Grid Era," *Trends in Renewable Energy*, vol. 5, no. 1, pp. 12 – 46, Oct. 2018. [Online]. Available: http://futureenergysp.com/index.php/tre/article/view/81/pdf

[2]   A. G. Lazaropoulos, "Measurement Differences, Faults and Instabilities in Intelligent Energy Systems – Part 1: Identification of Overhead High-Voltage Broadband over Power Lines Network Topologies by Applying Topology Identification Methodology (TIM)," *Trends in Renewable Energy*, vol. 2, no. 3, pp. 85 – 112, Oct. 2016. [Online]. Available: http://futureenergysp.com/index.php/tre/article/download/26/32

[3]   A. G. Lazaropoulos, "Measurement Differences, Faults and Instabilities in Intelligent Energy Systems – Part 2: Fault and Instability Prediction in Overhead High-Voltage Broadband over Power Lines Networks by Applying Fault and Instability Identification Methodology (FIIM)," *Trends in Renewable Energy*, vol. 2, no. 3, pp. 113 – 142, Oct. 2016. [Online]. Available: http://futureenergysp.com/index.php/tre/article/view/27/33

[4]   A. G. Lazaropoulos, "Power Systems Stability through Piecewise Monotonic Data Approximations – Part 2: Adaptive Number of Monotonic Sections and Performance of L1PMA, L2WPMA and L2CXCV in Overhead Medium-Voltage Broadband over Power Lines Networks," *Trends in Renewable Energy*, vol. 3, no. 1, pp. 33 – 60, Jan. 2017. [Online]. Available: http://futureenergysp.com/index.php/tre/article/view/30/35

[5]   A. G. Lazaropoulos, "Power Systems Stability through Piecewise Monotonic Data Approximations – Part 1: Comparative Benchmarking of L1PMA, L2WPMA and L2CXCV in Overhead Medium-Voltage Broadband over Power Lines Networks," *Trends in Renewable Energy*, vol. 3, no. 1, pp. 2 – 32, Jan. 2017. [Online]. Available: http://futureenergysp.com/index.php/tre/article/view/29/34

[6]   A. G. Lazaropoulos, "Main Line Fault Localization Methodology in Smart Grid – Part 1: Extended TM2 Method for the Overhead Medium-Voltage Broadband over Power Lines Networks Case," *Trends in Renewable Energy*, vol. 3, no. 3, pp. 2-25, Dec. 2017. [Online]. Available: http://futureenergysp.com/index.php/tre/article/view/36

[7]   A. G. Lazaropoulos, "Main Line Fault Localization Methodology in Smart Grid – Part 2: Extended TM2 Method, Measurement Differences and L1 Piecewise Monotonic Data Approximation for the Overhead Medium-Voltage Broadband over Power Lines Networks Case," *Trends in Renewable Energy*, vol. 3, no. 3, pp. 26-61, Dec. 2017. [Online]. Available: http://futureenergysp.com/index.php/tre/article/view/37

[8]   A. G. Lazaropoulos, "Main Line Fault Localization Methodology in Smart Grid – Part 3: Main Line Fault Localization Methodology (MLFLM)," *Trends in*

Renewable Energy, vol. 3, no. 3, pp. 62-81, Dec. 2017. [Online]. Available: http://futureenergysp.com/index.php/tre/article/view/38

[9]   A. G. Lazaropoulos, "Towards Modal Integration of Overhead and Underground Low-Voltage and Medium-Voltage Power Line Communication Channels in the Smart Grid Landscape: Model Expansion, Broadband Signal Transmission Characteristics, and Statistical Performance Metrics (Invited Paper)," *ISRN Signal Processing*, vol. 2012, Article ID 121628, pp. 1-17, 2012. [Online]. Available: http://www.hindawi.com/isrn/sp/2012/121628/

[10] A. G. Lazaropoulos, "Towards broadband over power lines systems integration: Transmission characteristics of underground low-voltage distribution power lines," *Progress in Electromagnetics Research B*, 39, pp. 89-114, 2012. [Online]. Available: http://www.jpier.org/PIERB/pierb39/05.12012409.pdf

[11] A. G. Lazaropoulos and P. G. Cottis, "Transmission characteristics of overhead medium voltage power line communication channels," *IEEE Trans. Power Del.*, vol. 24, no. 3, pp. 1164-1173, Jul. 2009.

[12] A. G. Lazaropoulos and P. G. Cottis, "Capacity of overhead medium voltage power line communication channels," *IEEE Trans. Power Del.*, vol. 25, no. 2, pp. 723-733, Apr. 2010.

[13] A. G. Lazaropoulos and P. G. Cottis, "Broadband transmission via underground medium-voltage power lines-Part I: transmission characteristics," *IEEE Trans. Power Del.*, vol. 25, no. 4, pp. 2414-2424, Oct. 2010.

[14] A. G. Lazaropoulos and P. G. Cottis, "Broadband transmission via underground medium-voltage power lines-Part II: capacity," *IEEE Trans. Power Del.*, vol. 25, no. 4, pp. 2425-2434, Oct. 2010.

[15] A. G. Lazaropoulos, "Broadband transmission characteristics of overhead high-voltage power line communication channels," *Progress in Electromagnetics Research B*, vol. 36, pp. 373-398, 2012. [Online]. Available: http://www.jpier.org/PIERB/pierb36/19.11091408.pdf

[16] A. G. Lazaropoulos, "Green Overhead and Underground Multiple-Input Multiple-Output Medium Voltage Broadband over Power Lines Networks: Energy-Efficient Power Control," *Springer Journal of Global Optimization*, vol. 2012 / Print ISSN 0925-5001, pp. 1-28, Oct. 2012.

[17] A. G. Lazaropoulos, "Deployment Concepts for Overhead High Voltage Broadband over Power Lines Connections with Two-Hop Repeater System: Capacity Countermeasures against Aggravated Topologies and High Noise Environments," *Progress in Electromagnetics Research B*, vol. 44, pp. 283-307, 2012. [Online]. Available: http://www.jpier.org/PIERB/pierb44/13.12081104.pdf

[18] A. G. Lazaropoulos, "Broadband transmission and statistical performance properties of overhead high-voltage transmission networks," *Hindawi Journal of Computer Networks and Commun.*, 2012, article ID 875632, 2012. [Online]. Available: http://www.hindawi.com/journals/jcnc/aip/875632/

[19] P. Amirshahi and M. Kavehrad, "High-frequency characteristics of overhead multiconductor power lines for broadband communications," *IEEE J. Sel. Areas Commun.*, vol. 24, no. 7, pp. 1292-1303, Jul. 2006.

[20] T. Calliacoudas and F. Issa, ""Multiconductor transmission lines and cables solver," An efficient simulation tool for plc channel networks development," presented at the *IEEE Int. Conf. Power Line Communications and Its Applications*, Athens, Greece, Mar. 2002.

[21] T. Sartenaer and P. Delogne, "Deterministic modelling of the (Shielded) outdoor powerline channel based on the multiconductor transmission line equations," *IEEE J. Sel. Areas Commun.*, vol. 24, no. 7, pp. 1277-1291, Jul. 2006.

[22] C. R. Paul, *Analysis of Multiconductor Transmission Lines*. New York: Wiley, 1994.

[23] H. Meng, S. Chen, Y. L. Guan, C. L. Law, P. L. So, E. Gunawan, and T. T. Lie, "Modeling of transfer characteristics for the broadband power line communication channel," *IEEE Trans. Power Del.*, vol. 19, no. 3, pp. 1057-1064, Jul. 2004.

[24] B. Li, D. Mansson, and G. Yang, "An efficient method for solving frequency responses of power-line networks," *Progress in Electromagnetics Research B*, Vol. 62, 303-317, 2015. DOI: 10.2528/PIERB15013008 http://www.jpier.org/pierb/pier.php?paper=15013008

[25] M. Chaaban, K. El KhamlichiDrissi, and D. Poljak, "Analytical model for electromagnetic radiation by bare-wire structures," *Progress in Electromagnetics Research B*, Vol. 45, 395-413, 2012. DOI:10.2528/PIERB12091102 http://www.jpier.org/pierb/pier.php?paper=12091102

[26] Y. H. Kim, S. Choi, S. C. Kim, and J. H. Lee, "Capacity of OFDM two-hop relaying systems for medium-voltage power-line access networks," *IEEE Trans. Power Del.*, vol. 27, no. 2, pp. 886-894, Apr. 2012.

[27] A. G. Lazaropoulos, "Best L1 Piecewise Monotonic Data Approximation in Overhead and Underground Medium-Voltage and Low-Voltage Broadband over Power Lines Networks: Theoretical and Practical Transfer Function Determination," *Hindawi Journal of Computational Engineering*, vol. 2016, Article ID 6762390, 24 pages, 2016. DOI:10.1155/2016/6762390. [Online]. Available: https://www.hindawi.com/journals/jcengi/2016/6762390/cta/

[28] A. G. Lazaropoulos, "New Coupling Schemes for Distribution Broadband over Power Lines (BPL) Networks," *Progress in Electromagnetics Research B*, vol. 71, pp. 39-54, 2016. [Online]. Available: http://www.jpier.org/PIERB/pierb71/02.16081503.pdf

[29] A. G. Lazaropoulos, "Broadband Performance Metrics and Regression Approximations of the New Coupling Schemes for Distribution Broadband over Power Lines (BPL) Networks," *Trends in Renewable Energy*, vol. 4, no. 1, pp. 43 – 73, 2018. [Online]. Available: http://www.futureenergysp.com/index.php/tre/article/view/59/pdf

[30] OPERA1, D44: Report presenting the architecture of plc system, the electricity network topologies, the operating modes and the equipment over which PLC access system will be installed, IST Integr. Project No 507667, Dec. 2005.

[31] OPERA1, D5: Pathloss as a function of frequency, distance and network topology for various LV and MV European powerline networks. IST Integrated Project No 507667, Apr. 2005.

[32] A. G. Lazaropoulos, "Factors Influencing Broadband Transmission Characteristics of Underground Low-Voltage Distribution Networks," *IET Commun.*, vol. 6, no. 17, pp. 2886-2893, Nov. 2012.

[33] J. Anatory, N. Theethayi, and R. Thottappillil, "Power-line communication channel model for interconnected networks-Part II: Multiconductor system," *IEEE Trans. Power Del.*, vol. 24, no. 1, pp. 124-128, Jan. 2009.

[34] J. Anatory, N. Theethayi, R. Thottappillil, M. M. Kissaka, and N. H. Mvungi, "The effects of load impedance, line length, and branches in typical low-voltage channels

of the BPLC systems of developing countries: transmission-line analyses," *IEEE Trans. Power Del.*, vol. 24, no. 2, pp. 621-629, Apr. 2009.

[35] A. G. Lazaropoulos, "Special Cases during the Detection of the Hook Style Energy Theft in Overhead Low-Voltage Power Grids through HS-DET Method – Part 2: Different Measurement Differences, Feint "Smart" Hooks and Hook Interconnection Issues," *Trends in Renewable Energy*, DOI: 10.17737/tre.2019.5.1.0083.

Special Cases during the Detection of the Hook Style Energy Theft in Overhead Low-Voltage Power Grids through HS-DET Method – Part 2: Different Measurement Differences, Feint "Smart" Hooks and Hook Interconnection Issues

Athanasios G. Lazaropoulos[*]

School of Electrical and Computer Engineering / National Technical University of Athens / 9 Iroon Polytechniou Street / Zografou, GR 15780

On the basis of [1] and [2], this paper investigates the possibility of jamming the method of the detection of the hook style energy theft (HS-DET method) that is used for the detection of the hook style energy theft in the overhead low-voltage (OV LV) power grids. Three more sophisticated scenarios, which have been revealed in [2] and are the evolution of the three main suspicious issues of [1], are further investigated in this paper. The detection efficiency of HS-DET method is assessed by using the already validated percent error sum (PES) submetrics and appropriate contour plots.

1. Introduction

The hook style energy theft detection method (HS-DET method), which has been proposed in [1] and partially tested on its detection performance during a set of special cases in [2], aims at detecting the hook style energy theft in overhead low-voltage (OV LV) power grids that exploit broadband over powerlines (BPL) technology conveniences. HS-DET method is added in the existing portfolio of BPL broadband applications, such as Topology Identification Methodology (TIM) [3], Fault and Instability Identification Methodology (FIIM) [4], methodology to preserve power system stability [5], [6] and main line fault localization methodology (MLFLM) [7]-[9], while its application is considered valid when all the problematic cases of TIM, FIIM and MLFLM are excluded. The portfolio of BPL broadband applications focuses on a more accurate and more reliable monitoring, metering and controlling of distribution power grids.

HS-DET method is based on the hybrid model [10]-[27] while the hook style energy theft is detected by HS-DET method through $\overline{\Delta PES}$ metric, which is the suitable percent error sum (PES) submetric for energy theft detection, and its relevant contour plots. Actually, $\overline{\Delta PES}$ evaluates the asymmetry between the original and the modified

OV LV BPL topology where the modified OV LV BPL topology comes from the original OV LV BPL topology after the hook insertion. If $\overline{\Delta PES}$ remains above the strict $\overline{\Delta PES}$ threshold, which is equal to 10%, a safe detection of a hook style energy theft can be received. If $\overline{\Delta PES}$ remains between the above the loose $\overline{\Delta PES}$ threshold, which is equal to 0%, and the strict $\overline{\Delta PES}$ threshold, a less safe detection of a hook style energy theft can be received. Here, it should be noted that HS-DET method can give reliable decisions concerning the existence of the energy theft regardless of the existence of very intense measurement differences due to the $\overline{\Delta PES}$ definition that can significantly mitigate them (see [1] and Appendix of [2]).

In accordance with [1], three special issues have been addressed there and it has been proven in [2] that these three special issues cannot jam HS-DET method. More specifically, the concluding remarks concerning these three special issues can be synopsized as: (i) There is no threshold of CUD maximum values a_{CUD} of measurement differences below 20 dB that HS-DET method could not detect the hook style energy theft; (ii) The installation of very long hooks in order to mask the hook existence during the application of HS-DET method can indeed make the energy theft detection less easy by HS-DET method but again in all the cases HS-DET method can detect the hook style energy theft through its strict and loose $\overline{\Delta PES}$ thresholds; and (iii) The $\overline{\Delta PES}$ behavior of "smart" hook technique resembles to the respective behavior of very long hooks and hence the energy theft detection of "smart" hook technique by HS-DET method remains as easy as in the very long hook technique. In all the three special issues, HS-DET method detected the energy theft through strict and loose $\overline{\Delta PES}$ thresholds.

In accordance with [2], three more sophisticated scenarios have been proposed that aspire, by exploiting and extending the strengths of the three special cases, to distract further HS-DET method. With reference to [1] and [2], these three sophisticated scenarios are: (a) the existence of different CUD measurement differences of the same maximum value a_{CUD} when the coupling transfer functions of the original and the modified OV LV BPL topologies are measured; (b) The installation of a second "smart" hook, which acts as a feint device, so that the first "smart" hook that is responsible for the energy theft can be camouflaged; and (c) The impact of the full interconnection assumption of the "smart" hook during the computations of HS-DET method.

The rest of this paper is organized as follows: In Section 2, numerical results and discussion are provided, aiming at practically evaluating the efficiency of the three sophisticated scenarios towards the jamming of HS-DET method. Section 3 concludes this paper.

2. Numerical Results and Discussion

The numerical results of this Section focus on assessing the performance of HS-DET method and describe the behavior of HS-DET method when the aforementioned three sophisticated scenarios occur. All these three scenarios try to jam HS-DET method, each one exploiting its own strengths presented in [2]. For that reason, the robustness of decisions of HS-DET method is also evaluated as well as the road map towards safer decisions concerning the detection of hook style energy thefts. As the circuital, topological and coupling scheme characteristics of OV LV BPL networks are concerned, these remain the same with [1], [2].

2.1 Different CUD Measurement Differences and HS-DET Method Jamming

The influence of measurement differences of maximum value a_{CUD} up to 5 dB has been thoroughly discussed in [1] while the influence of measurement differences of maximum value a_{CUD} above 5 dB has been evaluated in [2]. It has been proven that there is no threshold of CUD maximum values a_{CUD} of measurement differences below 20 dB that HS-DET method could not detect the hook style energy theft. Actually, in the vast majority of the cases examined, HS-DET method detected the energy theft through its strict $\overline{\Delta PES}$ threshold while the loose $\overline{\Delta PES}$ threshold of HS-DET method have been used in special cases such as urban OV LV BPL topologies when very high measurement differences occur.

With reference to eqs. (2)-(4) of [2], HS-DET method can successfully detect the hook style energy theft regardless of the CUD maximum values a_{CUD} of measurement differences when measurements of original measured coupling scheme channel transfer function and modified measured coupling scheme channel transfer functions are available at the same time. However, the cost of a non-real time and continuous HS-DET method in terms of $\overline{\Delta PES}$ is going to be assessed in this subsection.

If simultaneous measurements of original measured coupling scheme channel transfer function and modified measured coupling scheme channel transfer functions are not available, the aforementioned measured transfer functions suffer from different measurement differences. Supposing that the environmental and circuital conditions of the examined OV LV power grid remain the same due the short time interval between the two measurements, two different CUD measurement differences of the same maximum values a_{CUD} affect the original measured coupling scheme channel transfer function and the modified measured coupling scheme channel transfer functions. In this paper, the influence of average measurement differences (*i.e.,* measurement differences of maximum value a_{CUD} between 0 dB and 5 dB) is evaluated in this paper. In accordance with [2], the performance of HS-DET method against different measurement differences will be assessed in terms of $\overline{\Delta PES}$, $\overline{PES_{or}}$ and $\overline{Rob}$.

With reference to Fig. 2(b) of [1] and the indicative original OV LV BPL topologies as reported in Table 1 of [1], let assume that a hook of length L_{bh} is inserted at distance D_h from the transmitting end. In Fig. 1(a), $\overline{\Delta PES}$ is plotted with respect to the maximum value a_{CUD} when $L_{bh} = 5m$ and $D_h = 300m$ are assumed for the five indicative original OV LV BPL topologies. Note that two different CUD measurement differences are used during the determination of the original measured coupling scheme channel transfer function and the modified measured coupling scheme channel transfer functions. In Figs. 1(b) and 1(c), same curves with Fig. 1(a) are given but for $\overline{PES_{or}}$ and $\overline{Rob}$, respectively.
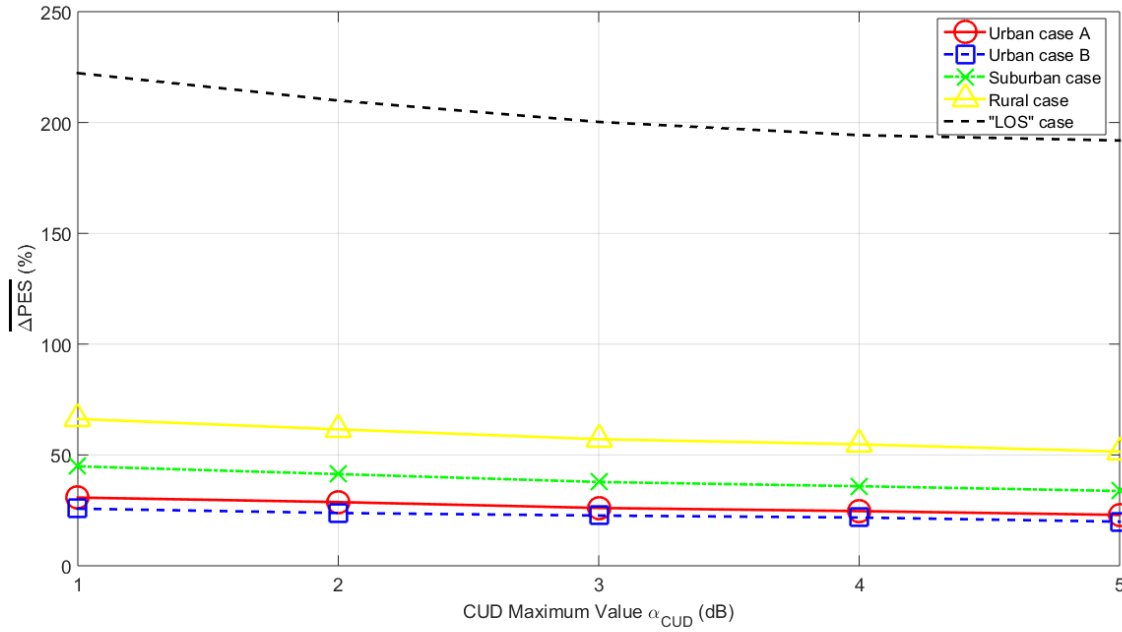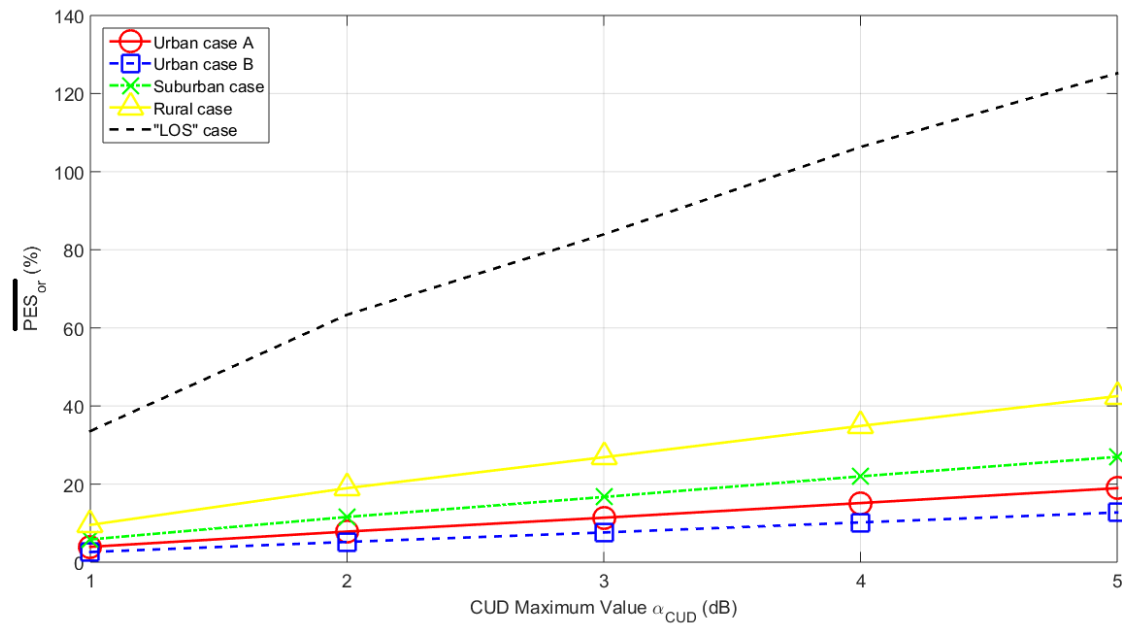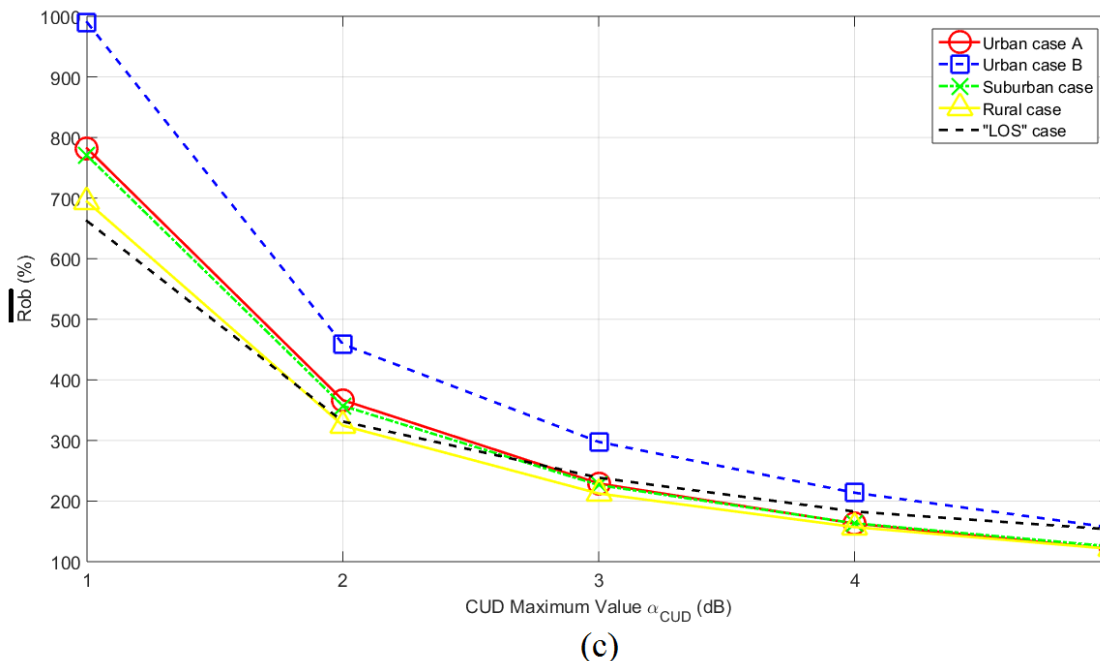
(a)

(b)

(c)

Fig. 1. PES submetrics of HS-DET method for the five original indicative OV LV BPL topologies of [1] when hook length of 5 m, hook distance from the transmitting end of 300 m and open-circuit hook termination are assumed for two different CUD measurement differences and various maximum values a_{CUD}. (a) $\overline{\Delta PES}$. (b) $\overline{PES_{or}}$. (c) $\overline{Rob}$.

From Figs. 1(a)-(c), it is evident that HS-DET method can easily detect the hook style energy theft even if unintentional / intentional different measurement differences occur during the determination of the original measured coupling scheme channel transfer function and the modified measured coupling scheme channel transfer functions. This easily can be explained since all $\overline{\Delta PES}$ and $\overline{Rob}$ values of all the indicative OV LV BPL topologies remain well above the respective $\overline{\Delta PES}$ and $\overline{Rob}$ strict thresholds, which have been described in [2] (*i.e.,* strict $\overline{\Delta PES}$ and $\overline{Rob}$ thresholds are assumed to be equal to 10% and 20%, respectively).

In accordance with [2], the three categories of OV LV BPL topologies concerning the hook style energy theft detection through $\overline{\Delta PES}$, say, "LOS", good channel and bad channel cases, also remain the same despite the different CUD measurement differences. Similarly to the case of common CUD measurement differences during the determination of the original measured coupling scheme channel transfer function and the modified measured coupling scheme channel transfer functions, the easiest decision concerning the energy theft detection remains in original "LOS" case while the most precarious one remains in the bad channel case.

Although the detection of the energy theft is based on the strict $\overline{\Delta PES}$ and $\overline{Rob}$ thresholds in all the examined OV LV BPL topologies and CUD maximum values, the uncertainty degree of the two different CUD measurement differences, which is intrinsically added in the $\overline{\Delta PES}$ and $\overline{Rob}$ curves of respective Figs. 1(a) and 1(c), need to be assessed. This assessment will highlight the possibility of jamming the decision concerning the energy theft. In Appendix, the sole influence of the two different CUD measurement differences of the same maximum value a_{CUD} is assessed in terms of $\overline{\Delta PES}$,

$\overline{PES_{or}}$ and $\overline{Rob}$. As it is shown in the Appendix, the effect of two different CUD measurement differences on $\overline{\Delta PES}$ and $\overline{Rob}$ values remains marginal (*i.e.,* below 3% and 4% for $\overline{\Delta PES}$ and $\overline{Rob}$, respectively) and remain as a small fraction of the respective $\overline{\Delta PES}$ and $\overline{Rob}$ values in all the cases examined in Figs. 1(a) and 1(c). However, the effect of two different CUD measurement differences on $\overline{\Delta PES}$ and $\overline{Rob}$ values cannot be neglected in the cases where the decision concerning the existence of hook style energy theft needs to be taken by using the respective loose $\overline{\Delta PES}$ and $\overline{Rob}$ thresholds (see decisions with loose $\overline{\Delta PES}$ and $\overline{Rob}$ thresholds in [2]).

Since the impact of two different CUD measurement differences on the detection of hook style energy theft is negligible in the cases examined in this paper, a common CUD measurement difference during the determination of the original theoretical coupling scheme channel transfer function and the modified theoretical coupling scheme channel transfer function is considered in the following analysis. Anyway, this is the typical procedure that has been followed until now and further implies the existence of a real time and continuous HS-DET method.

Also, by comparing Figs. 1(a) and 1(c), there are no areas of maximum value a_{CUD} uncertainty where $\overline{\Delta PES}$ and $\overline{Rob}$ give conflicting results concerning the existence of hook style energy theft. Therefore, only $\overline{\Delta PES}$ plots are going to be used in the following analysis.

2.2 Two "Smart" Hooks and HS-DET Method Jamming

In accordance with [2], the installation of additional equipment on the power grid can be easily detectable by the authorized maintenance personnel. However, the small size of "smart" hooks can be camouflaged in comparison with other energy theft techniques such as the very long hooks technique. Anyway, HS-DET method can detect any hook style energy theft that is based on the concept of "smart" hooks but in few cases such as the aggravated urban OV LV BPL topologies that suffer from intentional / unintentional measurement differences, the detection has been made through the loose $\overline{\Delta PES}$ threshold [2].

The concept of this subsection is that the use of two "smart" hooks, where the first one (hook A) will perform the energy theft and the second one (hook B) will try to jam HS-DET method as a feint hook, could significantly decrease $\overline{\Delta PES}$ values. As indicated in Sec.2.1, the success of this combined use of "smart" hooks would be accomplished if $\overline{\Delta PES}$ values can remain below 5%. Although $\overline{\Delta PES}$ values that are below 5% can be detected by the loose $\overline{\Delta PES}$ threshold, these $\overline{\Delta PES}$ values can be considered as various small measurement differences, which have not been mitigated and finally ignored by the authorized maintenance personnel. Anyway, $\overline{\Delta PES}$ values that are below 5% have been detected neither in [1] nor in [2] in all the cases examined.

To investigate the possibility of camouflaging the hook style energy theft through the use of two "smart" hooks, in Fig. 2(a), $\overline{\Delta PES}$ is plotted versus the hook A distance from the transmitting end and the hook B distance from the transmitting end when the OV LV BPL topology of urban case A is assumed, and maximum value a_{CUD} of 1 dB is applied. In Figs. 2(b) and 2(c), same contour plots with Fig. 2(a) are given but for maximum value a_{CUD} of 2 dB and 5 dB, respectively. In Figs. 3, 4, 5 and 6, same plots with Fig. 2 are given but for the case of the urban case B, suburban case, rural case and "LOS" case, respectively. In accordance with [1], the hook A and B distance from the transmitting end span is assumed to be equal to 50 m, the terminations of hook A and B

are assumed to be matched while the hook A and B length is assumed to be equal to 5m for all the examined contour plots of this paper. Note that the range of the hook A distance from the transmitting end is from 1 m to 951 m for all the examined contour plots of this paper while the respective range of the hook B is from 2 m to 952 m.
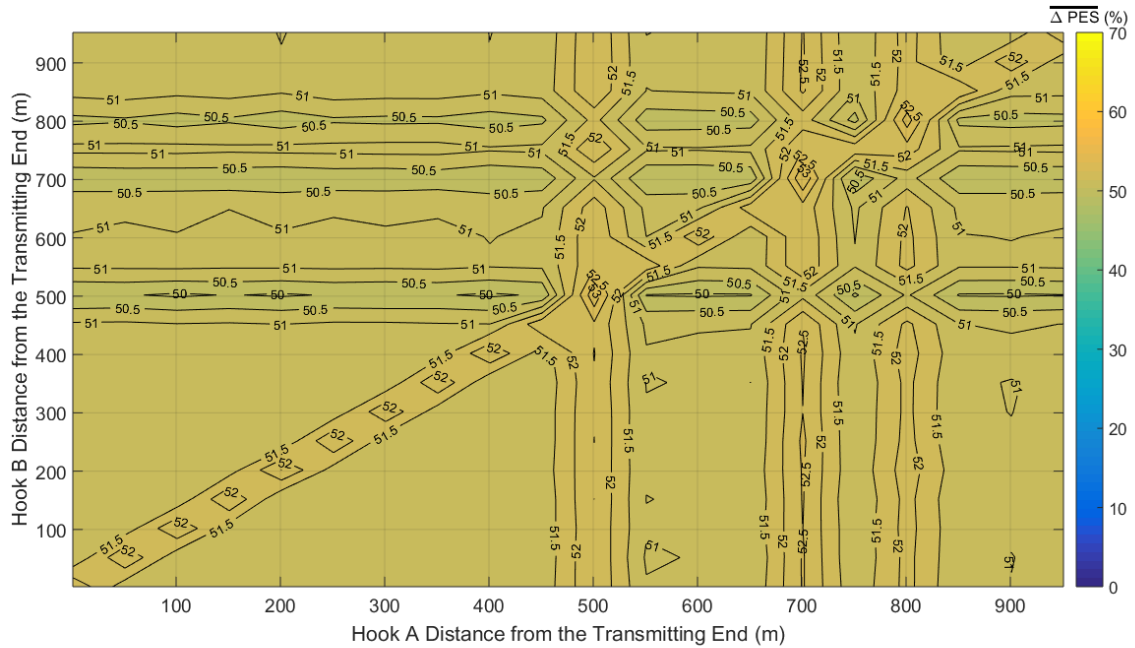
(a)
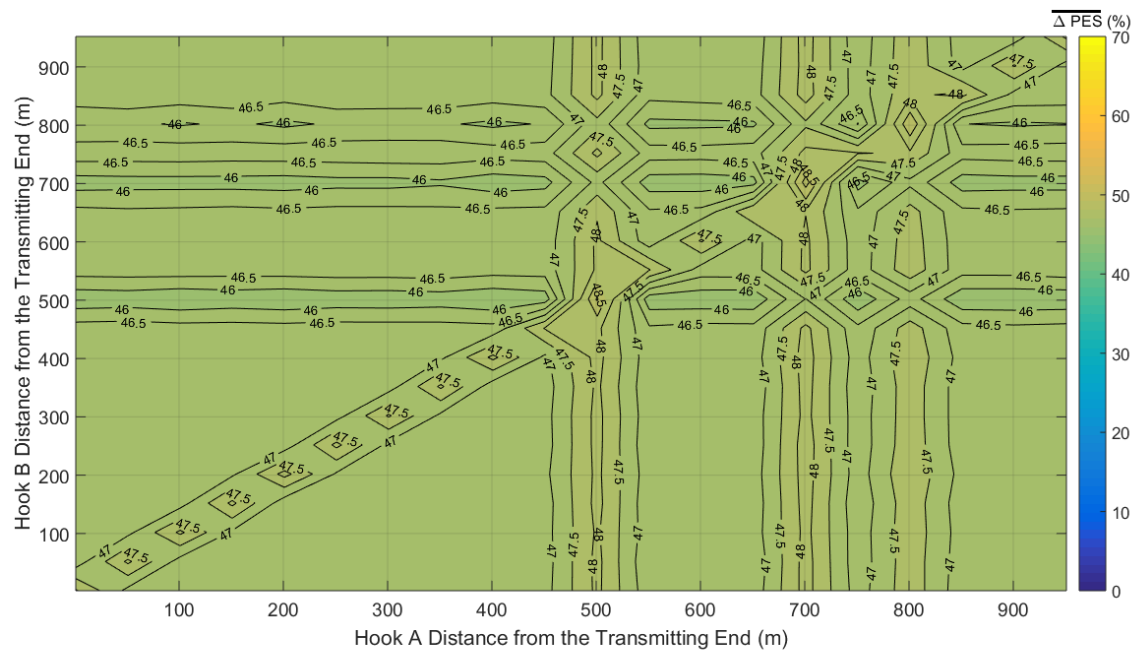
(b)
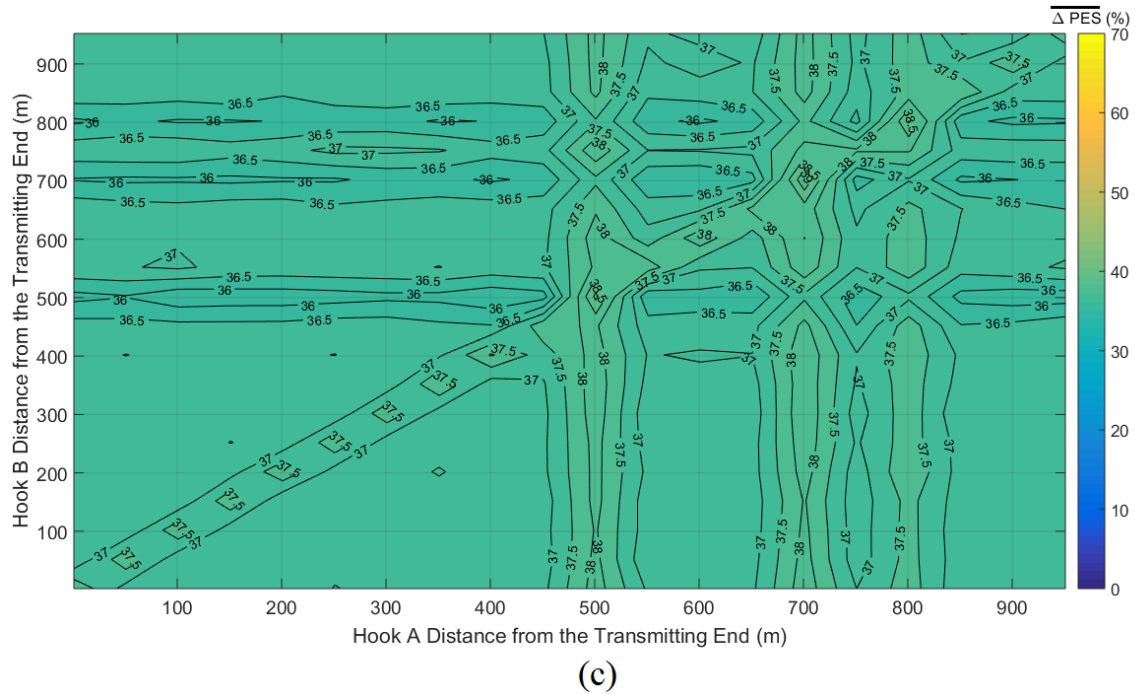
(c)

Fig. 2. $\overline{\mathit{\Delta PES}}$ of the urban case A of the indicative OV LV BPL topologies in the 3-88MHz frequency band for various hook A and hook B distances from the transmitting end. (a) $a_{CUD} = 1\text{dB}$. (b) $a_{CUD} = 2\text{dB}$. (c) $a_{CUD} = 5\text{dB}$.
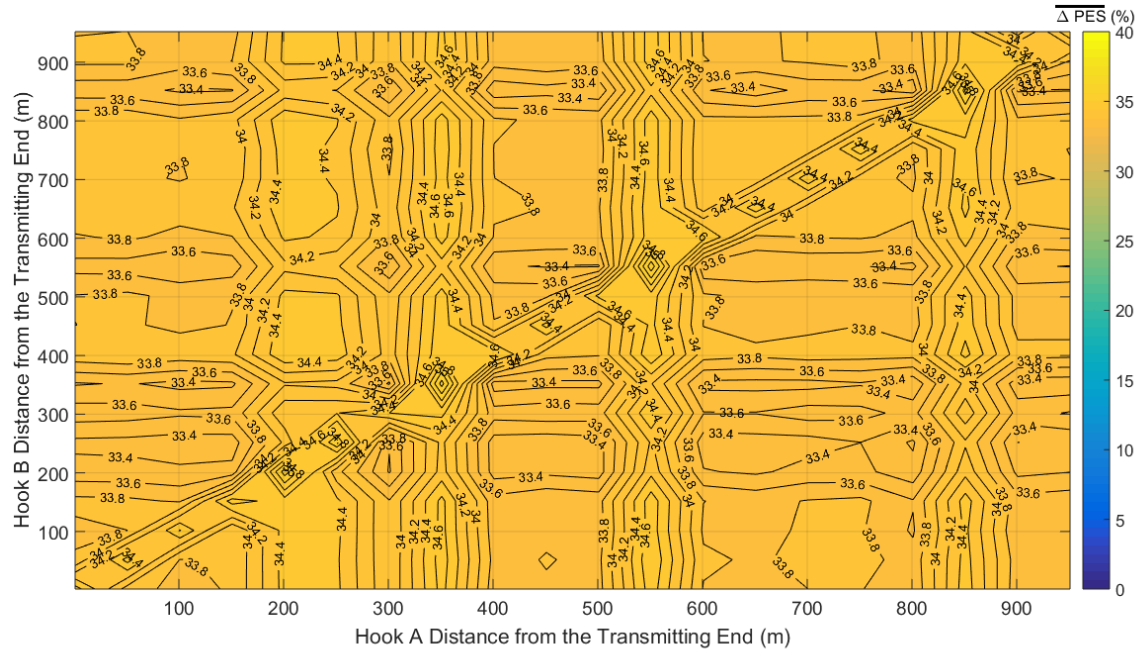
(a)
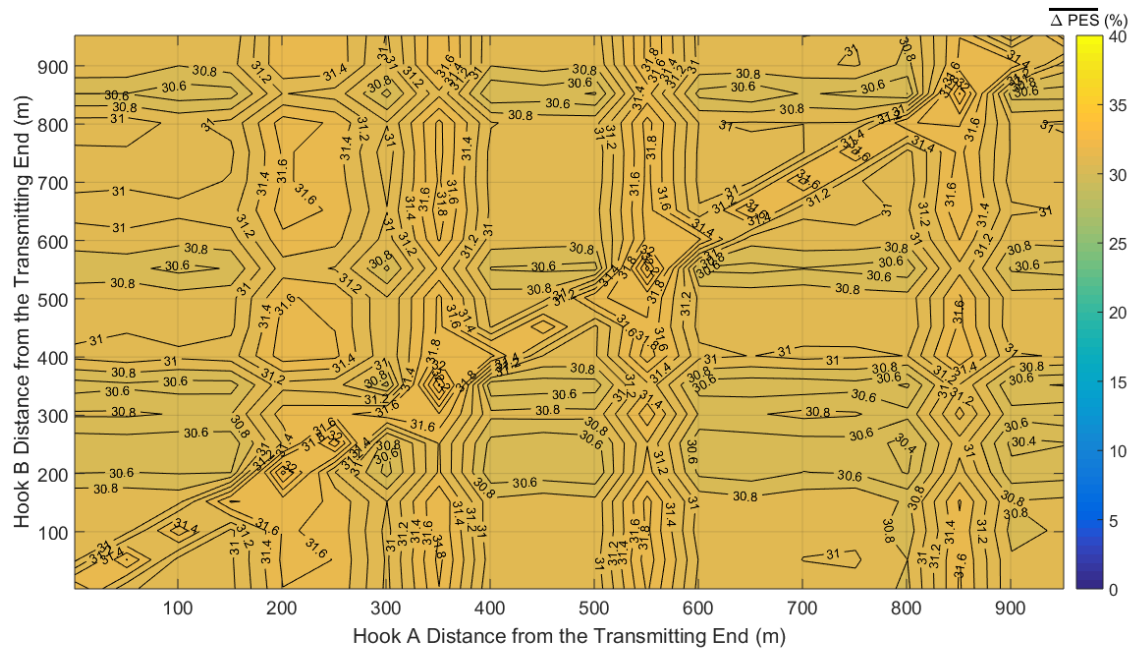
(b)

Fig. 3. Same curves with Fig. 2 but for the urban case B.
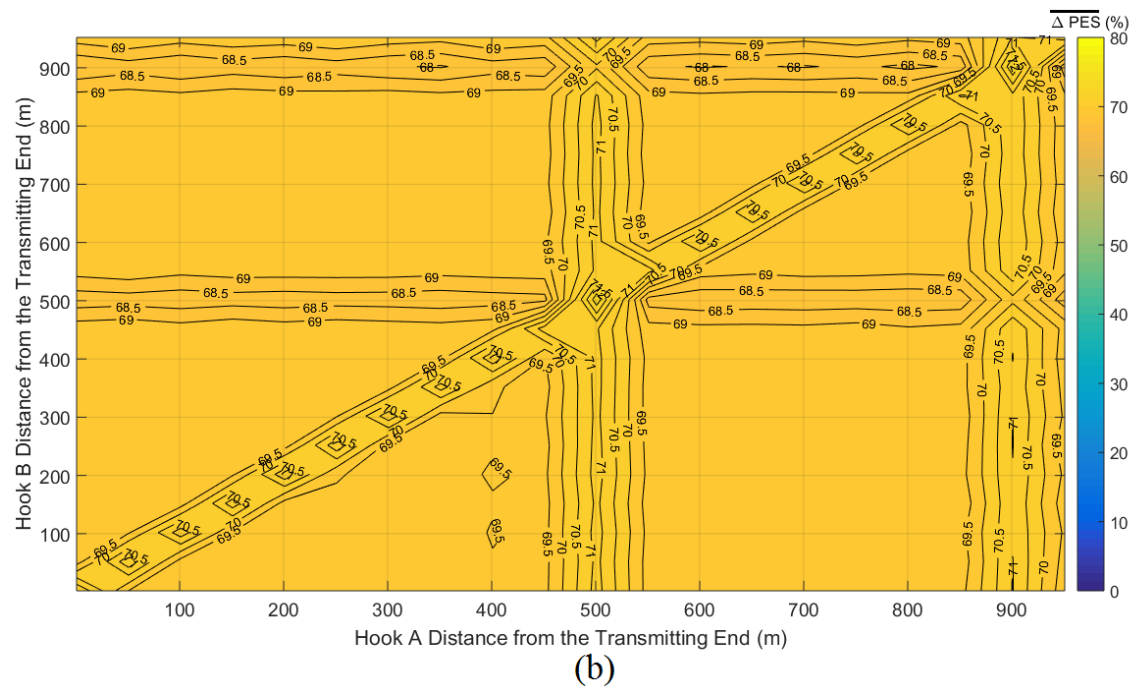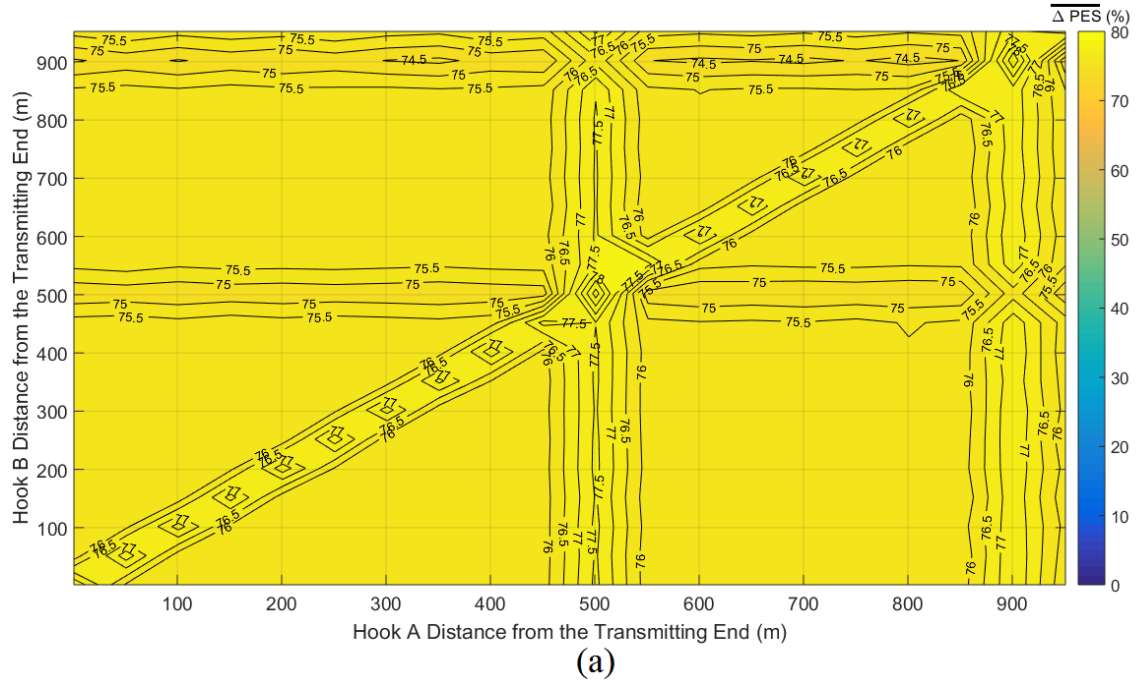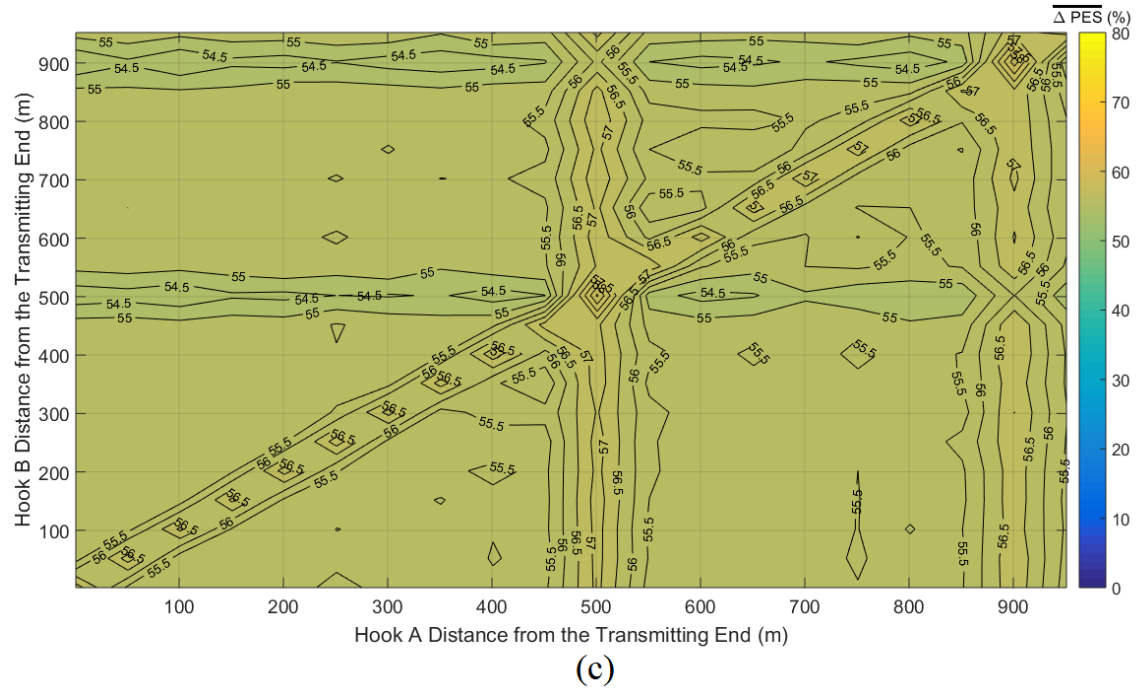
(a)

(b)

Fig. 4. Same curves with Fig. 2 but for the suburban case.
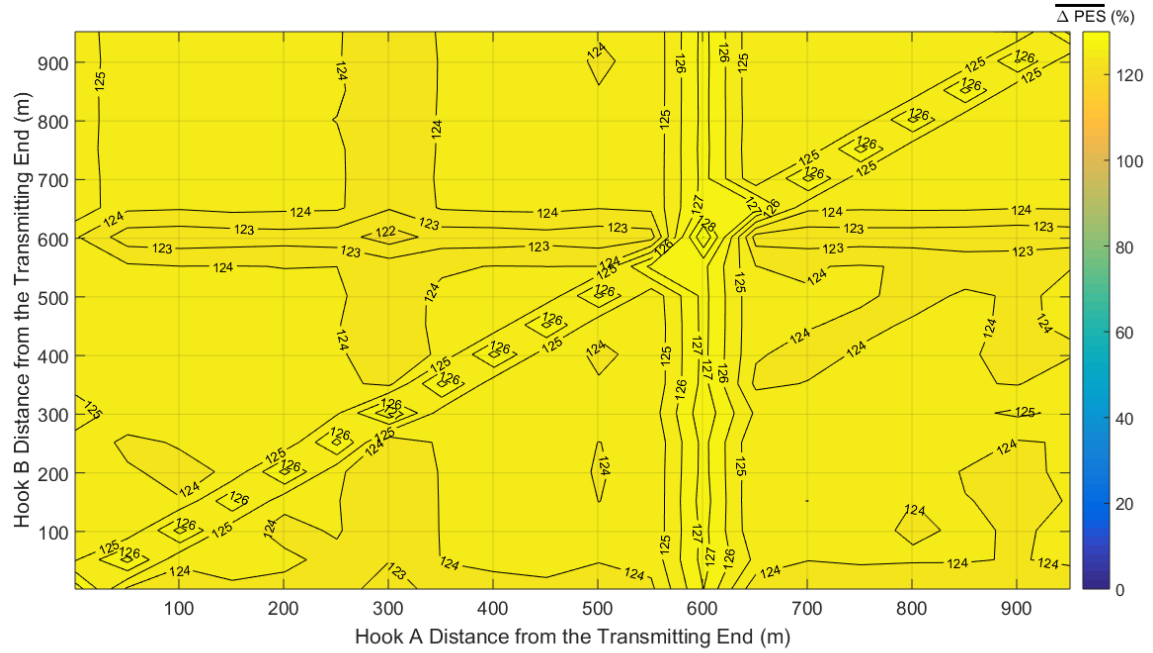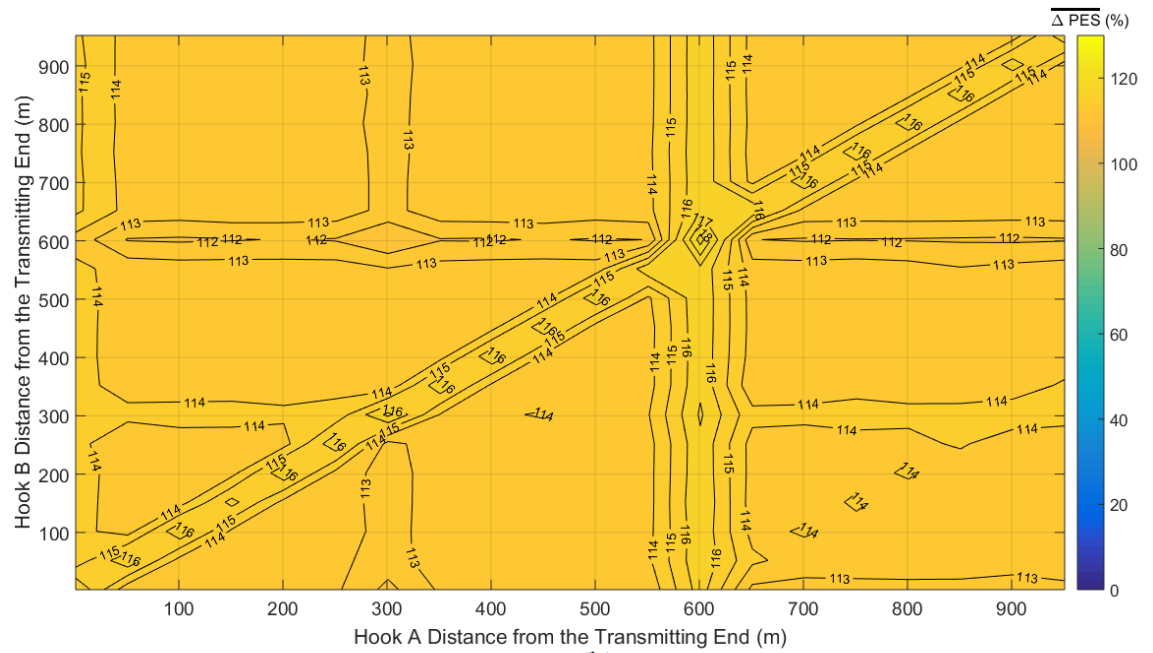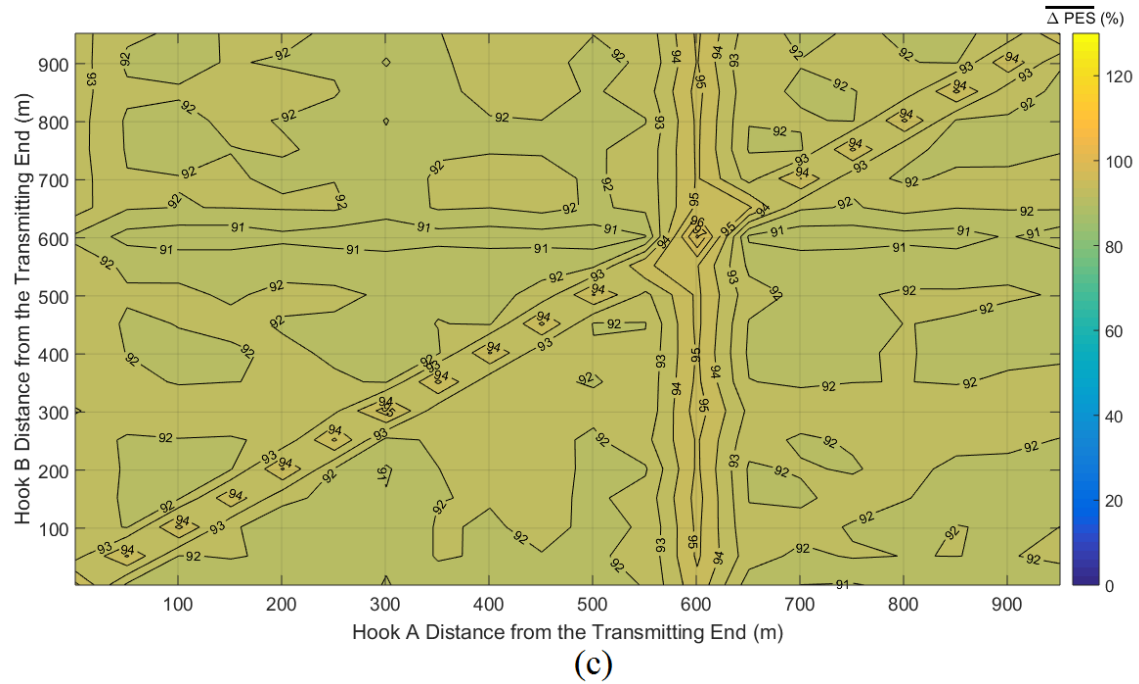
(a)

(b)

(c)

Fig. 5. Same curves with Fig. 2 but for the rural case.

(a)

(b)

(c)
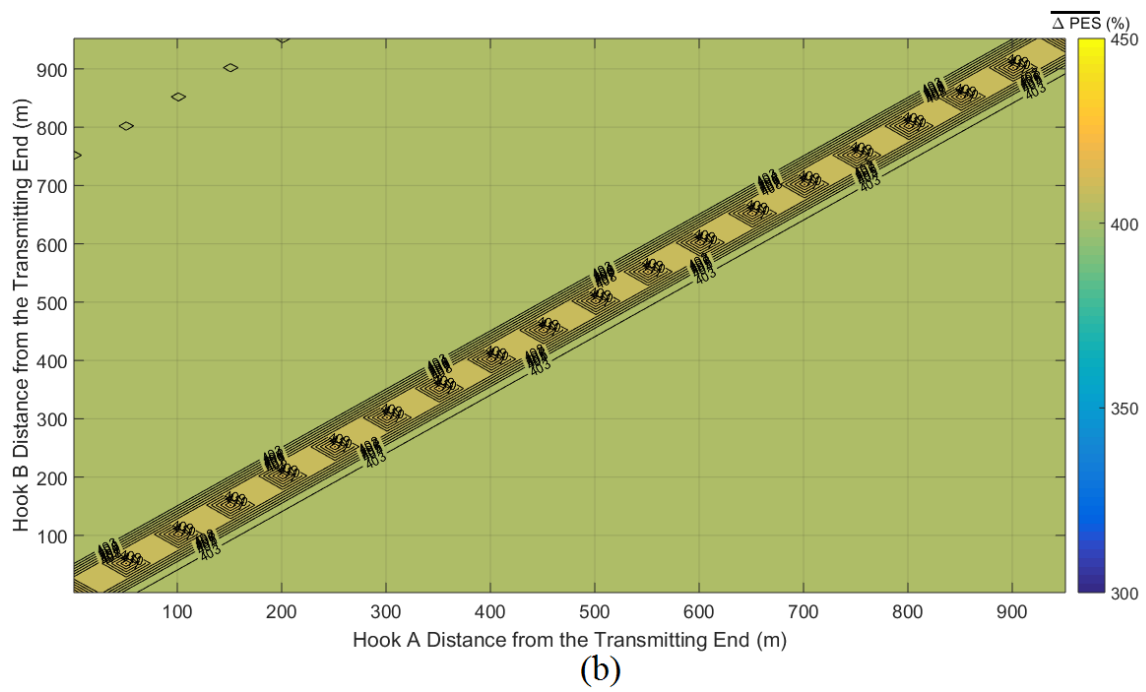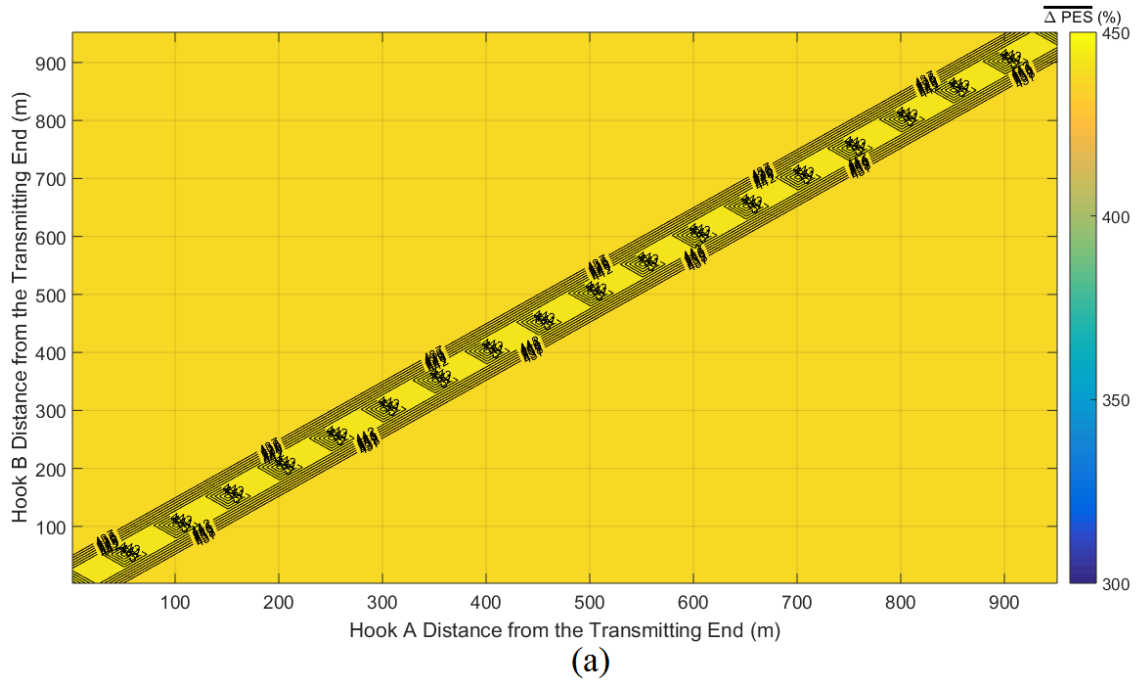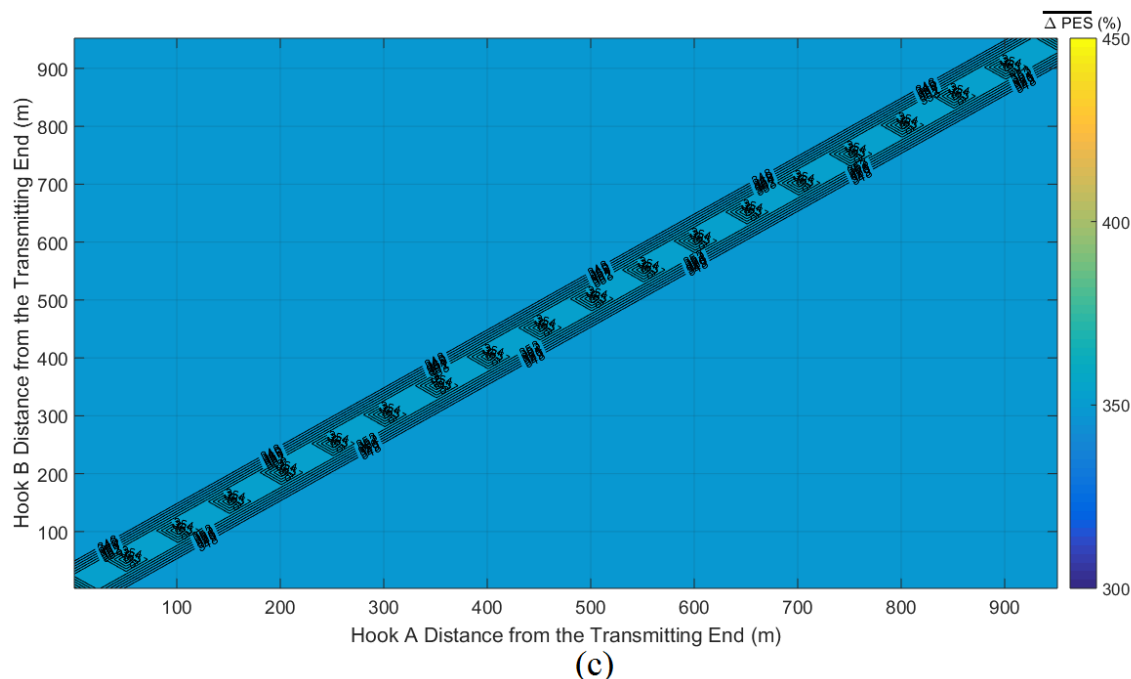
Fig. 6. Same curves with Fig. 2 but for the "LOS" case.

From Figs. 2-6, the insertion of the feint "smart" hook significantly increases $\overline{\Delta PES}$ values for given OV LV BPL topology, "smart" hook A distance from the transmitting end and maximum value a_{CUD}. Instead of reducing $\overline{\Delta PES}$ values, HS-DET method now more easily detects the energy theft; when the feint "smart" hook is employed, $\overline{\Delta PES}$ values of Figs. 2-6 are more than twice as high as those of the respective Figs. 2-6 of [2] in all the cases examined. In addition, higher $\overline{\Delta PES}$ values are observed when two "smart" hooks remain close enough due to the fact that the comparable distance of two hooks allows the creation of new significant multipath channels [10], [12]. Furthermore, $\overline{\Delta PES}$ difference between the highest and lowest $\overline{\Delta PES}$ value for given figure remains below 3% in all the cases examined.

In addition, each of Figs. 2-6 presents a strong symmetry with respect to the diagonal linking the top of the axes with the top right top. This implies that the overall $\overline{\Delta PES}$, which is shown in Figs. 2-6, can be regarded as the additive result of the partial $\overline{\Delta PES}$ of the two "smart" hooks.

Anyway, by comparing Figs. 2-6 with Fig. 7(a) of [2], it is clear that the two-"smart"-hooks technique cannot jam HS-DET method by its own. Actually, the effect of feint "smart" hook on $\overline{\Delta PES}$ values can be described as a small $\overline{\Delta PES}$ fluctuation to the existing $\overline{\Delta PES}$ values of the first "smart" hook while the effect of higher maximum value a_{CUD} becomes significantly stronger. The last conclusion is also validated by the almost the same color tone presented in each of the Figs. 2-6.

In general, the belief that adding feint "smart" hooks can allow the bypass of HS-DET method is misleading. HS-DET method can detect the hook style energy theft via two or more "smart" hooks with the same difficulty as HS-DET method does when one "smart" hook is installed across the OV LV lines.

3.3 Full Interconnection Assumption, Hybrid Method and HS-DET Method Jamming

Hybrid model is extensively employed to examine the behavior of various multiconductor transmission line (MTL) configurations in transmission and distribution BPL networks [10]-[24] while it is the core element of HS-DET method. Actually, the hybrid model consists of two interconnected modules, namely: (i) the bottom-up approach module; and (ii) the top-down approach module. The top-down approach module of the hybrid model is based on the concatenation of multidimensional transmission matrices of the cascaded network BPL connections and, among others, through its interconnection multidimensional transmission matrix $\mathbf{C}_k$ describes the connection between the distribution and branch TLs (i.e., the interconnection between the phases and the neutral of two TLs) [10].

Until now [1], [2], full interconnections between the hook and the distribution TLs have been considered while the impact of partial interconnection (*i.e.,* hook hung on one phase) is here investigated. The full interconnection allows the hook to be treated as a branch by the hybrid model and, hence, the simplicity of the analysis is enhanced. To proceed with the partial interconnection, the hook is assumed to be hung only on one phase, say phase A or the green conductor of Fig. 1 of [1]. As it is obvious, the partial interconnection is more realistic way of hook style energy theft while this may have an impact on the coupling scheme that is used to detect hook style energy theft. In the case of hook hung on phase A and with reference to [10], the interconnection multidimensional transmission matrix is equal to zero array apart from the element of the first row and first column that is equal to 1.

To investigate the effect of partial interconnections during the energy theft detection by HS-DET method, with reference to Fig. 2(b) of [1] and the indicative original OV LV BPL topologies as reported in Table 1 of [1], let assume again that an open-circuit hook of length L_{bh} is inserted at distance D_{h} from the transmitting end. In Fig. 7(a), $\overline{\mathit{\Delta PES}}$ is plotted with respect to the maximum value a_{CUD} when $L_{\mathrm{bh}} = 5\mathrm{m}$ and $D_{\mathrm{h}} = 300\mathrm{m}$ are assumed for the five indicative original OV LV BPL topologies, hook is hung on the phase A and WtG[1] coupling scheme is applied. In Figs. 7(b) and 7(c), same curves with Fig. 7(a) are given but for the cases of WtG[2] and WtG[3] coupling schemes, respectively.
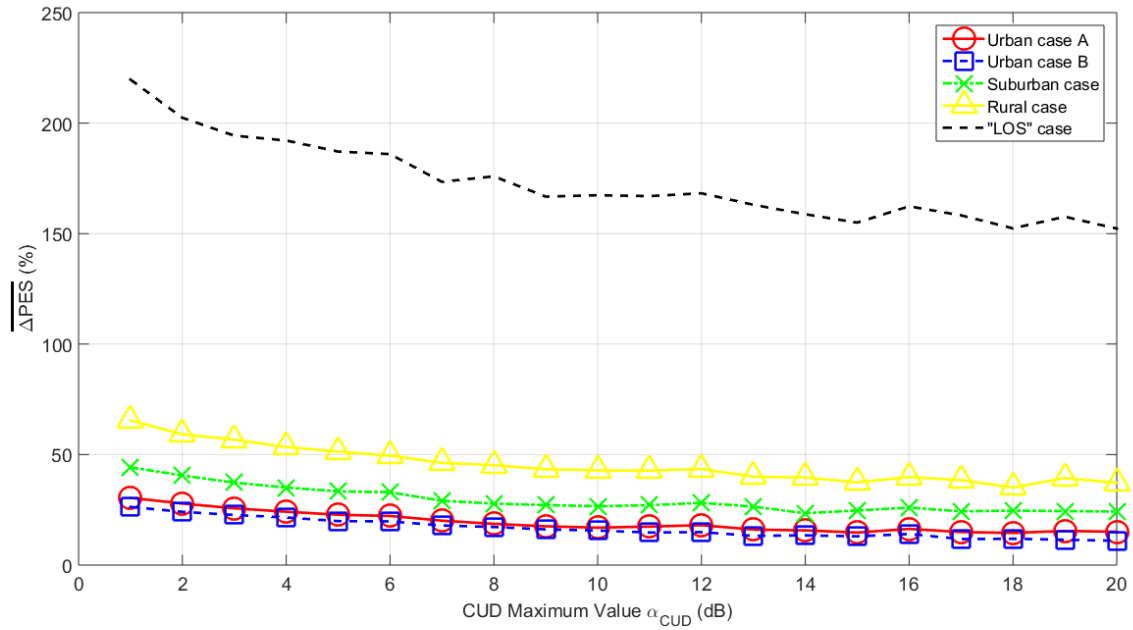
(a)
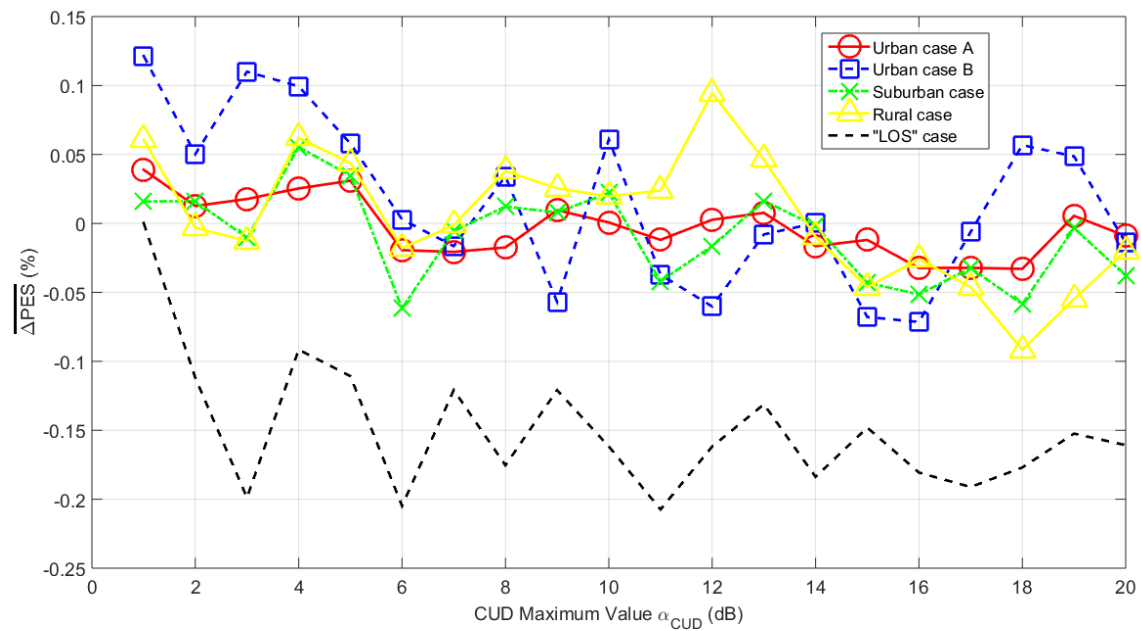
(b)
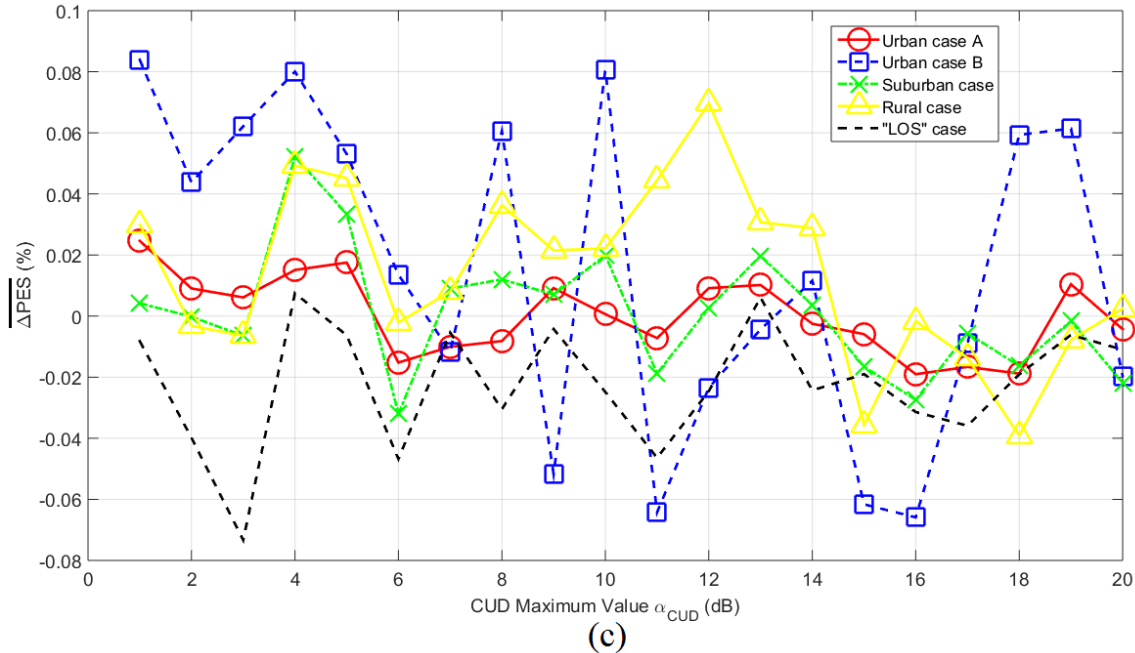
Fig. 7. $\overline{\Delta PES}$ of HS-DET method for the five original indicative OV LV BPL topologies of [1] when hook of 5m-length, of 300m-distance from the transmitting end, hung at phase A and with open-circuit termination is assumed for different WtG coupling schemes. (a) WtG[1]. (b) WtG[2]. (c) WtG[3].

From Figs. 7(a)-(c), interesting findings can be reported concerning the detection of hook style energy theft when the hook is hung on only one phase. More specifically:

- Comparing Fig. 7(a) with Fig. 1(a) of [2], $\overline{\Delta PES}$ plots are identical as expected. This means that when the applied WtG coupling scheme comprises the conductor where the hook is hung, $\overline{\Delta PES}$ plots present no differences compared with $\overline{\Delta PES}$ plots of fully interconnected hooks. Therefore, all the results of this paper, [1] and [2] occur without changes when the conductor of hook is the same with the conductor of WtG coupling scheme.

- Comparing Figs. 7(b) and 7(c) with Fig. 1(a) of [2], when the applied WtG coupling scheme does not comprise the conductor where the hook is hung, $\overline{\Delta PES}$ values are close to zero resembling with the difference measurement difference $\overline{\Delta PES}$ behavior of Fig. 8(a) of the Appendix. However, if the case of different CUD measurement differences during the determination of the original theoretical coupling scheme channel transfer function and the modified theoretical coupling scheme channel transfer function can be excluded (see Sec.2.1), the loose $\overline{\Delta PES}$ threshold may detect the hook style energy theft through the fluctuating or negative $\overline{\Delta PES}$ values even though the hook is hung on different conductor with reference to the conductor of the employed WtG coupling schemes. Therefore, with reference to Sec.2.1, a real time and continuous HS-DET method can trigger the hook style energy theft detection alarm even if the hook is hung intentionally on different conductor from the BPL injector / extractors.

- In [28]-[31], new coupling schemes for transmission and distribution BPL networks have been presented through the adoption of CS2 module. Actually, CS2 module can exploit all the available conductors of the examined MTL

configuration and, hence, the detection of the hook style energy theft can be accomplished through a periodic surveillance test of the supported multiple input multiple output (MIMO) channels.

Concluding this subsection, there are three ways of detecting the hook style energy theft when the hook is hung on only one conductor, namely: (i) through $\overline{\Delta PES}$ values when the employed WtG coupling scheme comprises the conductor where the hook is hung; (ii) through the existence of a real time and continuous HS-DET method. The exclusion of all other problematic cases can be ensured and the small $\overline{\Delta PES}$ fluctuations can imply a hook style energy theft through a different conductor from the one that is used by the applied WtG coupling scheme, and (iii) by exploiting WtW and MtM coupling schemes of CS2 module. These coupling schemes exploit all the conductors of the examined MTL configuration and, thus, the hook style energy theft detection can be easily achieved through a periodic check of the MIMO channel health.

3. Conclusions

This paper has focused on the performance of HS-DET method when the three more sophisticated scenarios of [2] are addressed. In fact, these sophisticated cases are considered as the further consideration of special cases presented in [1] and investigated in [2]. As the first sophisticated scenario has been examined, the effect of two different CUD measurement differences on $\overline{\Delta PES}$ and $\overline{Rob}$ values remains marginal in comparison with the respective $\overline{\Delta PES}$ and $\overline{Rob}$ values when one CUD measurement difference is assumed during the computation of the original theoretical coupling scheme channel transfer function and the modified theoretical coupling scheme channel transfer function. In all the cases of average values of CUD maximum values a_{CUD}, the hook style energy theft has been detected by HS-DET method through strict $\overline{\Delta PES}$ and $\overline{Rob}$ thresholds. As the second sophisticated scenario has been investigated, HS-DET method more easily detects the energy theft when a second "smart" hook, either acting as a feint "smart" hook or not, is installed across OV LV TLs. In fact, $\overline{\Delta PES}$ values for given OV LV BPL topology with two "smart" hooks are significantly higher than the respective ones of the same OV LV BPL topology with one "smart" hook regardless of the distance between them. Hence, by generalizing the findings of two "smart" hooks, the myth of many "smart" hooks that can jam HS-DET method has been disproven. The third sophisticated scenario that has been examined was the impact of the assumption of full interconnections during the computations of HS-DET method. When the hook is hung on only one conductor, three different detection cases have been analyzed that allow HS-DET method to securely detect the hook style energy theft. The three special cases of [1] and the three sophisticated scenarios of this paper have aimed at jamming HS-DET method. As it has been proven, HS-DET method can detect all the potential hook style energy thefts in OV LV BPL networks through its strict $\overline{\Delta PES}$ threshold in the vast majority of the cases and its loose $\overline{\Delta PES}$ threshold in few aggravated cases. Finally, the virtue of maintaining a real-time and continuous HS-DET method combined with CS2 module conveniences has been praised and its advantages have been analytically reported.

Appendix – Can Different CUD Measurement Differences Trigger the Hook Style Energy Theft Alarm of HS-DET Method

The impact of same CUD measurement difference during the determination of the original measured coupling scheme channel transfer function and the modified measured coupling scheme channel transfer functions on $\overline{\Delta PES}$, $\overline{PES_{or}}$ and $\overline{Rob}$ has been examined in the Appendix of [2]. In this Appendix, the sole influence of different CUD measurement differences but of the same maximum value a_{CUD} during the determination of the original measured coupling scheme channel transfer function and the modified measured coupling scheme channel transfer functions on the aforementioned three PES submetrics is evaluated. With reference to eqs (3)-(8) of [1], the modified theoretical coupling scheme channel transfer function $H_{mod}^{C}\{\cdot\}$ is assumed to be equal to the original theoretical coupling scheme channel transfer function $H_{or}^{C}\{\cdot\}$. With reference to eqs. (5) and (6) of [1], since different measurement differences are considered, $\overline{PES_{or}}$ stops being equal to $\overline{PES_{mod}}$ when the aforementioned assumption occurs. In general terms, the critical issue now is the difference between the two assumed CUD measurement differences for given frequency.

To examine the impact of the two different CUD measurement differences of the same maximum value a_{CUD}, in Fig. 8(a), $\overline{\Delta PES}$ is plotted with respect to the maximum value a_{CUD} when the modified OV LV BPL topology is assumed to be the same with the original one for the five indicative original OV LV BPL topologies of Table 1 of [1]. Note that two different CUD measurement differences of the same maximum value a_{CUD} are used during the determination of the original measured coupling scheme channel transfer function and the modified measured coupling scheme channel transfer functions. In Figs. 8(b) and 8(c), same curves with Fig. 8(a) are given but for $\overline{PES_{or}}$ and $\overline{Rob}$, respectively.

(a)

(b)

(c)
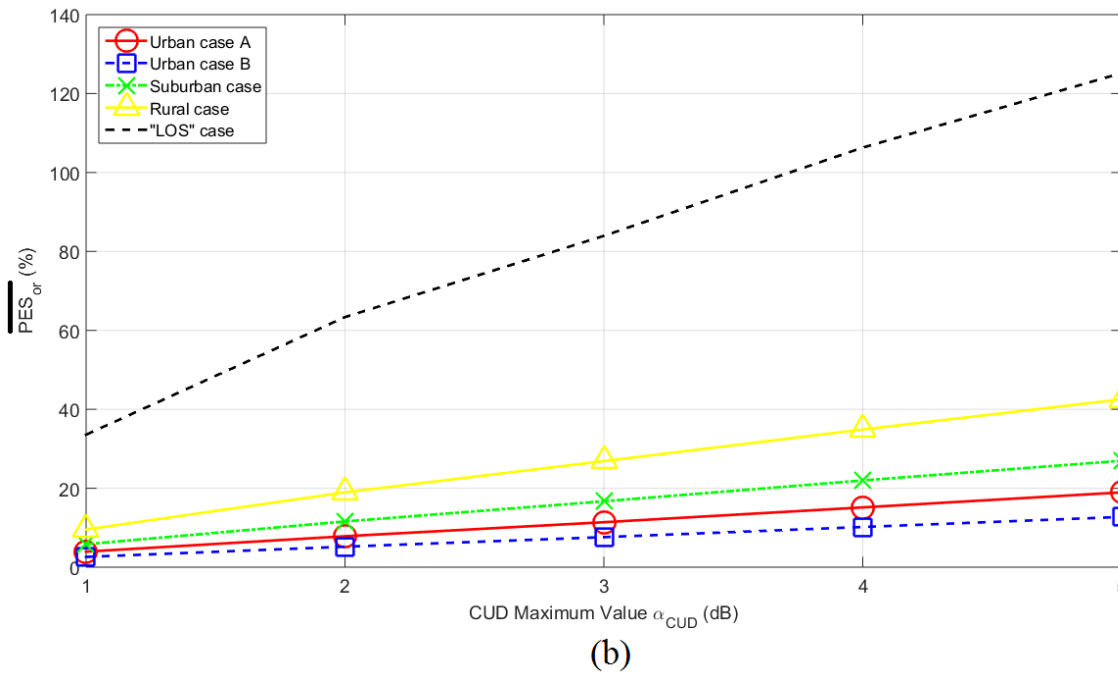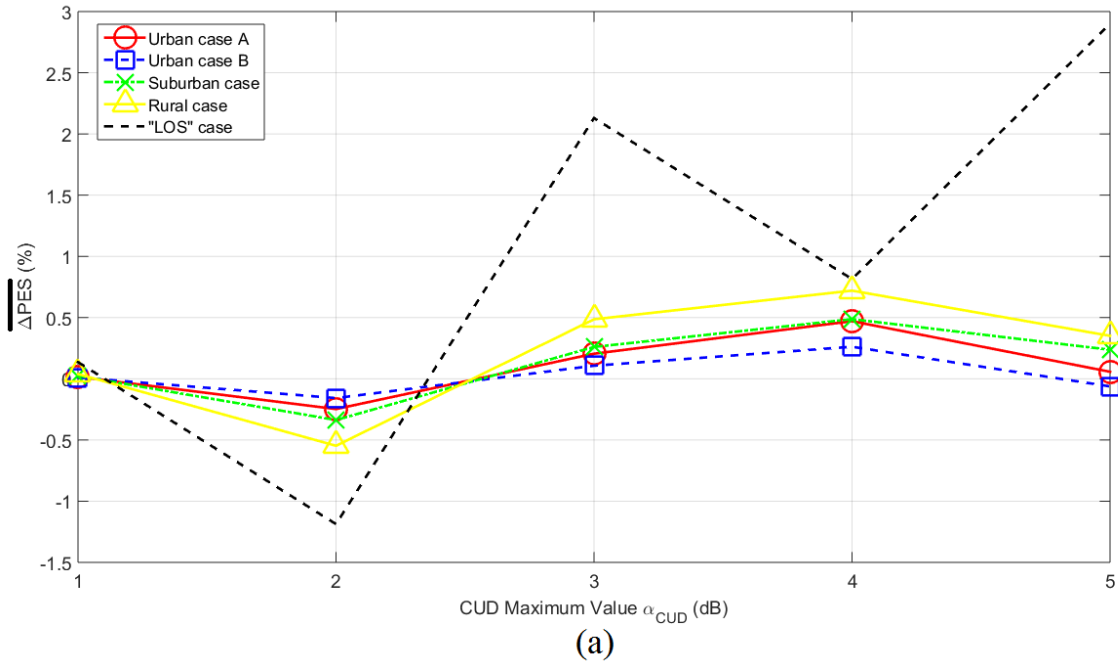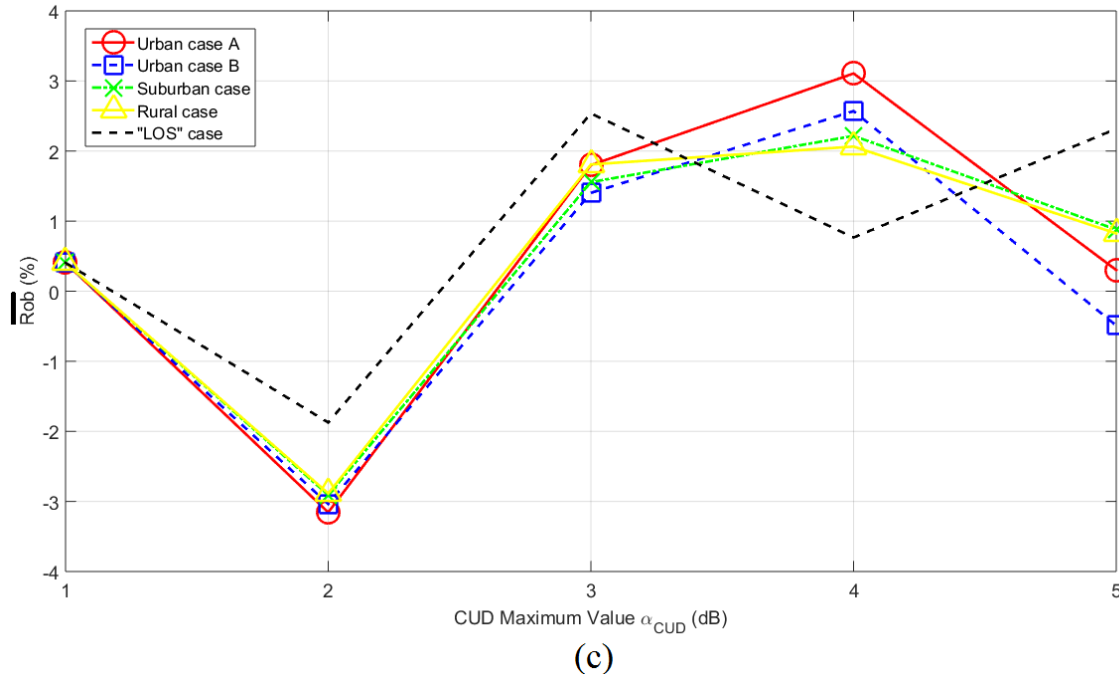
Fig. 8. PES submetrics of HS-DET method for the five original indicative OV LV BPL topologies of [1] when modified OV LV BPL topology is assumed the same with the original one and two different CUD measurement differences and various maximum values a_{CUD}. (a) $\overline{\Delta PES}$. (b) $\overline{PES_{or}}$. (c) $\overline{Rob}$.

By comparing Figs. 8(a)-(c) with the findings of [2], the following conclusions can be deduced concerning $\overline{\Delta PES}$, $\overline{PES_{or}}$ and $\overline{Rob}$, say:

- Due to the definition of $\overline{\Delta PES}$ and $\overline{Rob}$, their study is focused on weighted differences between the absolute values of different CUD measurement differences of the same maximum value a_{CUD} since the modified theoretical coupling scheme channel transfer function and the original theoretical coupling scheme channel transfer function are equal. Therefore, it is expected that $\overline{\Delta PES}$ and $\overline{Rob}$ behave as CUD variables of zero mean. Possible divergences are due to the weighted definition of $\overline{\Delta PES}$ and $\overline{Rob}$.

- Already been mentioned in [2], $\overline{PES_{or}}$ is independent of the modified measured coupling scheme channel transfer function since it depends only on the original measured and original theoretical coupling scheme channel transfer function. Hence, the increase of the considered maximum value a_{CUD} is reflected on the increased values of $\overline{PES_{or}}$.

- The influence of the different CUD measurement differences to $\overline{\Delta PES}$ and $\overline{Rob}$ values remain marginal and significantly lower than the respective strict $\overline{\Delta PES}$ and $\overline{Rob}$ thresholds. However, $\overline{\Delta PES}$ and $\overline{Rob}$ values render precarious such a decision based on the loose $\overline{\Delta PES}$ and $\overline{Rob}$ thresholds.

Concluding this Appendix, the effect of two different CUD measurement differences on $\overline{\Delta PES}$ and $\overline{Rob}$ values remains marginal allowing the decision concerning the existence of hook style energy theft by using the respective strict $\overline{\Delta PES}$ and $\overline{Rob}$ thresholds. However, the cost of a non-real time and continuous HS-DET method in

terms of $\overline{\Delta PES}$ and $\overline{Rob}$ is that decisions concerning the hook style energy theft that are based on the loose $\overline{\Delta PES}$ and $\overline{Rob}$ can be considered as risky ones.

CONFLICTS OF INTEREST

The author declares that there is no conflict of interests regarding the publication of this paper.

References

[1]   A. G. Lazaropoulos, "Detection of Energy Theft in Overhead Low-Voltage Power Grids – The Hook Style Energy Theft in the Smart Grid Era," *Trends in Renewable Energy*, vol. 5, no. 1, pp. 12 – 46, Oct. 2018. [Online]. Available: http://futureenergysp.com/index.php/tre/article/view/81/pdf

[2]   A. G. Lazaropoulos, "Special Cases during the Detection of the Hook Style Energy Theft in Overhead Low-Voltage Power Grids through HS-DET Method – Part 1: High Measurement Differences, Very Long Hook Technique and "Smart" Hooks," *Trends in Renewable Energy*, vol. 5, no. 1, pp. 60 – 89, Dec. 2018. DOI: 10.17737/tre.2019.5.1.0082

[3]   A. G. Lazaropoulos, "Measurement Differences, Faults and Instabilities in Intelligent Energy Systems – Part 1: Identification of Overhead High-Voltage Broadband over Power Lines Network Topologies by Applying Topology Identification Methodology (TIM)," *Trends in Renewable Energy*, vol. 2, no. 3, pp. 85 – 112, Oct. 2016. [Online]. Available: http://futureenergysp.com/index.php/tre/article/download/26/32

[4]   A. G. Lazaropoulos, "Measurement Differences, Faults and Instabilities in Intelligent Energy Systems – Part 2: Fault and Instability Prediction in Overhead High-Voltage Broadband over Power Lines Networks by Applying Fault and Instability Identification Methodology (FIIM)," *Trends in Renewable Energy*, vol. 2, no. 3, pp. 113 – 142, Oct. 2016. [Online]. Available: http://futureenergysp.com/index.php/tre/article/view/27/33

[5]   A. G. Lazaropoulos, "Power Systems Stability through Piecewise Monotonic Data Approximations – Part 2: Adaptive Number of Monotonic Sections and Performance of L1PMA, L2WPMA and L2CXCV in Overhead Medium-Voltage Broadband over Power Lines Networks," *Trends in Renewable Energy*, vol. 3, no. 1, pp. 33 – 60, Jan. 2017. [Online]. Available: http://futureenergysp.com/index.php/tre/article/view/30/35

[6]   A. G. Lazaropoulos, "Power Systems Stability through Piecewise Monotonic Data Approximations – Part 1: Comparative Benchmarking of L1PMA, L2WPMA and L2CXCV in Overhead Medium-Voltage Broadband over Power Lines Networks," *Trends in Renewable Energy*, vol. 3, no. 1, pp. 2 – 32, Jan. 2017. [Online]. Available: http://futureenergysp.com/index.php/tre/article/view/29/34

[7]   A. G. Lazaropoulos, "Main Line Fault Localization Methodology in Smart Grid – Part 1: Extended TM2 Method for the Overhead Medium-Voltage Broadband over Power Lines Networks Case," *Trends in Renewable Energy*, vol. 3, no. 3, pp. 2-25,

Dec.   2017.   [Online].   Available:
http://futureenergysp.com/index.php/tre/article/view/36

[8]   A. G. Lazaropoulos, "Main Line Fault Localization Methodology in Smart Grid –
       Part 2: Extended TM2 Method, Measurement Differences and L1 Piecewise
       Monotonic Data Approximation for the Overhead Medium-Voltage Broadband
       over Power Lines Networks Case," *Trends in Renewable Energy*, vol. 3, no. 3, pp.
       26-61,   Dec.   2017.   [Online].   Available:
       http://futureenergysp.com/index.php/tre/article/view/37

[9]   A. G. Lazaropoulos, "Main Line Fault Localization Methodology in Smart Grid –
       Part 3: Main Line Fault Localization Methodology (MLFLM)," *Trends in
       Renewable Energy*, vol. 3, no. 3, pp. 62-81, Dec. 2017. [Online]. Available:
       http://futureenergysp.com/index.php/tre/article/view/38

[10]   A. G. Lazaropoulos, "Towards Modal Integration of Overhead and Underground
       Low-Voltage and Medium-Voltage Power Line Communication Channels in the
       Smart Grid Landscape: Model Expansion, Broadband Signal Transmission
       Characteristics, and Statistical Performance Metrics (Invited Paper)," *ISRN Signal
       Processing*, vol. 2012, Article ID 121628, pp. 1-17, 2012. [Online]. Available:
       http://www.hindawi.com/isrn/sp/2012/121628/

[11]   A. G. Lazaropoulos, "Towards broadband over power lines systems integration:
       Transmission characteristics of underground low-voltage distribution power lines,"
       Progress in Electromagnetics Research B, 39, pp. 89-114, 2012. [Online].
       Available: http://www.jpier.org/PIERB/pierb39/05.12012409.pdf

[12]   A. G. Lazaropoulos and P. G. Cottis, "Transmission characteristics of overhead
       medium   voltage   power   line   communication   channels,"
       IEEE Trans. Power Del., vol. 24, no. 3, pp. 1164-1173, Jul. 2009.

[13]   A. G. Lazaropoulos and P. G. Cottis, "Capacity of overhead medium voltage power
       line communication channels," *IEEE Trans. Power Del.*, vol. 25, no. 2, pp. 723-
       733, Apr. 2010.

[14]   A. G. Lazaropoulos and P. G. Cottis, "Broadband transmission via underground
       medium-voltage power lines-Part I: transmission characteristics," *IEEE Trans.
       Power Del.*, vol. 25, no. 4, pp. 2414-2424, Oct. 2010.

[15]   A. G. Lazaropoulos and P. G. Cottis, "Broadband transmission via underground
       medium-voltage   power   lines-Part   II: capacity,"
       IEEE Trans. Power Del., vol. 25, no. 4, pp. 2425-2434, Oct. 2010.

[16]   A. G. Lazaropoulos, "Broadband transmission characteristics of overhead high-
       voltage power line communication channels," *Progress in Electromagnetics
       Research B*, vol. 36, pp. 373-398, 2012. [Online]. Available:
       http://www.jpier.org/PIERB/pierb36/19.11091408.pdf

[17]   A. G. Lazaropoulos, "Green Overhead and Underground Multiple-Input Multiple-
       Output Medium Voltage Broadband over Power Lines Networks: Energy-Efficient
       Power Control," *Springer Journal of Global Optimization*, vol. 2012 / Print ISSN
       0925-5001, pp. 1-28, Oct. 2012.

[18]   A. G. Lazaropoulos, "Deployment Concepts for Overhead High Voltage Broadband
       over Power Lines Connections with Two-Hop Repeater System: Capacity
       Countermeasures against Aggravated Topologies and High Noise Environments,"
       Progress in Electromagnetics Research B, vol. 44, pp. 283-307, 2012. [Online].
       Available: http://www.jpier.org/PIERB/pierb44/13.12081104.pdf

[19] A. G. Lazaropoulos, "Broadband transmission and statistical performance properties of overhead high-voltage transmission networks," *Hindawi Journal of Computer Networks and Commun.*, 2012, article ID 875632, 2012. [Online]. Available: http://www.hindawi.com/journals/jcnc/aip/875632/

[20] P. Amirshahi and M. Kavehrad, "High-frequency characteristics of overhead multiconductor power lines for broadband communications," *IEEE J. Sel. Areas Commun.*, vol. 24, no. 7, pp. 1292-1303, Jul. 2006.

[21] T. Calliacoudas and F. Issa, ""Multiconductor transmission lines and cables solver," An efficient simulation tool for plc channel networks development," presented at the *IEEE Int. Conf. Power Line Communications and Its Applications*, Athens, Greece, Mar. 2002.

[22] T. Sartenaer and P. Delogne, "Deterministic modelling of the (Shielded) outdoor powerline channel based on the multiconductor transmission line equations," *IEEE J. Sel. Areas Commun.*, vol. 24, no. 7, pp. 1277-1291, Jul. 2006.

[23] C. R. Paul, *Analysis of Multiconductor Transmission Lines*. New York: Wiley, 1994.

[24] H. Meng, S. Chen, Y. L. Guan, C. L. Law, P. L. So, E. Gunawan, and T. T. Lie, "Modeling of transfer characteristics for the broadband power line communication channel," *IEEE Trans. Power Del.*, vol. 19, no. 3, pp. 1057-1064, Jul. 2004.

[25] B. Li, D. Mansson, and G. Yang, "An efficient method for solving frequency responses of power-line networks," *Progress in Electromagnetics Research B*, Vol. 62, 303-317, 2015. DOI: 10.2528/PIERB15013008 http://www.jpier.org/pierb/pier.php?paper=15013008

[26] M. Chaaban, K. El KhamlichiDrissi, and D. Poljak, "Analytical model for electromagnetic radiation by bare-wire structures," *Progress in Electromagnetics Research B*, Vol. 45, 395-413, 2012. DOI:10.2528/PIERB12091102 http://www.jpier.org/pierb/pier.php?paper=12091102

[27] Y. H. Kim, S. Choi, S. C. Kim, and J. H. Lee, "Capacity of OFDM two-hop relaying systems for medium-voltage power-line access networks," *IEEE Trans. Power Del.*, vol. 27, no. 2, pp. 886-894, Apr. 2012.

[28] A. G. Lazaropoulos, "New Coupling Schemes for Distribution Broadband over Power Lines (BPL) Networks," *Progress in Electromagnetics Research B*, vol. 71, pp. 39-54, 2016. [Online]. Available: http://www.jpier.org/PIERB/pierb71/02.16081503.pdf

[29] A. G. Lazaropoulos, "Broadband Performance Metrics and Regression Approximations of the New Coupling Schemes for Distribution Broadband over Power Lines (BPL) Networks," *Trends in Renewable Energy*, vol. 4, no. 1, pp. 43 – 73, 2018. [Online]. Available: http://www.futureenergysp.com/index.php/tre/article/view/59/pdf

[30] A. G. Lazaropoulos, "Smart Energy and Spectral Efficiency (SE) of Distribution Broadband over Power Lines (BPL) Networks – Part 1: The Impact of Measurement Differences on SE Metrics," *Trends in Renewable Energy*, vol. 4, no. 2, pp. 125-184, Aug. 2018. [Online]. Available: http://futureenergysp.com/index.php/tre/article/view/76/pdf

[31] A. G. Lazaropoulos, "Smart Energy and Spectral Efficiency (SE) of Distribution Broadband over Power Lines (BPL) Networks – Part 2: L1PMA, L2WPMA and L2CXCV for SE against Measurement Differences in Overhead Medium-Voltage BPL Networks," *Trends in Renewable Energy*, vol. 4, no. 2, pp. 185-212, Aug.

2018.   [Online].   Available:
http://futureenergysp.com/index.php/tre/article/view/77/pdf

Trends in Renewable Energy (TRE) is an open accessed, peer-reviewed semi-annual journal publishing reviews and research papers in the field of renewable energy technology and science. The aim of this journal is to provide a communication platform that is run exclusively by scientists. This journal publishes original papers including but not limited to the following fields:

✧ Renewable energy technologies
✧ Catalysis for energy generation, Green chemistry, Green energy
✧ Bioenergy: Biofuel, Biomass, Biorefinery, Bioprocessing, Feedstock utilization, Biological waste treatment,
✧ Energy issues: Energy conservation, Energy delivery, Energy resources, Energy storage, Energy transformation, Smart Grid
✧ Environmental issues: Environmental impacts, Pollution
✧ Bioproducts
✧ Policy, etc.

We publish the following article types: peer-reviewed reviews, mini-reviews, technical notes, short-form research papers, and original research papers.

The article processing charge (APC), also known as a publication fee, is fully waived for the Trends in Renewable Energy.

Call for Editorial Board Members

We are seeking scholars active in a field of renewable energy interested in serving as volunteer Editorial Board Members.

Qualifications

Ph.D. degree in related areas, or Master's degree with a minimum of 5 years of experience.
All members must have a strong record of publications or other proofs to show activities in the energy related field.
If you are interested in serving on the editorial board, please email CV to
editor@futureenergysp.com.